MASTER

UCRL-9130
UC-34 Physics and Mathematics
TID-4500 (15th Ed.)

UNIVERSITY OF CALIFORNIA
Lawrence Radiation Laboratory
Berkeley, California
Contract No. W-7405-eng-48

THE RUBIDIUM-85–RUBIDIUM-86 HYPERFINE-STRUCTURE ANOMALY

Norman Braslau

(Thesis)

March 21, 1960

DISCLAIMER

This report was prepared as an account of work sponsored by an agency of the United States Government. Neither the United States Government nor any agency Thereof, nor any of their employees, makes any warranty, express or implied, or assumes any legal liability or responsibility for the accuracy, completeness, or usefulness of any information, apparatus, product, or process disclosed, or represents that its use would not infringe privately owned rights. Reference herein to any specific commercial product, process, or service by trade name, trademark, manufacturer, or otherwise does not necessarily constitute or imply its endorsement, recommendation, or favoring by the United States Government or any agency thereof. The views and opinions of authors expressed herein do not necessarily state or reflect those of the United States Government or any agency thereof.

DISCLAIMER

Portions of this document may be illegible in electronic image products. Images are produced from the best available original document.

THE RUBIDIUM-85–RUBIDIUM-86 HYPERFINE-STRUCTURE ANOMALY

Contents

THE RUBIDIUM-85–RUBIDIUM-86 HYPERFINE-STRUCTURE ANOMALY

Norman Braslau

Lawrence Radiation Laboratory
University of California
Berkeley, California

March 21, 1960

ABSTRACT

The atomic-beam magnetic-resonance method with separated oscillatory fields has been used to measure the hyperfine-structure separation and magnetic dipole moment of the isotopes Rb^{85} and Rb^{86}. Observation of a $\Delta F = \pm 1$ doublet in the magnetic field region where its mean value is a minimum gives the values of these observables; the doublet separation is proportional to the nuclear g factor and the mean doublet frequency is proportional to the hyperfine-structure separation.

Results obtained on Rb^{85} are in excellent agreement with previously published values, and indicate that the transition frequencies calculated from the Breit-Rabi energy-level equation agree with the experiment to better than one part per million.

For the radioactive isotope Rb^{86}, the following values are obtained for the $^2S_{1/2}$ electronic ground state:

$$\Delta\nu = 3946.883(2)\ \text{Mc},$$
$$g_I = -4.590(4)\times 10^{-4},$$
$$\mu_I = -1.6856(14)\ \text{nm}.$$

The hyperfine-structure anomaly is defined as the deviation from equality of the ratio of the hyperfine-splitting factors of two isotopes to the ratio of their nuclear g factors. For these two isotopes its value is found to be

$$\Delta = 0.17(9)\ \%.$$

Details of the apparatus constructed for the purpose of measuring these anomalies in radioactive alkali isotopes are presented, as well as the comparison of the experimental result with values predicted for the anomaly by using various nuclear models and the Bohr-Weisskopf theory.

I. INTRODUCTION

The measurement of various intrinsic nuclear properties such as spin and magnetic and electric multipole moments and comparison of these experimental values to values calculated on the basis of an assumed nuclear model have contributed to the development of a comprehensive theory of nuclear structure. At present the subject is in a rapid state of development; no one relatively simple model can account for all the observed properties of a very complex nucleus, but theories are reaching such a state of refinement and sophistication that a theory should be expected to predict rather well at least related observable properties.

There is a nuclear property, which may be described as the distribution of nuclear magnetism (EIS 58), whose effect is small but measurable and somewhat difficult to discuss theoretically, but which may provide a sensitive test to differentiate between various nuclear models.

The obvious probe of the distribution of magnetism in a nucleus is the deeply penetrating s electron of that atom. Accurate measurements of the hyperfine interaction due to the magnetic coupling of the nuclear magnetic moment to the electronic magnetic moment have contributed most of the experimental knowledge of this effect. Except for a few cases (EIS 52, STR 57) this effect has been measured only for pairs of stable isotopes scattered over the periodic table. The experimental difficulty of making accurate measurements on radioactive isotopes can be overcome, and it is hoped that information on the distribution of nuclear magnetism can be obtained for series of adjacent isotopes, making available the results of adding one neutron after another, and leading to an understanding of this effect as predicted by various nuclear models.

The most accurate means of measuring the hyperfine interaction in an atom is atomic beam magnetic resonance spectroscopy as introduced by Rabi (RAB 38). Refinement of techniques and associated instrumentation have made this a very widely used tool in atomic and

molecular beam research. Indeed, probably the most accurate physical measurement made to date has been that of the hyperfine interaction in Cs^{133} (ESS 58), which serves as the basis of atomic time standards. Several books and review articles have appeared in the past few years on the general field of atomic and molecular beams (RAM 56, SMI 55, KUS 59), and are recommended for a more complete treatment of the subject.

The apparatus described in this thesis utilizes the "flop-in" method first used by Zacharias (ZAC 42), which has proved very successful in the study of radioactive isotopes. The basic principle of the experimental method is as follows. An atom emerges from a small hole in a heated container and finds itself in a highly evacuated space. It travels in a straight line until it hits an obstacle such as a wall or other atom, or until some force is exerted on it. It is essentially alone in space and does not interact with other atoms in the effused beam. By means of defining slits the atom is directed to pass between the pole faces of an electromagnet whose field is inhomogeneous and pointed horizontally. If the atom possesses a magnetic moment, it is deflected slightly and then passes through the field of another electromagnet whose field is also inhomogeneous and pointed in the same direction. If the atom's magnetic moment has not changed the atom is further deflected and misses a detector placed at the position of the undeflected beam. If the magnetic moment has somehow changed its sign in the region between the two magnets, its deflection in the second magnet is opposite in direction to its deflection in the first and cancels, so that the atom strikes the detector.

A uniform magnetic field is placed between the two deflecting fields and when an oscillating radio-frequency magnetic field is superimposed on it, transitions between magnetic substates of the atom can occur when the oscillator frequency equals the Bohr frequency, i. e., the energy difference between two states divided by h, Planck's constant. If the initial and final states of the transition are such that the atomic moment has changed sign, the effect can be detected.

Observation of the detector reading as the oscillator frequency is varied allows the radio-frequency spectrum of the atom to be traced out; from the frequencies and structure of the spectral components, the magnetic-interaction constants can be determined.

Since the effect of the distributed magnetic moment of a nucleus cannot be compared experimentally to the idealized point magnetic moment (which is easier to treat theoretically), it is necessary to compare ratios of the hyperfine interaction in two isotopes of the same element. The deviation of this ratio from the ratio of the nuclear moments expected from a point dipole theory is a measure of the difference of the distribution of magnetism and is called the hyperfine-structure (hfs) anomaly of the two isotopes.

An apparatus has been constructed in the Atomic Beam Laboratory at the University of California by Dr. Gilbert O. Brink, Jhan M. Khan, and the author to make precision measurements of the hfs anomaly in radioactive alkali isotopes. Extensive work on atomic beams of radioactive substances has been under way in this group for several years (NIE 57, HUB 59, SHU 57), and this apparatus represents a refinement of the existing machines, techniques, and instrumentation.

The second section of this thesis develops the theory of the hyperfine interaction and the details of the resonance techniques, together with the theory from which the interaction constants can be obtained. Present ideas on the structure of the nucleus are mentioned in Section III, as also is the existing theory of the hfs anomaly. Section IV deals with details of the design and construction of the apparatus. The fifth section includes a description of the operation of the machine, the experimental procedure, and results of studies on stable isotopes which establish the machine characteristics. By comparing results obtained for Rb^{85} with previously published constants for this isotope, the reliability of the device and techniques may be checked. Section VI covers the determination of the Rb^{85} - Rb^{86} hfs anomaly. Section VII attempts to compare this result to predictions of nuclear models.

II. THEORY OF THE EXPERIMENT

A. The Hyperfine Interaction

Pauli (PAU 24) first suggested that the hyperfine structure found in high-resolution optical spectroscopy might be due to the action of a magnetic moment of the nucleus on the motion of the atomic electrons. Since this idea was presented, the effects of nuclear moments have been studied by many different methods. All observations so far are consistent with the following basic assumptions (RAM 53):

a. The nucleus contains a charge +Ze confined to a small region in the center of an atom.

b. A nucleus whose mass number is odd obeys Fermi statistics, while a nucleus whose mass number is even obeys Bose statistics.

c. A nucleus has a spin angular momentum that can be described by a quantum mechanical angular momentum vector $\vec{a}$ (CON 35) given by the relation

$$\vec{a} = \hbar\vec{I},$$

where I is called the nuclear spin. I is half integral if the mass number of the isotope is odd and integral if the mass number is even.

d. The nuclear magnetic dipole moment is related to the spin by the equation

$$\vec{\mu}_I = \gamma_I \hbar\vec{I} = g_I\mu_0\vec{I}, \qquad \text{(II. 1)}$$

where μ_0 is the Bohr magneton, g_I is the nuclear g factor, and γ_I is the nuclear gyromagnetic ratio. Similarly, for the atomic electrons, if $\vec{J}$ is the total electron angular momentum,

$$\vec{\mu}_J = \gamma_J \hbar\vec{J} = g_J\mu_0\vec{J}. \qquad \text{(II. 2)}$$

The magnetic interaction between a nucleus and the surrounding electrons may be regarded as the interaction between nuclear magnetic moment and the magnetic field, due to the electrons, at the position of the nucleus. The set of discrete energy levels arising from the allowed orientations of the nuclear moment and magnetic field gives rise to the hyperfine structure of the atom.

In the approximation that the nucleus can be regarded as a point dipole moment, the interaction can be written

$$\mathcal{H}_m = -\vec{\mu}_I \cdot \vec{H}_J, \qquad \text{(II. 3)}$$

where $\vec{H}_J$ is the magnetic field, due to the electrons, at the position of the nucleus. Since the work described here pertains only to atoms in the $^2S_{1/2}$ electronic state, all interactions other than the magnetic dipole one are zero. The spherical symmetry of the $^2S_{1/2}$ configuration precludes the existence of an electric field gradient or higher-order gradients at the nuclear position and, although the nucleus may possess multipole moments of higher order, no interaction can result that will modify the Hamiltonian $\mathcal{H}$ in Eq. (II. 3).

Since the magnetic field $\vec{H}_J$ is proportional to $\vec{J}$ for the matrix elements diagonal in J, and since μ_I is proportional to I by Eq. (II. 1), the interaction becomes

$$\mathcal{H}_m = ha\vec{I} \cdot \vec{J}, \qquad \text{(II. 4)}$$

where a contains all the constants and is known as the hfs splitting factor:

$$ha = -\left(\frac{\mu_I}{I}\right) \frac{\vec{H}_J \cdot \vec{J}}{\vec{J} \cdot \vec{J}} . \qquad \text{(II. 5)}$$

Assuming the nucleus to be a point charge, Fermi (FER 30) calculated the field $\vec{H}_J$ at the nucleus for hydrogenlike atoms to be

$$\vec{H}_J = \frac{8\pi}{3} g_J \mu_0 |\psi(0)|^2 \vec{J}, \qquad \text{(II. 6)}$$

where $|\psi(0)|^2$ is the expectation value of the electron wave function evaluated at the nucleus.

From Eqs. (II. 5) and (II. 6), the hfs splitting factor becomes

$$ha = -\frac{8\pi}{3} g_I g_J \mu_0^2 |\psi(0)|^2. \qquad \text{(II. 7)}$$

If the ratio of the splitting factor is taken for two isotopes of the same element, the electronic factors cancel and the Fermi-Segrè equation is obtained,

$$\frac{a_1}{a_2} = \frac{g_{I_1}}{g_{I_2}} . \qquad \text{(II. 8)}$$

The total angular momentum, $\vec{F}$, of an atom is given by

$$\vec{F} = \vec{I} + \vec{J}. \qquad \text{(II. 9)}$$

The angular momentum state of an atom may be expressed for this case by designating the value as F and the component of $\vec{F}$ as m_F, along the field direction. For the state of a given F and m_F, the interaction energy is obtained by taking the diagonal matrix element of the interaction Hamiltonian,

$$W_m^F = \langle IJFm_F | \mathcal{H}_m | IJFm_F \rangle = ha \langle IJFm_F | \vec{I} \cdot \vec{J} | IJFm_F \rangle$$

$$= \frac{ha}{2} [F(F+1) - I(I+1) - J(J+1)]. \qquad \text{(II. 10)}$$

F takes on the values $I + J$, $I + J - 1$, ..., $|I - J|$. The energy difference between a state F and a state $F - 1$ is, according to II. 10:

$$\Delta W^F = W_m^F - W_m^{F-1} = \frac{ha}{2} [F(F+1) - (F-1)F] = haF. \qquad \text{(II. 11)}$$

This relation is known as the interval rule of hyperfine structure. For $^2S_{1/2}$ electronic states, where $J = 1/2$, F can take on only the values $I + 1/2$ and $I - 1/2$. The separation of these two levels is

$$\Delta W = h\Delta\nu = \frac{ha}{2} (2I + 1) \qquad \text{(II. 12)}$$

The quantity $\Delta\nu$ defined in this way is called the hyperfine-structure separation, and is usually expressed in megacycles per second. For alkali atoms, $\Delta\nu$ is of the order of 100 to 10,000 megacycles.

B. The Atom in an External Magnetic Field

When an external magnetic field $\vec{H}_0$ is introduced, there are additional interactions due to the coupling of both the nuclear and electronic moments to the external field. The Hamiltonian can be written

$$\mathcal{H} = a\vec{I}\cdot\vec{J} - \vec{\mu}_I\cdot\vec{H}_0 - \vec{\mu}_J\cdot\vec{H}_0$$

$$= a\vec{I}\cdot\vec{J} - g_I\mu_0\vec{I}\cdot\vec{H}_0 - g_J\mu_0\vec{J}\cdot\vec{H}_0. \qquad \text{(II. 13)}$$

The F, m_F representation is valid, and for small values of H_0 the off-diagonal matrix elements may be neglected. Then

$$W(F, m_F) = \left\langle Fm_F|\mathcal{H}|Fm_F\right\rangle = \frac{ha}{2}\,[F(F+1) - I(I+1) - J(J+1)]$$

$$- g_J[F(F+1) + J(J+1) - I(I+1)]\,\frac{\mu_0 H_0}{2F(F+1)}\,m_F$$

$$- g_I[F(F+1) + I(I+1) - J(J+1)]\,\frac{\mu_0 H_0}{2F(F+1)}\,m_F. \qquad \text{(II. 14)}$$

The splitting of the magnetic sublevels of a state F is then

$$\left\langle Fm_F|g_J\mu_0\vec{J}\cdot\vec{H}_0 + g_I\mu_0\vec{I}\cdot\vec{H}_0|Fm_F\right\rangle = g_F\mu_0 H_0 m_F, \qquad \text{(II. 15)}$$

where

$$g_F = g_J\,\frac{F(F+1)+J(J+1)-I(I+1)}{2F(F+1)} + g_I\,\frac{F(F+1)+I(I+1)-J(J+1)}{2F(F+1)}. \qquad \text{(II. 16)}$$

Since $g_J \approx 10^3 g_I$, the second term of Eq. (II. 16) is negligible and the state W^F breaks up into $2F+1$ equally spaced energy levels in weak field with a separation

$$\frac{W_m - W_{m-1}}{h} = \frac{2\mu_0 H_0}{(2I+1)h} \simeq \frac{2.8\ H}{2I+1}\ \text{Mc.} \qquad \text{(II. 17)}$$

Transitions between these energy levels and the energy levels of the state $F \pm 1$ give rise to the Zeeman spectrum of the hyperfine-structure interaction.

In the limit where I and J are completely decoupled because of the much stronger interaction of each with the external magnetic field, F is no longer a good quantum number and the energy can be written in a representation of quantum numbers m_I and m_J, which represent the component of I and J, respectively, along the field direction. In this case the energy of a state $|m_I m_J\rangle$ is

$$W(m_I m_J) = \langle m_I m_J | \mathcal{H} | m_I m_J \rangle = h a m_I m_J - g_J \mu_0 m_J H_0 - g_I \mu_0 m_I H_0$$

(II. 18)

When I and J are decoupled the atom is spoken of as being in the Paschen-Back region. There are two sets of (2I+1) equally spaced levels of separation $\Delta\nu/(2I+1)$.

In the intermediate region the situation is more complicated as the coupling of I and J is of the same order of magnitude as the coupling of J to H_0. For the important case of $J = 1/2$, an analytic expression for the energy can be obtained by using either representation (BRE 31, RAM 56). The solution, known as the Breit-Rabi equation, can be written

$$W(F, m_F) = -\frac{h\Delta\nu}{2(2I+1)} - g_I \mu_0 H_0 m_F \pm \frac{h\Delta\nu}{2}\left[1 + \frac{4m_F}{2I+1}\, x + x^2\right]^{1/2}$$

(II. 19a)

when $\Delta\nu$ is the hfs separation defined in Eq. (II. 12) and the dimensionless parameter x is given by

$$x = (g_I - g_J)\ \frac{\mu_0 H_0}{h\Delta\nu} \qquad \text{(II. 19b)}$$

The positive sign before the square root in Eq. (II. 19a) refers to the state $F = I + 1/2$ and the negative sign to the state $F = I - 1/2$.

If the energy in units of $h\Delta\nu$ is plotted for all states of the atomic-nuclear system as a function of x, the resulting graph is called a Breit-Rabi diagram. An example is shown in Fig. 1 for the case $I = 2$ and $g_I < 0$. The effect of a positive nuclear moment is to rotate the diagram 180 deg about the abscissa. For the state $F = I + 1/2$, $\vec{\mu}_I$ and $\vec{H}_J$ are antiparallel for $g_I > 0$ so that the state has greater energy than the state $F = I - 1/2$. For $g_I < 0$, the situation is reversed. These diagrams show the general behavior of the various energy levels as a function of magnetic field and are very useful in illustrating the observable transitions in an atomic beam apparatus.

Only energy differences between levels are observable and it is easy to write the transition frequency between any two levels by use of Eq. (II. 19a). The transition ν_{12} between levels 1 and 2 is

$$\nu_{12} = -\frac{g_I \mu_0 H_0}{h}(m_1 - m_2) + \frac{\Delta\nu}{2}\left\{(\pm)_1\left[1 + \frac{4m_1}{2I+1}x + x^2\right]^{1/2} - (\pm)_2\left[1 + \frac{4m_2}{2I+1}x + x^2\right]^{1/2}\right\}, \qquad \text{(II. 20)}$$

where $(\pm)_1 = (\pm)_2$ if m_1 and m_2 belong to the same F, and $(\pm)_1 = -(\pm)_2$ if m_1 and m_2 belong to different F.

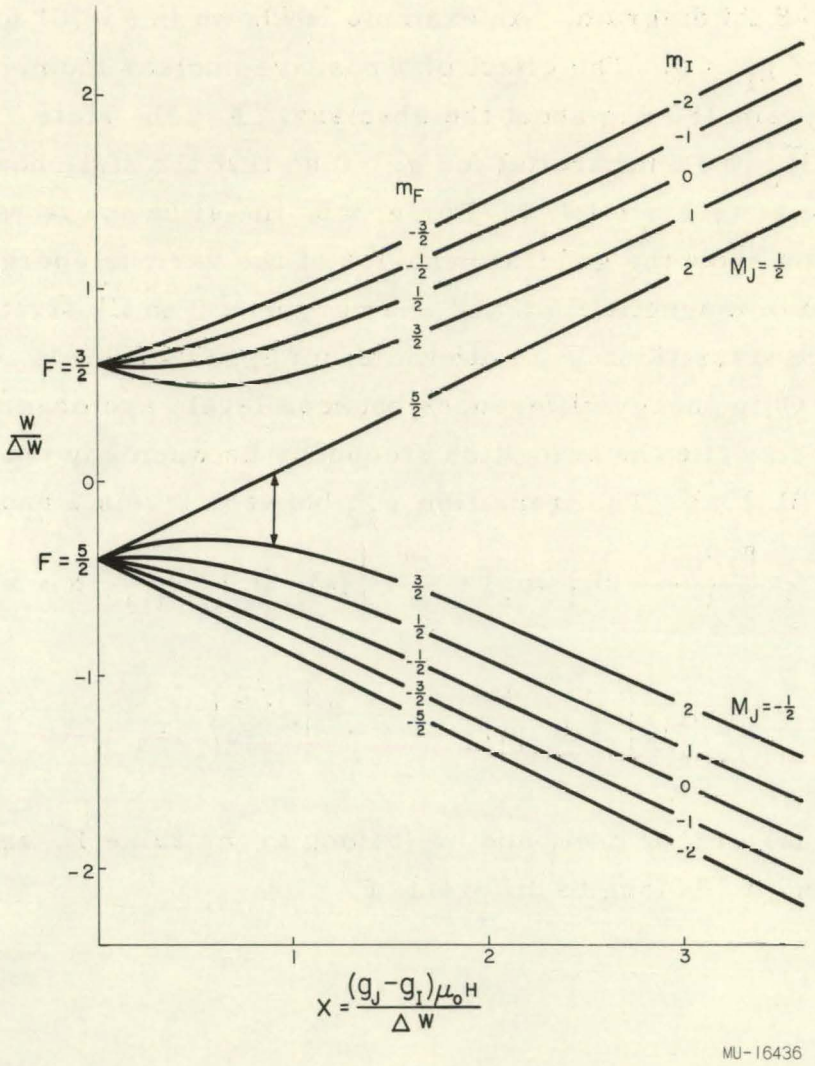

Fig. 1. Breit-Rabi diagram. I = 2, J = 1/2, g_I negative.

C. The "Flop-In" Technique and Observable Transitions

An atom possessing a magnetic moment $\vec{\mu}$ experiences a force in an inhomogeneous magnetic field H given by

$$\vec{F} = - \nabla W = - \frac{\partial W}{\partial H} \nabla H = \mu_{eff} \nabla H, \qquad \text{(II. 21)}$$

where μ_{eff} is the component of $\vec{\mu}$ along H. The value of μ_{eff} may be obtained by differentiation of the Breit-Rabi equation (Eq. (II. 19a)) with respect to H, or if H is large and the $m_I m_J$ representation is valid, Eq. (II. 18) gives

$$\mu_{eff} = g_J \mu_0 m_J + g_I \mu_0 m_I.$$

For $J = 1/2$ $|\mu_{eff}|$ has the value μ_0 since g_I is much smaller than g_J. Since the effective moment is the negative slope of curves drawn on a Breit-Rabi diagram, reference to Fig. 1 shows the variation of effective moment with magnetic field. For $x > 2$ all states have essentially the same slope with a value $\pm \mu_0$. No matter what magnetic substate an atom may be in, a large magnetic field sees it as a moment of one Bohr magneton, pointing either parallel or antiparallel to the field. This property can be used to describe the operation of the apparatus, schematically shown in Fig. 2. If the A and B magnets have their gradients pointing in the same direction the force experienced by a magnetic moment oriented similarly in these two fields must be in the same direction in both fields. If an atom starts from the oven in a given state and receives a deflection in the A magnet, it receives a further deflection in the B magnet assuming that the state of the atom has been maintained between the two fields. This atom is deflected away from the detector (path 1). If, however, the state of the atom is changed in the region between the A and B fields so that its effective moment has changed sign in the high-field region, the atom is re-focused around the stop wire S (path 2) and strike the detector placed at the focus of the machine. This is called the "flop-in" method. It is also possible to reverse one of the inhomogeneous magnets; then all atoms are refocused except those which have undergone a suitable change of magnetic substate. This is called the "flop-out" method.

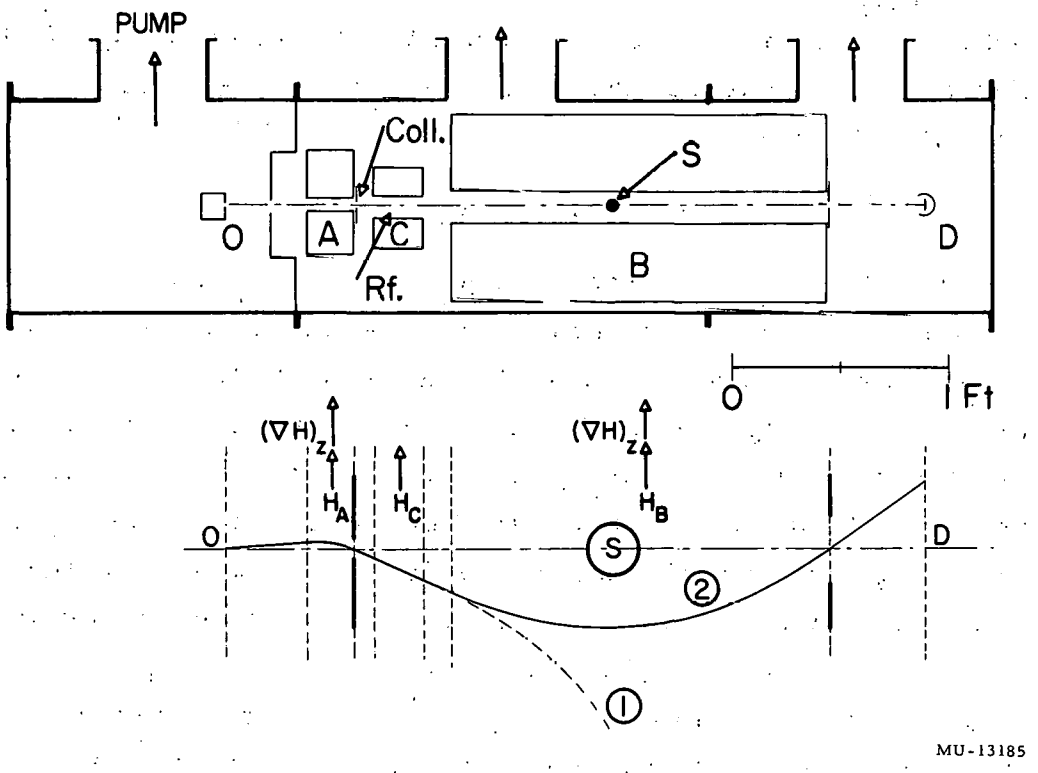

Fig. 2. Schematic diagram of an atomic-beam apparatus, showing arrangement of fields for flop-in operation.

The means used to change the state of an atom is to introduce a suitable perturbation as the atom passes through the homogeneous C magnet (Fig. 2). The experiment consists of setting the A, B, and C magnets to desired fields and monitoring a detector placed at the focus while the radio frequency is changed. When the rf energy $h\nu$ is equal to the energy difference between two states that satisfy the refocusing condition above, atoms are deflected into the detector and an increase in the detector reading is noted.

Transitions between different hfs levels are induced by an oscillating magnetic field $\vec{H}_1 \cos \omega t$ superimposed on a static magnetic field $\vec{H}_0$ (the C field). The oscillating field contributes to the Hamiltonian, Eq. (II. 13) a time-dependent term

$$V = \mu_0 g_J \vec{J} \cdot \vec{H}_1 \cos \omega t + \mu_0 g_I \vec{I} \cdot \vec{H}_1 \cos \omega t.$$

The matrix elements of this perturbation in the F, m_F representation determine the selection rules (KUS 59):

$\Delta F = 0, \pm 1, \quad \Delta m_F = 0,$ (σ transitions) for the z component of H_1;

$\Delta F = 0, \pm 1, \quad \Delta m_F = \pm 1,$ (π transitions) for the x and y components of H_1,

where the z coordinate is defined as the direction of $\vec{H}_0$. For strong fields the selection rules are

$\Delta m_J = 0, \quad \Delta m_I = 0,$ for z component of H_1,

$\Delta m_J = 0, \pm 1, \quad \Delta m_I = 0, \pm 1,$ for x and y components of H_1.

The restriction imposed by the refocusing condition requires that the initial and final states have equal and opposite signs of effective moment in the Paschen-Back region where the deflecting magnets operate. Reference to the Breit-Rabi diagram (Fig. 1) shows that when H_0 is small there is only one transition that satisfies the selection rule $\Delta F = 0$ which simultaneously satisfies the refocusing condition, namely the transition $F = I + 1/2, m_F = -I - 1/2 \leftrightarrow m_F = -I + 1/2$ whose frequency is, by Eq. (II. 17),

$$\nu \cong \frac{2.8\, H_0}{2I+1} \text{ Mc.} \qquad \text{(II. 22)}$$

All other observable transitions are of the order of $\Delta\nu$, which is a much higher frequency.

The collimator (Fig. 2) serves to define the beam dimensions and the stop wire S is placed on the axis of the beam to intercept the very fast atoms in the tail of the Maxwellian velocity distribution which would not be deflected far enough away from the detector and would contribute an undesirable background.

In the absence of a perturbing rf field, it is possible for atoms to undergo transitions when they pass through weak fields whose direction varies rapidly in space, such as may be possible in the intermagnet regions. These are called Majorana transitions (MAJ 32). Furthermore, when the field H_0 in the C magnet is zero, the atoms passing through the region no longer have a preferred sense of orientation and some have randomly reoriented during their passage into a refocusable state. This type of Majorana transition sets a lower limit on the value of H_0 at which useful experiments can be done without increased and erratic background due to these transitions. This problem is not encountered with the flop-out method, but since a typical resonance is about 2% of the full beam intensity it is obvious that the flop-in method is more suitable for radioactive detection, since it is easier and more reliable to see a change in a small background rather than in a large one.

If the A and B magnets are on and no oscillatory field is applied, all atoms either are deflected or impinge on some obstacle. If the detector is moved horizontally in a plane normal to the beam a pattern symmetrical about the undeflected position is seen, having a single well-defined peak (for $J = 1/2$). If the width of the undeflected beam is much smaller than the deflection S_m of the peak, it can be shown (RAM 56) that

$$S_m \cong \frac{1}{3} S_a ,$$

where S_a is the deflection of an atom with the most probable velocity, $a = \sqrt{\frac{2kT}{m}}$, in the oven. For a symmetrical apparatus where the A

and B fields are identical and operated at a field H,

$$S_a = K \frac{H}{kT} ,$$

where K is a numerical constant taking into account the geometry of the apparatus and the properties of the inhomogeneous magnets. The intensity of the deflected beam at that position can be shown to be a function only of S_a and the total rate of effusion from the oven. For small changes in oven temperature and deflecting fields (as during a run), the beam intensity at the deflected peak is a function only of the total rate of effusion of the oven and serves as a convenient means of monitoring the change in total beam intensity during an experiment.

D. Calculation of $\Delta\nu$

It is assumed that a "hairpin" such as is described in Section IV is in position which can excite π transitions by providing an oscillatory magnetic field perpendicular to the static C field, H_0. If two isotopes (1 and 2) are present in a beam and the spin of one is known, observation of the $\Delta F = 0$ refocusable transition of each one in the same field H_0 having the value of a few gauss gives, by Eq. (II. 22),

$$\nu_1 = \frac{2I_2 + 1}{2I_1 + 1} \nu_2, \qquad \text{(II. 23)}$$

and the spin of the other is easily found. Since a beam of radioactive isotopes for practical reasons must be formed together with a beam of stable isotopes, it is not usually difficult to perform this measurement.

After the spin of an isotope is known, this $\Delta F = 0$ transition is followed as H_0 is increased so that the quadratic dependence of the transition frequency on the field is observed. By expansion of Eq. (II. 20), neglecting the small g_I term, we obtain

$$\nu \cong \frac{2.8\ H_0}{2I + 1} + \left[\frac{2.8\ H_0}{2I + 1}\right]^2 \frac{2I}{\Delta\nu} \text{ Mc.} \qquad \text{(II. 24)}$$

These measurements confirm the spin assignment and place a lower limit on $\Delta\nu$. At higher values of H_0, in the region of intermediate coupling, Eq. (II. 20) can be solved exactly to yield

$$\Delta\nu = \frac{\left(\nu + \frac{g_I \mu_0 H_0}{h}\right)\left(-\frac{g_J \mu_0 H_0}{h} - \nu\right)}{\left[\nu + \frac{g_J \mu_0 H_0}{(2I+1)h} + \frac{2I}{2I+1}\frac{g_I \mu_0 H_0}{h}\right]} \quad . \qquad \text{(II. 25)}$$

All the quantities on the right side of Eq. (II. 25) are known or observable except g_I. Its numerical value can be found to within a few percent by the Fermi-Segrè formula, Eq. (II. 8), or its equivalent,

$$\frac{\Delta\nu_1}{|g_{I_1}|(2I_1+1)} = \frac{\Delta\nu_2}{|g_{I_2}|(2I_2+1)} \quad . \qquad \text{(II. 26)}$$

Two different values of $\Delta\nu$ are obtained by using Eqs. (II. 25) and (II. 26), first assuming a positive g_I and then a negative one. Observations are made at several values of H_0 and the $\Delta\nu$'s associated with one sign or the other shows a consistency. This consistency establishes the sign of g_I and as H_0 is increased the uncertainty in $\Delta\nu$ is reduced.

When the uncertainty in $\Delta\nu$ has been reduced to a few megacycles it is possible to move H_0 back to the Zeeman region ($x \ll 1$) and search for $\Delta F = \pm 1$ transitions whose frequencies are of the order of $\Delta\nu$. The spectrum consists of $2I$ π lines with a unit separation of $2\left(\frac{2.8\ H_0}{2I+1}\right)$ Mc. The lower $2I-1$ lines are unresolved doublets centered on $\Delta\nu$ and the highest line is a singlet. When I is integral, the central doublet is very close to $\Delta\nu$, having only a second-order field correction of a few kilocycles. Observation of this field-independent line enables $\Delta\nu$ to be determined very accurately, limited only by the width of the resonance and the quality of the radio-frequency gear.

Details of these calculations for the isotopes of interest are given in Appendix B. If I is half integral, the field-independent line near $\Delta\nu$ is a σ transition and cannot be observed unless a hairpin is available in which H_1 is parallel to H_0. Such hairpins usually do not give as narrow resonance lines as those exciting π transitions, as is explained in Section IV E.

In the early days of atomic beam work before World War II, when microwave oscillators were not available, the direct observation of these weak-field $\Delta F = \pm 1$ transitions was not possible. It was sometimes possible to observe at very high fields the almost field-independent $\Delta m_J = 0, \Delta m_I = \pm 1$ doublet for which the mean frequency is equal to $\Delta\nu/(2I+1)$ (KUS 40). In order to observe these transitions, however, the refocusing condition must be changed since the sign of the atomic moment in strong fields does not differ in the two states. However, if fields in the A and B magnets are reduced to a value corresponding to $x \approx 0.3$, these states have slopes of opposite sign (see Fig. 1) but the effective atomic moment is very small. Long deflecting magnets with large field gradients such as are used in molecular-beam experiments can be used under these conditions to observe the $\Delta m_J = 0$ transitions. By suitable placement of the magnitude of the deflecting fields, any transiton allowed by the selection rules can be observed with such an apparatus. Unfortunately, in order to use these deflecting magnets, the width of the beam must be reduced, since the gap in the inhomogeneous pole faces must be smaller. The narrow beam, together with the necessary increase in total length of the apparatus, makes this technique unsuitable for detection of radioactive isotopes by counting of the deposited activity as is done here, since exposure times would have to be prohibitively long in order to get usable counting rates. If such an apparatus is available, there are $\Delta F = 0$ transitions that go through a maximum value in intermediate fields (RAM 56) from which $\Delta\nu$ can be accurately determined.

E. Calculation of g_I

In order to obtain an experimental value of the hfs anomaly, an independent measurement of g_I must be made. With stable isotopes it is usually possible to measure the moment ratio of two isotopes by standard nuclear magnetic resonance methods (LAU 58) to very high precision. There are usually far too few radioactive atoms available in a sample to give a detectable signal, so the atomic beam resonance method must be used for radioactive isotopes.

Because of the presence of the term involving g_I in Eq. (II. 18) all the $\Delta m_J = 0$ $\Delta m_I = \pm 1$ lines mentioned in the preceding section are actually doublets with a separation

$$\nu^+ - \nu^- = 2g_I \frac{\mu_0 H_0}{h}, \qquad \text{(II. 27)}$$

where ν^+ and ν^- are the upper and lower components, respectively. If the resolution of the apparatus is high enough, g_I can be determined to about one part in ten thousand if the transitions are observed in high fields. The doublet of particular interest for measuring g_I is

$$F^+ = I + 1/2, \quad (\pm)m = -F^+ + 2 \leftrightarrow (\pm)m = -F^+ + 1,$$
$$F^- = I - 1/2, \quad (\pm)m = -F^- \leftrightarrow (\pm)m = -F^- + 1,$$

where the positive sign of m is for a positive g_I, and the negative sign of m is used for a negative g_I. Note that these are $\Delta F = 0$, $\Delta m = \pm 1$ transitions and are not ordinarily refocusable except for machines capable of handling small moments as described above. If a detector of high sensitivity is available, such as a mass spectrometer following an ionizer, the moments of radioactive isotopes can be determined with machines of low transmission (EIS 52, STR 57).

Fortunately, the $\Delta F = \pm 1$ doublet involving the four levels $\mp F^+ \pm 2 \leftrightarrow \mp F^-$ and $\mp F^+ \pm 1 \leftrightarrow \mp F^- \pm 1$ is refocusable in the sense of Section II. C, where the upper signs are used for positive g_I, the lower signs for negative g_I. The separation of this doublet is also $2g_I \frac{\mu_0 H_0}{h}$. These transitions also go through a field-independent

point, but it is not as broad and occurs at not as high a field as the $\Delta F = 0$ doublet above. The frequencies involved are of the order of $\Delta\nu$ and the experimenter is forced into the undesirable situation of taking the difference of two large numbers. If very narrow resonance lines can be obtained, it is possible to measure g_I to one part in a thousand or a little better and to obtain a usable experimental value of the hfs anomaly, if it is not too small. This method has recently been employed at Heidelberg University to measure the moment of stable Au^{197} (FRI 59).

The position of the minimum of the mean value of this doublet on a Breit-Rabi diagram is a function only of the spin I. Its value at this point is a function only of $\Delta\nu$. It is possible to obtain a value of $\Delta\nu$ from this doublet, often more accurately than can be done in weak fields as described in the previous section, especially for isotopes of half-integral spin where the field-independent transition is a σ transition. Details of the calculations involving this measurement for Rb^{85} and Rb^{86} are included in Appendix B.

When an external field H is applied to an atom, the electrons acquire an induced diamagnetic current which produces a field $-\sigma H$ at the nuclear position, where σ is called the shielding constant. This induced field partially cancels the applied field, and--since it is proportional to the applied field--it cannot be eliminated experimentally. This has the effect of making the nuclear moment smaller than it really is and must be calculated theoretically (LAM 41) when the true magnitude of the nuclear moment is to be inferred. Since the correction is a function of Z, it is the same for two isotopes of the same element and is usually neglected in the determination of hfs anomalies, since a ratio of moments is desired. All values of nuclear moments used or calculated in this work are uncorrected for this effect. Tables of the diamagnetic correction are available (KOP 58) if corrected values are desired.

F. Calculation of the Hyperfine-Structure Anomaly

Since the observed splitting factor a for an isotope differs from the Fermi value (Eq. (II. 7)) by a small factor $1 + \epsilon$ (see Section III. B), the Fermi-Segrè formula, Eq. (II. 26), may be written

$$\frac{\Delta\nu_1}{\Delta\nu_2} = \frac{g_{I_1}}{g_{I_2}} \left(\frac{2I_1 + 1}{2I_2 + 1} \right) (1 + \Delta), \qquad \text{(II. 28)}$$

where $\Delta = \epsilon_1 = \epsilon_2$, neglecting higher-order terms. Solving for the hfs anomaly Δ,

$$\Delta = \left[\frac{\Delta\nu_1}{\Delta\nu_2} \left(\frac{2I_2 + 1}{2I_1 + 1} \right) \frac{g_{I2}}{g_{I_1}} \right] - 1. \qquad \text{(II. 29)}$$

By convention (SCH 57, EIS 58), isotope 1 is the lighter of the two. The anomaly is usually less than 0.5%.

III. NUCLEAR STRUCTURE AND THE THEORY OF THE HYPERFINE-STRUCTURE ANOMALY

A. Nuclear Models

At present it is impossible to treat the interactions between many bodies with any degree of rigor, and the nucleus is indeed a very complex structure of many particles. It is necessary to postulate relatively simple models of the nucleus from semiclassical and simple quantum-mechanical considerations and see to what extent these models can account for the experimental data. Various models have been extensively discussed in the literature (MAY 55, BOH 53, NOY 58, BLI 57), and only a brief outline is given here.

Models are usually classified according to the emphasis on effects of single-nucleon states or on collective effects of many nucleons. In postulating the shell model, Mayer (MAY 55) made the assumption that the internucleon interaction was such that an even number of like nucleons in a given angular-momentum level coupled to spin zero, while an odd number coupled to spin j of that level. This model assumes that the interaction is one of an odd particle moving in a potential well due to the other particles in the nucleus. The effective magnetic properties of the nucleus are essentially those of the odd single particle. This model has had considerable success in predicting spins, but cannot be expected to predict nuclear moments very well.

For nuclei in the region of closed angular-momentum shells it is expected that the equilibrium shape of the nucleus is approximately spherical and that nucleons move in an essentially spherical potential well. In regions far removed from closed shells, the nucleus may favor some nonspherical shape, and there may be collective oscillations about this equilibrium shape that modify the effective nuclear field and couple to the motions of the odd nucleons, thus modifying the magnetic properties of the nucleus as a whole. This collective or asymmetric-core model (BOH 53) has been somewhat successful in predicting quadrupole moments (since nonspherical shapes are postulated) and in understanding low-energy nuclear spectra. Spin predictions are

usually not very different from those of the single-particle shell model, and predictions of nuclear moments have not been too successful. For more details the review article of Bohr and Mottelson (BOH 53) and the recent work of Nilsson (NIL 55, MOT 55) are recommended.

Residual internucleon forces may lead to a mixing of single-particle states with other configurations that have the same parity and angular momentum as the original one. Since the magnetic moment is an expectation value and not a quantum number, it is very sensitive to these possible admixtures. Blin-Stoyle (BLI 53) and Arima and Horie (ARI 54, NOY 58), using this model, have been able to account fairly well for the observed nuclear moments in isotopes of odd mass number. Recently the model has been extended to odd proton-odd neutron nuclei (CAI 56, NOY 58), but the agreement with observations is less satisfactory.

B. The Bohr-Weisskopf Theory

Since the derivation of the Fermi-Segrè formula involved the assumption that the nucleus is a point charge, the observed deviation from this relation is a measure of the volume distribution of the magnetic moment. This was first pointed out by Bitter (BIT 49) when accurate measurements of $\Delta\nu$ and moment ratios for Rb^{85} and Rb^{87} indicated an anomaly of 0.35%.

For nuclei heavy enough that the protons may be treated as a continuous charge distribution, Bohr and Weisskopf (BOH 50) have developed a quantitative theory to explain the effects of the volume distribution of magnetism on hyperfine structure. This theory has been extended by Bohr (BOH 51a, 51b), Eisinger and Jaccarino (EIS 58) and Stroke (STR 59).

Two kinds of magnetism are considered--spin magnetism and orbital magnetism. The former is caused by the distribution of particles throughout the nucleus, each of which possesses an intrinsic spin angular momentum and magnetic moment; the latter is due to circulating currents in the nucleus caused by the movement of charged

particles. The orbital part contributes less to the correction of the point dipole picture, since the effective dipole distribution of a current loop has a maximum at the center of the loop. The Bohr-Weisskopf effect is important only for electronic s states in which the density of the electronic wave function at the nuclei is large. It is very small for pure $p_{1/2}$ states and negligible for states of higher J.

The fractional reduction of the hyperfine-structure separation for a given isotope is

$$\epsilon = -(\bar{K}_s a_s + \bar{K}_\ell a_\ell), \tag{III. 1}$$

where a_s and a_ℓ are the respective fractions of the nuclear magnetism that are due to spin and orbital angular momentum, and $\bar{K}_s$ and $\bar{K}_\ell$ are the averages of K_s and K_ℓ over the nuclear radial coordinate, where

$$K_s \equiv \int_0^R \left[1 + \zeta \frac{r}{R}\right]^3 FG\, dr \Big/ \int_0^\infty FG\, dr,$$

$$K_\ell \equiv \int_0^R \left[1 - \frac{r}{R}\right]^3 FG\, dr \Big/ \int_0^\infty FG\, dr.$$

F and G are the Dirac radial wave functions for an electron, R is the nuclear radial coordinate, and ζ takes into account the angular asymmetry of the spin distribution. It depends on the particular model and has been calculated by Bohr (BOH 51b). In particular, for the single-particle model Bohr finds:

$$\zeta = \frac{2I - 1}{4(I + 1)} \quad \text{for } I = \ell + \frac{1}{2},$$

$$\zeta = \frac{2I + 3}{4I} \quad \text{for } I = \ell - \frac{1}{2}. \tag{III. 2}$$

The integrals above may be evaluated by writing F and G as a power series in (r/R) inside a uniformly charged sphere of radius R_0 and matching these functions at the nuclear radius with the standard solutions for an unscreened Coulomb potential (ROS 32). In their original paper Bohr and Weisskopf included only terms in the expansion to $(R/R_0)^2$, approximating the contributions of higher-order terms. The results of their calculations are

$$\bar{K}_s = (1 + 0.38\,\zeta)\, b\overline{\left(\frac{R}{R_0}\right)^2}\,,$$

$$K_\ell = 0.62\, b\overline{\left(\frac{R}{R_0}\right)^2}, \qquad \text{(III. 3)}$$

so that

$$\epsilon = -(1 + 0.38\,\zeta)\, a_s + 0.62\, a_\ell\, b\overline{\left(\frac{R}{R_0}\right)^2}, \qquad \text{(III. 4)}$$

where b is a function of R_0 and Z, the nuclear charge; it is tabulated elsewhere (BOH 50). Note that the value $r_0 = 1.5\times10^{-13}$ cm was used in the relation $R_0 = r_0 A^{1/3}$ in this early paper instead of the more recent value of $r_0 = 1.2\times10^{-13}$ cm (FOR 55).

The error introduced by neglecting the higher-order terms in the expansion is stated to be about 2%. Eisinger and Jaccarino (EIS 58) have extended this calculation to include terms in $(R/R_0)^4$, with the results

$$\bar{K}_s = (b_{s2} + b'_{s2})\overline{\left(\frac{R}{R_0}\right)^2} - (b_{s4} + b'_{s4})\overline{\left(\frac{R}{R_0}\right)^4}, \qquad \text{(III. 5)}$$

$$\bar{K}_\ell = b_{\ell 2}\overline{\left(\frac{R}{R_0}\right)^2} - b_{\ell 4}\overline{\left(\frac{R}{R_0}\right)^4},$$

with the constants b as tabulated (EIS 58) for $10 \leq Z \leq 90$.

It is necessary to make some assumptions about the particle distribution in the nucleus in order to evaluate the averages over the nuclear radial coordinate. As a compromise between the value 1 for a surface distribution and 3/5 for a uniform distribution, Bohr and Weisskopf assumed $(R/R_0)^2 = 0.8$, since an unpaired particle might tend to stay closer to the surface. Eisinger and Jaccarino assumed a single-particle model in which the odd nucleon moves in a spherically symmetric square potential well. Their calculations for these averages are presented in forms of graphs which are easily used.

There remains the problem of determining the fractional contributions a_s and a_ℓ. These can be calculated if a particular model is assumed. If the nuclear g factor is defined by the equation

$$g_I \vec{I} = g_s \vec{S} + g_\ell \vec{L}, \tag{III. 6}$$

the fractional contributions are given by

$$a_s = \frac{g_s}{g_I} \frac{g_I - g_\ell}{g_s - g_\ell}, \tag{III. 7}$$

$$a_\ell = 1 - a_s = \frac{g_\ell}{g_I} \frac{g_I - g_s}{g_s - g_\ell}.$$

If the spin and the orbital angular momenta can be expressed in terms of $\vec{S}$ and $\vec{L}$ respectively for the particular model, a_s and a_ℓ are known and ϵ (Eq. III. 4) can be determined.

Because of the uncertainty in normalization of the entire electronic wave function, it is difficult to get an accurate knowledge of the absolute magnitude of the interaction for the point dipole case. Comparing the ratio of the hfs interactions causes this uncertainty to almost vanish. If the isotopes are denoted by the subscripts 1 and 2, where, by convention, 2 is the heavier of the two, the hfs anomaly is defined as

$$\frac{a_1}{a_2} = \frac{g_{I_1}}{g_{I_2}} (1 + \Delta) \tag{III. 8}$$

and

$$\Delta = \frac{a_1}{a_2} \frac{g_{I_2}}{g_{I_1}} - 1; \qquad \text{(III. 9)}$$

Δ then measures the difference in the distribution of magnetism for the two isotopes. Because the asymmetry in the spin magnetization of certain nuclei enhances the spin contribution, and because the constants that weight the spin contributions are larger than the orbital ones, Δ can vary between zero and the same order of magnitude as ϵ.

C. Other Contribution Effects

Since the nucleus is not a point charge, the electrostatic potential in the neighborhood of the nucleus deviates from the pure Coulomb potential. The charge distribution for two isotopes generally is different and affects the ratio of the hfs interactions. This is known as the Breit-Rosenthal effect. Theoretical estimates (ROS 32, CRA 49) indicate that the contribution to Δ is of the order of 0.01%, which is negligible in this work but may in some cases exceed the Bohr-Weisskopf effect (LUR 56, TIN 57). Stroke (STR 59) has recently extended the work of Eisinger and Jaccarino to include the effects of the charge distribution, which enter into the evaluation of the coefficients b in Eq. (III. 5), so that the Breit-Rosenthal effect can be included in the framework of the Bohr-Weisskopf theory.

The reduced-mass correction to the electron wave function is $(1 + m/AM)^{-3}$, which, for two isotopes of different mass, gives an isotope-shift correction to Δ that is important for very light nuclei but negligible for heavier nuclei.

The presence of neighboring fine-structure levels will, in second order, perturb levels of the same F and modify the hfs interaction. This effect on $p_{1/2}$ electrons by the closely lying $p_{3/2}$ level--which has been treated by Clendennin (CLE 54)--affects the ratio of g_I's in the $p_{1/2}$ state. For $s_{1/2}$ states considered in this

work, this effect should be negligible. Since the parity of magnetic dipole radiation is even (EVA 55), the matrix elements between the s state and the closest states of higher J, the p states, vanish. The second-order perturbation effect is of the order of $(\Delta\nu)^2/\delta$, where δ is the fine-structure separation for the s state to the next states of even parity. For rubidium this is of the order 10^{-4} %, and is negligible in the ratio.

IV. THE DESIGN OF THE APPARATUS

An over-all picture of the apparatus is shown in Fig. 3. It consists of a large tank with associated pumps for maintaining a high vacuum through which the beam of atoms may pass (for several feet) without scattering. Inside the tank is a means of producing a beam, the three magnets previously mentioned, and detector for both the stable and radioactive components of the beam. Each system with its auxiliary equipment and instrumentation is described below in some detail.

A. The Geometry of the Apparatus

The vacuum tank and magnets built by Bemski (BEM 53) for molecular-beam experiments were used for this apparatus. New pole faces were built for the deflecting magnets, but the homogeneous C magnet was retained in its original form. The general layout of the machine is shown in Fig. 4.

Using the design equations from the thesis of R. J. Sunderland (SUN 56) we chose the dimensions and parameters for maximum refocusable signal at the detector consistent with the restriction imposed by the use of existing magnets and tank.

Since the A and B magnets are of equal length, it is convenient to make the machine symmetrical about the center of the C magnet, with the A and B fields equal in magnitude. On the basis of Cs^{133} as the design isotope, since minor adjustment allow any alkali to be refocused, the following dimensions were obtained (see Fig. 4), assuming a beam height of 1 cm at the detector:

ℓ_1 = 18.42 cm
ℓ_2 = 44.45 cm
ℓ_3 = 23.18 cm
ℓ_4 = 31.14 cm
ℓ_5 = 22.22 cm
ℓ_6 = 22.22 cm
ℓ_7 = 18.40 cm
ℓ_8 = 25.40 cm
ℓ_9 = 9.2 cm
L_3 = 85.08 cm = 33.89 in.
L_5 = 139.41 cm = 54.90 in.
L_6 = 100.98 cm = 39.75 in.
L = 187.03 cm = 73.65 in.
W_S = .056 in.
W_C = .035 in.
W_D = .075 in.

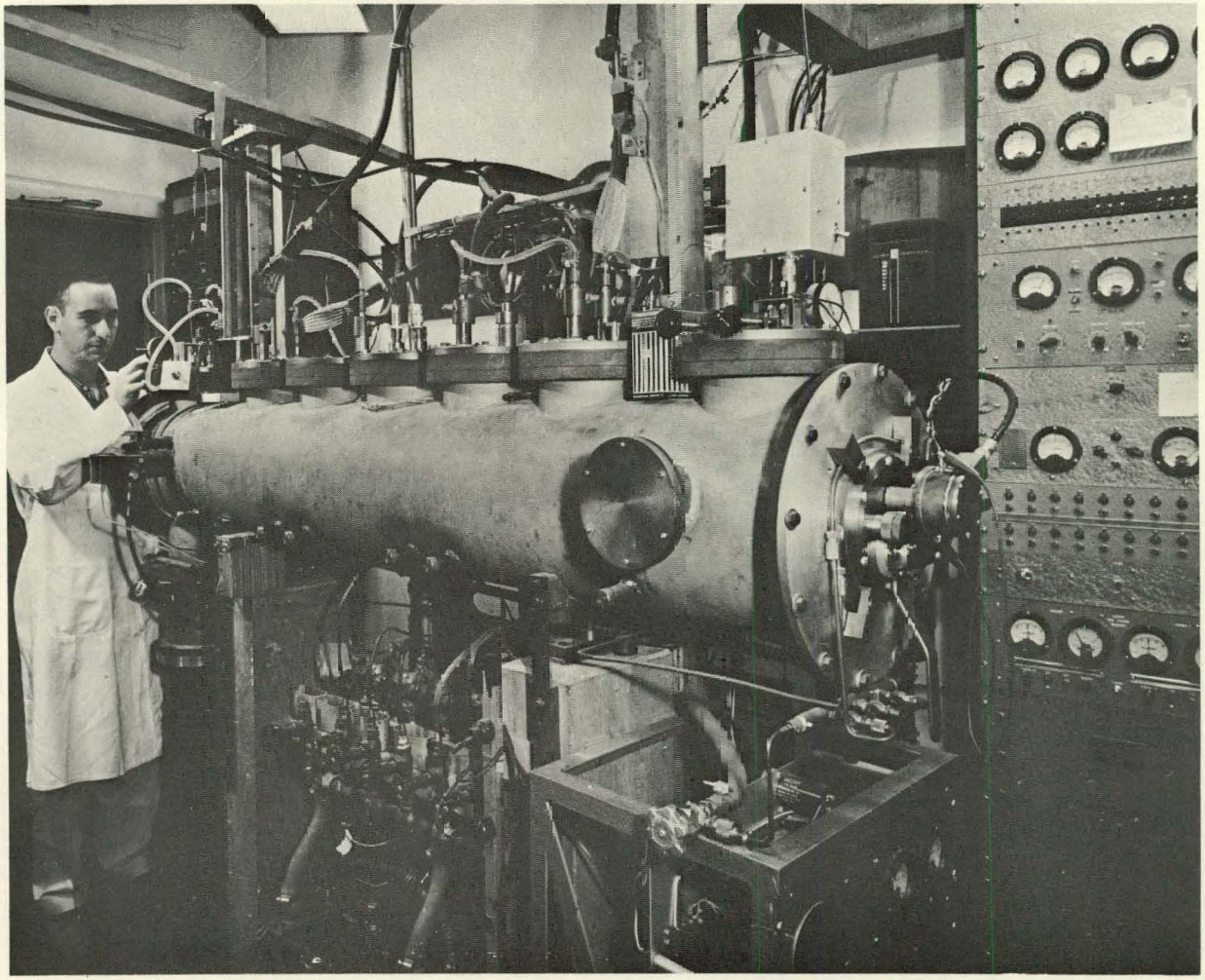

ZN-2055

Fig. 3. Over-all view of the apparatus, from the detector end.

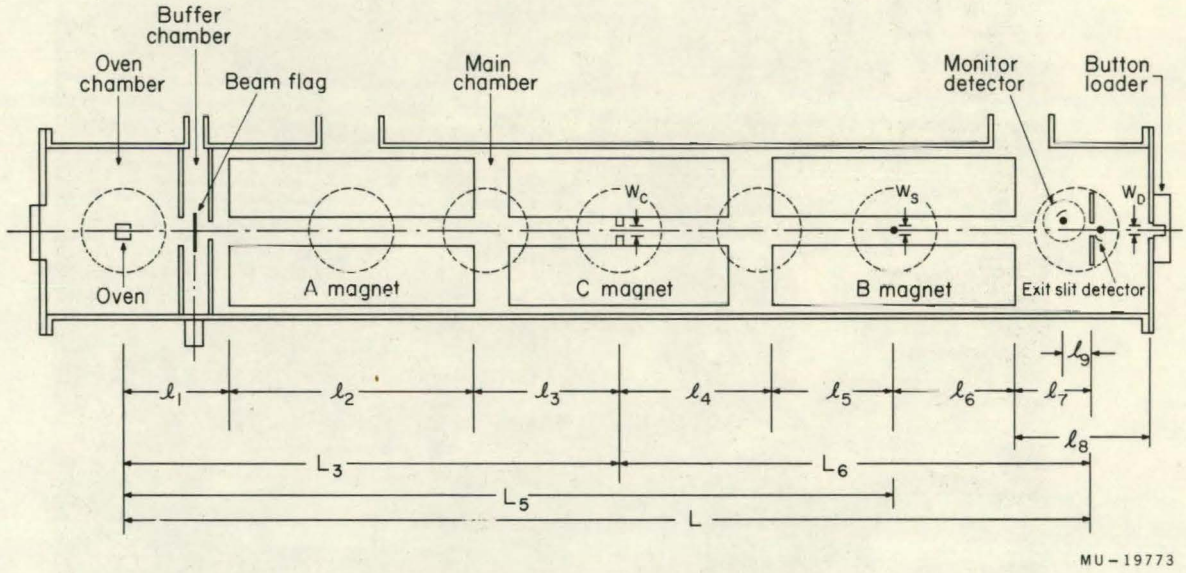

Fig. 4. Layout of the apparatus.

Note that the machine is not exactly symmetrical; ℓ_8 was made a little larger so that the focus would fall at the rear end plate.

B. The Vacuum System

The vacuum tank or "can" is rolled from 1/4-in. stainless steel sheet; it is 78-5/8 in. long and has an inside diameter of 12 in. There are two brass bulkheads separating the can into three sections: the oven chamber, the buffer chamber, and the main chamber. These bulkheads carry adjustable slits which allow the beam to pass yet allow differential pressures in the three sections. All flanges are made of 3/4-in. boiler plate. O-ring seals are used throughout for both static and sliding vacuum seals. The ends are closed with large aluminum plates. The plate on the oven end carries a quartz window; a button loader, described in Section IV-F, is mounted on the rear plate. Most connections to the inside are made through brass plates on top ports. These are labeled, in order from oven to detector, oven, A, C_1, RF, C_2, B, and detector. The can sits on a three-point suspension on concrete pillars set in the floor. All pumps hang from the can, allowing positioning of the apparatus with respect to the fixed pillars.

Oven and main chambers are pumped by Consolidated Vacuum Corp. MCF-700 oil diffusion pumps, two in the main chamber and one under the oven chamber. The buffer chamber is pumped by a Distillation Products Inc. VMF 260 oil diffusion pump. The outputs of the main chamber pumps are manifolded together and fed to a Consolidated Vacuum Corp. MCF 300 oil diffusion forepump. The oven and the buffer pump outputs are manifolded to the output of the MCF 300 forepump and backed by a Welch Duo-Seal mechanical forepump. Provision was made for two mechanical pumps operating in parallel but one gave satisfactory performance. Each diffusion pump except the main chamber forepump has its own liquid nitrogen trap mounted between it and the can. These traps prevent oil vapor from entering the can and condensing on interior surfaces. With this

pumping arrangement a vacuum of about 5×10^{-7} mm Hg can be reached. During an actual experiment the pressure is 10^{-5} to 10^{-6} mm Hg in the oven chamber and about 10^{-6} mm Hg in the main chamber. Gas scattering of the beam is negligible, since the mean free path of a molecule at these pressures is much greater than the length of the path. A rough-pumpout line is furnished, backed by a Welch Duo-Seal mechanical pump, which is used to evacuate chambers in the vacuum locks of the oven and button loaders described below. Fine-pumpout chambers in these vacuum locks are connected to the manifold behind the main-chamber diffusion pumps. There are thermocouple vacuum gauges with a range of 10^{-3} mm to 1 mm Hg mounted on the pumpout lines, manifolds, and in the oven and main chambers. Ion-current vacuum gauges with a range 10^{-7} mm to 2.5×10^{-4} mm Hg are mounted in the oven and main chambers for use at final operating pressures.

The machine has been extensively interlocked. All electronic components, relays, circuit breakers, and switches are standard items available at the Lawrence Radiation Laboratory. The essential feature of the interlock system is to automatically turn off any part of the apparatus when conditions become such that damage can occur. If there should, for example, be a large pressure rise in the can, all filaments and diffusion pump heaters are shut off. If cooling-water pressure drops, the oven heater is cut off, or if the flow of cooling water that runs through the magnet windings decreases, the magnet-current switch is opened. All interlocks except water-flow type can be by-passed by a switch on the "Y" panel.

A beam flag is provided in the buffer chamber which acts as a shutter, preventing any beam from entering the main chamber when it is in closed position. It consists of a small plate connected to a cylindrical plunger fitted in a horizontal port near the oven end of the can. A single sliding O-ring seal is used.

C. The Oven Loader and Ovens

For work with materials of short half-life it is necessary to provide a means of placing the oven in position inside the vacuum without waiting several hours for the machine to be pumped down to its operating condition from atmospheric pressure. A vacuum-lock arrangement was designed to allow insertion of an oven in a few minutes. A drawing of this device is shown in Fig. 5 and a view of the loader in its open position is shown in Fig. 6 with an oven inserted. When the loader is dropped into its closed position, it places the oven in position for conducting the experiment.

A plunger slides vertically through a tube containing three O rings with pumpout connections in the spaces between the O rings. The tube is fixed to a horizontal plate which makes a sliding seal with an O ring mounted on the oven port cover. Guide plates are provided to hold the plate and allow translational motion normal to the beam line. Precise positioning is facilitated by a micrometer screw and dial position indicator.

The oven mount fits inside the plunger. This consists of two long brass tubes with a copper block at the lower end, a spacer block higher up, and a flange at the top. The oven is placed on three pins on a metal plate which is insulated from the lower copper block by a quartz block. Leads for the oven filament are brought through the spacer block through glass insulators and through the upper flange by means of kovar seals. A third lead protrudes from the top flange, having a sliding O-ring seal and kovar seal, which makes contact with the oven cap. This lead supplies the high voltage to the oven and keeps the oven in position because of a slight downward force on this lead when under vacuum. The top flange is screwed to the top of the plunger, making the entire unit vacuumtight. A micrometer screw protrudes through this flange, allowing vertical positioning with respect to the port cover. A small vertical plate is mounted on this flange with horizontal screws for adjustment of rotation about the loader's vertical axis. Since there is a force of some 50 pounds tending to pull

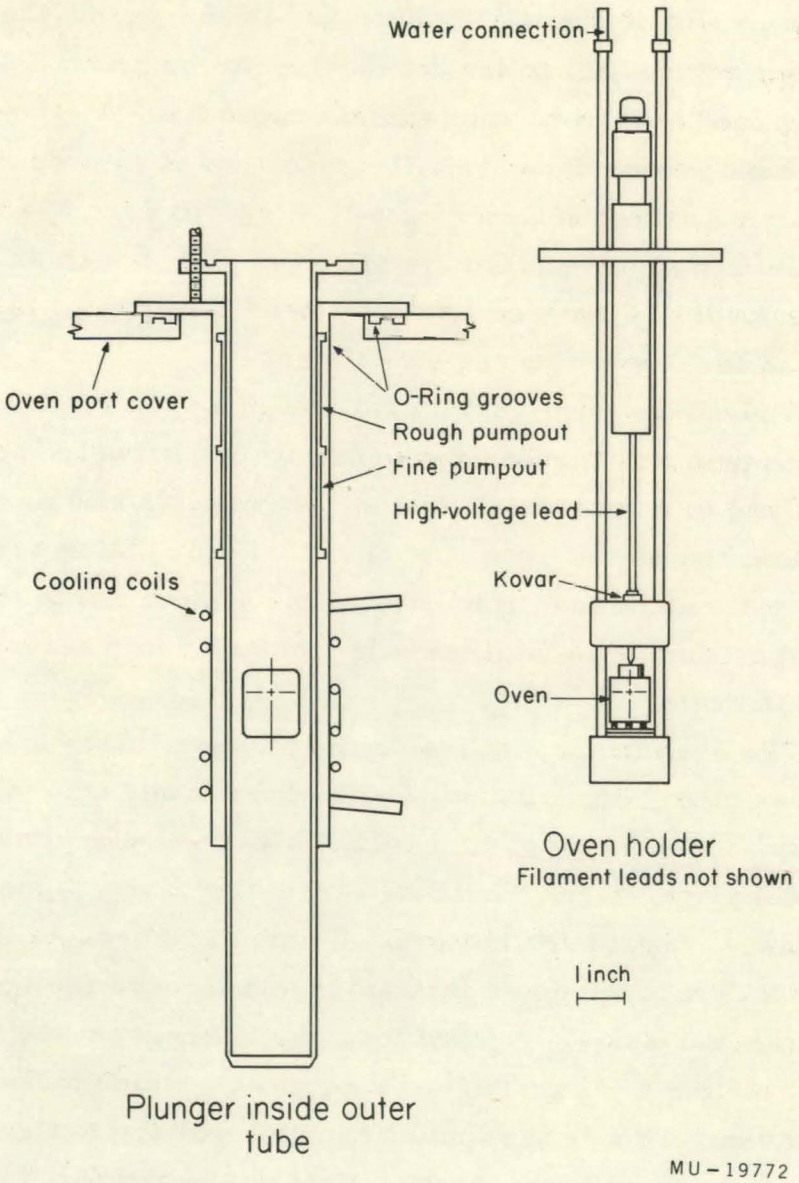

Fig. 5. Cutaway view of the oven loader in closed position.

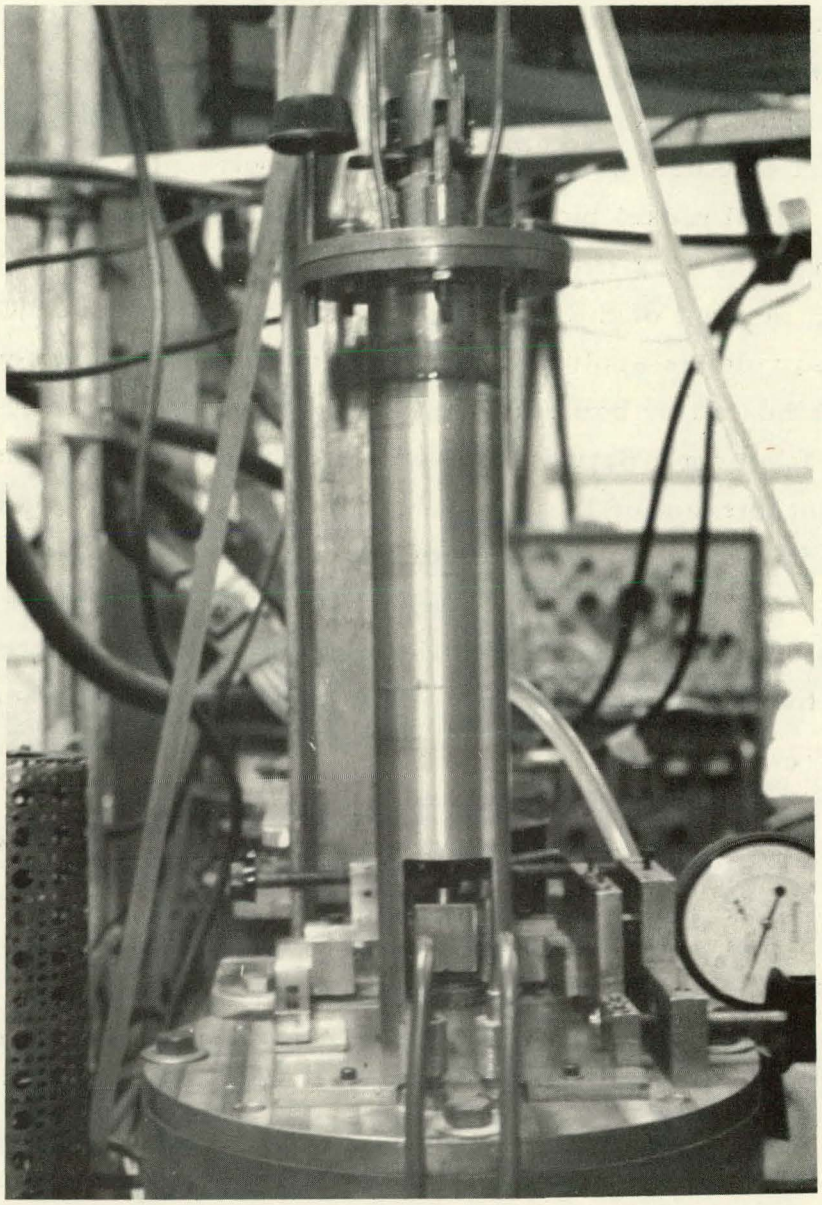

ZN-2393

Fig. 6. The oven loader in open position.

this unit into the vacuum, a counterweighted chain driven by a small electric motor is used to pull the oven loader up and to control its lowering into the vacuum.

The oven is heated by electron bombardment. A U-shaped filament of 0.020-in. thoriated tungsten wire is spot-welded at either end to small nickel blocks which are held onto the filament leads by set screws. This filament is positioned in the vertical plane about 1/8 in. in front of the oven and is heated to about 1500°C. Several hundred volts is applied between the oven and the filament and the oven is heated by bombardment of the accelerated electrons emitted by the filament. Satisfactory emission is usually obtained at a filament current of 12 amperes. Between 10 and 50 watts of electron power is required for beams of rubidium or other alkali.

Cooling water circulates through the brass tubes and copper blocks of the oven mount and through coils attached to the outer tube of the oven loader. Because of the high level of radioactivity of the oven loader, a steel-jacketed lead cylinder was fashioned which fits inside the oven chamber around the loader. This jacket has holes front and rear on the beam axis to allow the beam to pass and permit visual observation of the oven. It was also necessary to place an external lead shield around the liquid nitrogen trap of the oven chamber diffusion pump, which sits directly below the oven loader.

The ovens used were made of stainless steel blocks, 7/8×1×1-5/8 in. Figure 7 shows, from left to right, an assembled oven (front view), a disassembled oven, and an older type of oven no longer used. Slit jaws made of 1/8-in. stainless steel were screwed into place on the oven block. Two V-shaped slots, mutually perpendicular, were milled in the bottom to fit on the positioning pins of the oven mount. Material for producing a beam is placed in the cavity and the stainless steel press-fit cap is pushed into place with thumb pressure. (The older oven of Fig. 8 used a screw-on cap which tended to leak when heated. There was a small vapor chamber milled on the older oven, but it showed no improvement over the simple cylindrical hole drilled for the beam to emerge.) A slit width of 0.005 in. was used in this work, and no attempt was made to obtain further collimation.

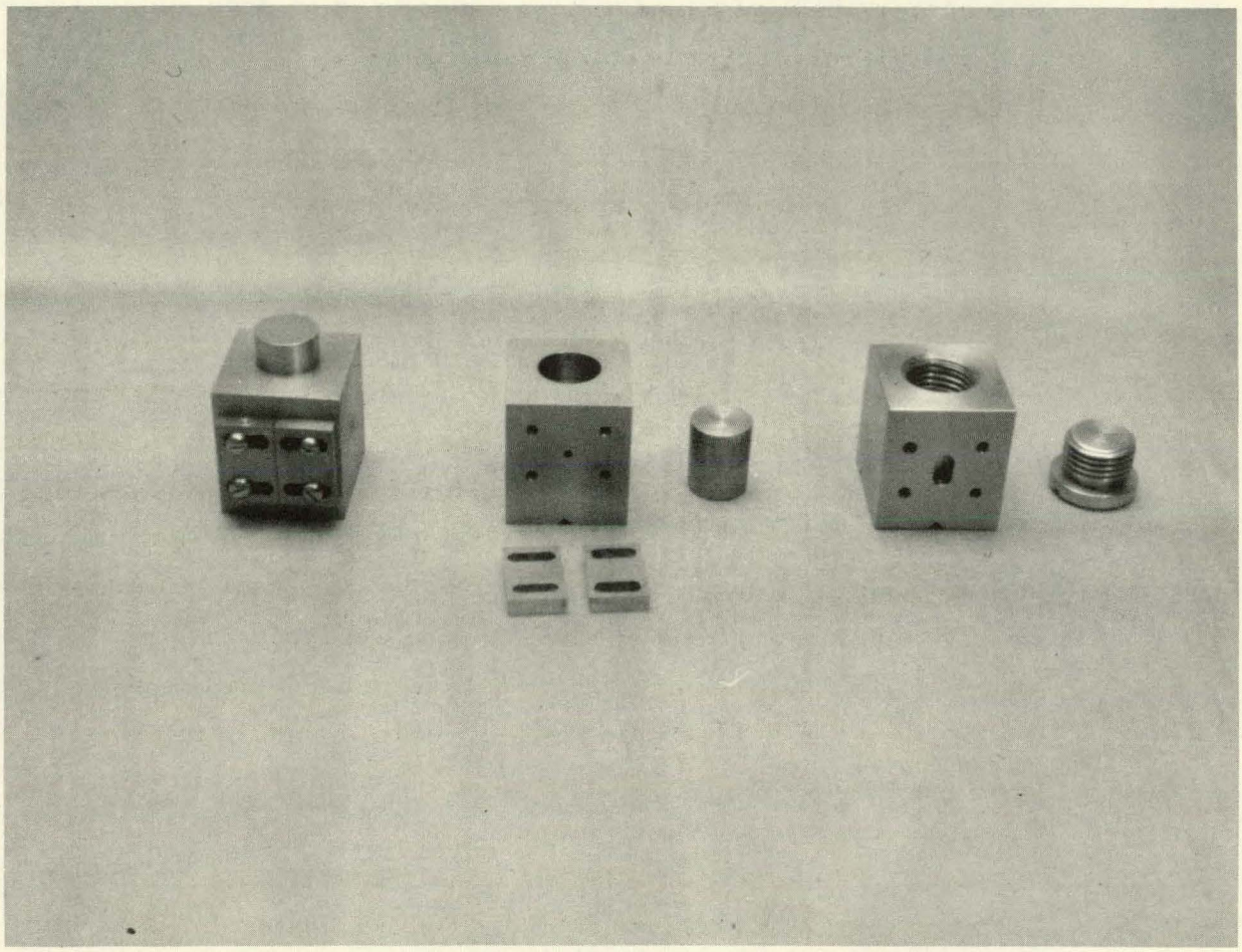

ZN-2391

Fig. 7. Stainless steel ovens, showing slit assembly.

Alkali beams were first produced by heating the pure metal whose surfaces were freshly cut before it was placed in the oven. It was easier, however (and necessary for radioactive runs), to obtain an alkali beam by reduction of a salt by calcium. About 50 mg of RbCl and a like volume of freshly filled calcium metal yielded a beam of 10^{-10} ampere for about 6 hours. A higher temperature is required to make the beam by the reduction method but it does not otherwise make any difference in the experiment.

D. The Magnet System

There are three magnets in the machine, usually labeled from the oven end, A, C, and B (see Fig. 4). All are low-impedence electromagnets. The A and B magnets are inhomogeneous magnets of the Rabi type. Yokes and coils are those used by Bemski. New pole tips suitable for deflection of larger atomic magnetic moments were constructed, the shape of which is shown in Fig. 8. These two magnets are identical except for a vertical slot milled in the center of the B magnet pole faces for the stop-wire motion. An over-all view of an assembled deflecting magnet is shown in Fig. 9. Figure 10 shows an end view of the B magnet.

Each magnet is wound in a one-piece coil consisting of flattened thick-wall copper tubing. Cooling water flows through the coils. In assembly, the layers of the coil are insulated from one another and from the magnet by 0.020-in. teflon strips.

The C magnet, shown in Fig. 11, has a homogeneous magnetic field. The pole tips are parallel surfaces with a gap 0.250 in. wide, 2 in. deep, and 15-5/8 in. long, and were set in place by using a template during assembly. No attempt was made to shim the field at that time. The winding consists of 20 turns of flattened copper tubing having a measured dc resistance of 0.0071 Ω. The magnet carries the collimator, Fig. 12, placed in the center of the magnet below the rf port.

Figure 13 shows the stop-wire structure which fits into the slot in the B magnet. Through a sliding O-ring seal in the cover

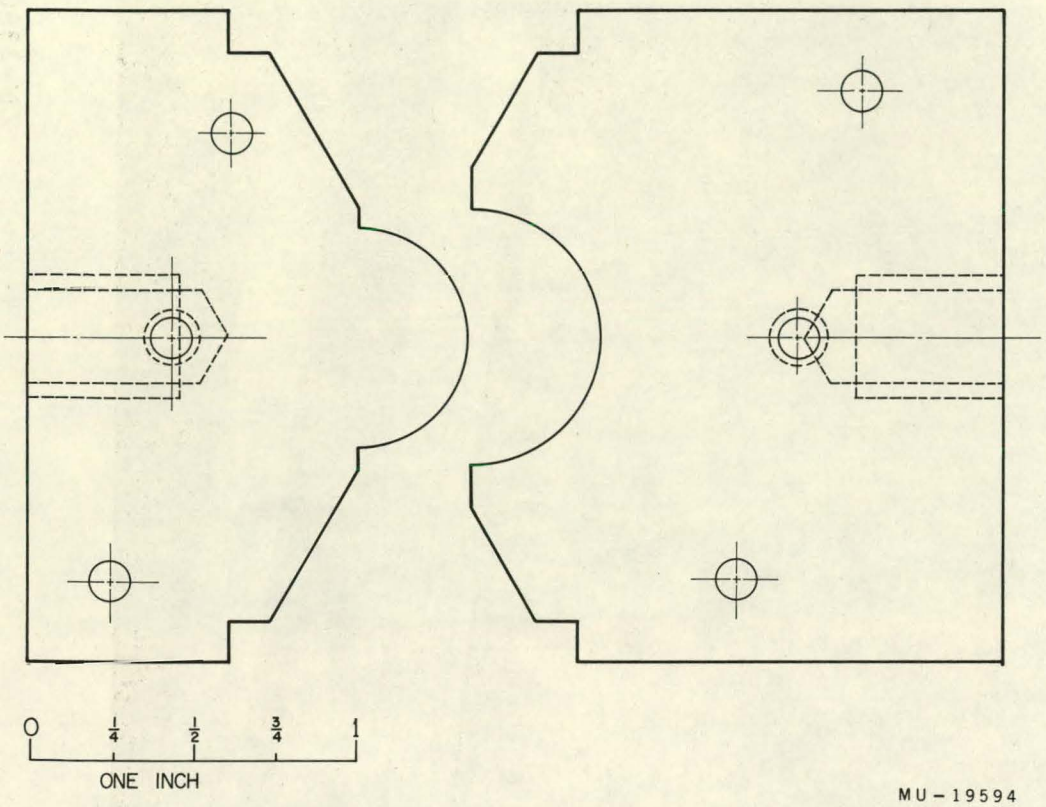

Fig. 8. Deflecting-magnet pole tips.

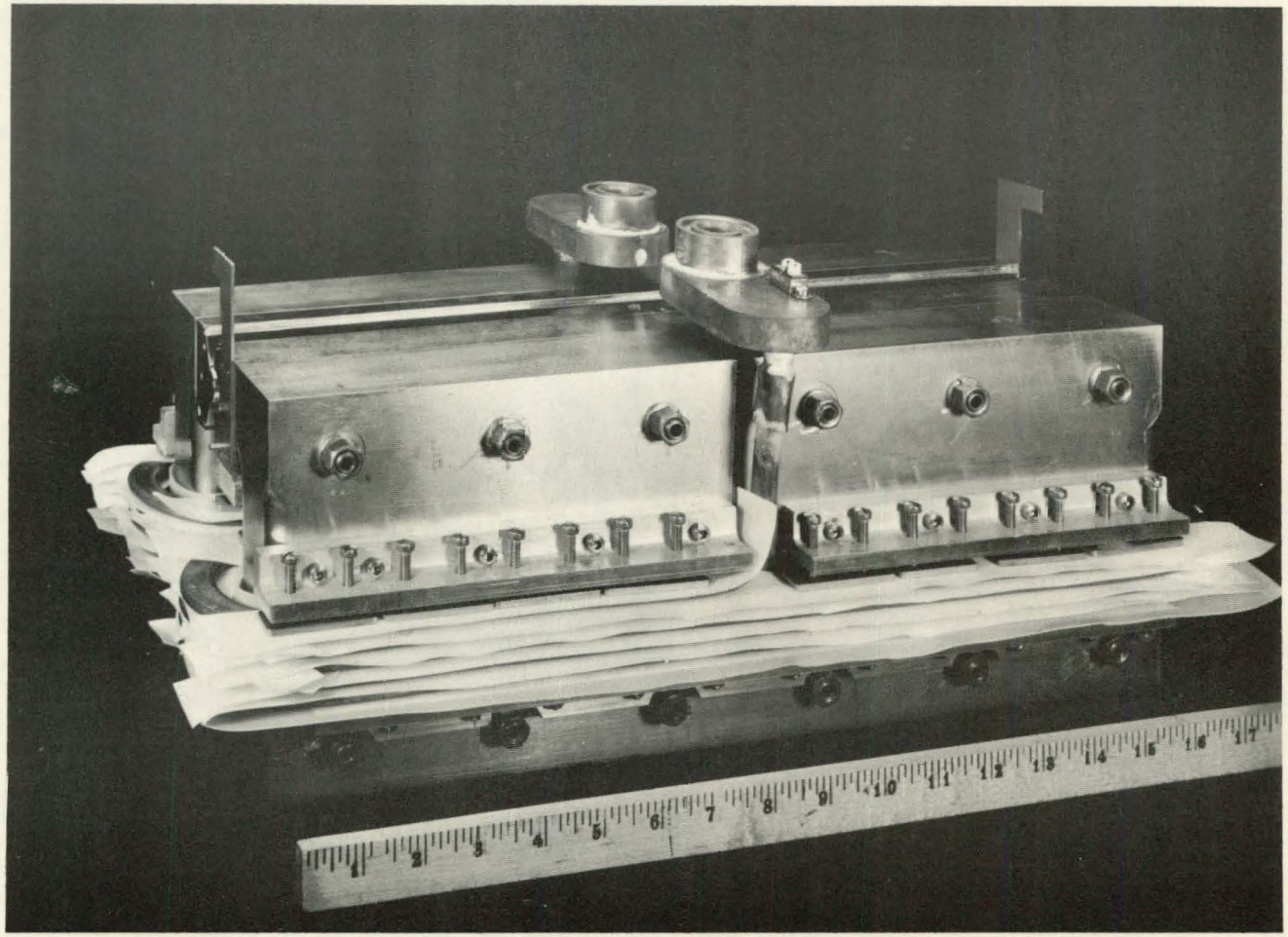

ZN-2380

Fig. 9. Over-all view of one of the deflecting magnets.

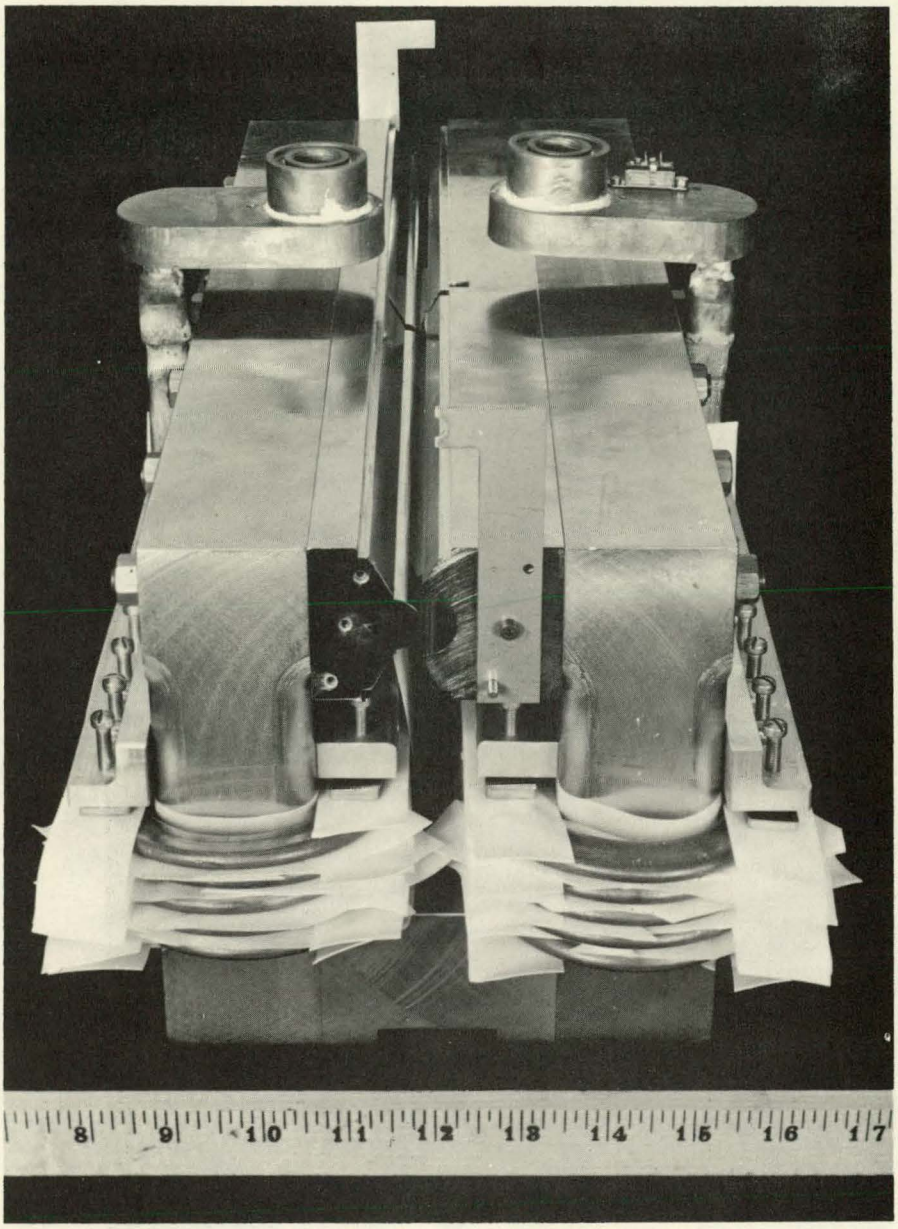

ZN-2379

Fig. 10. End view of a deflecting magnet.

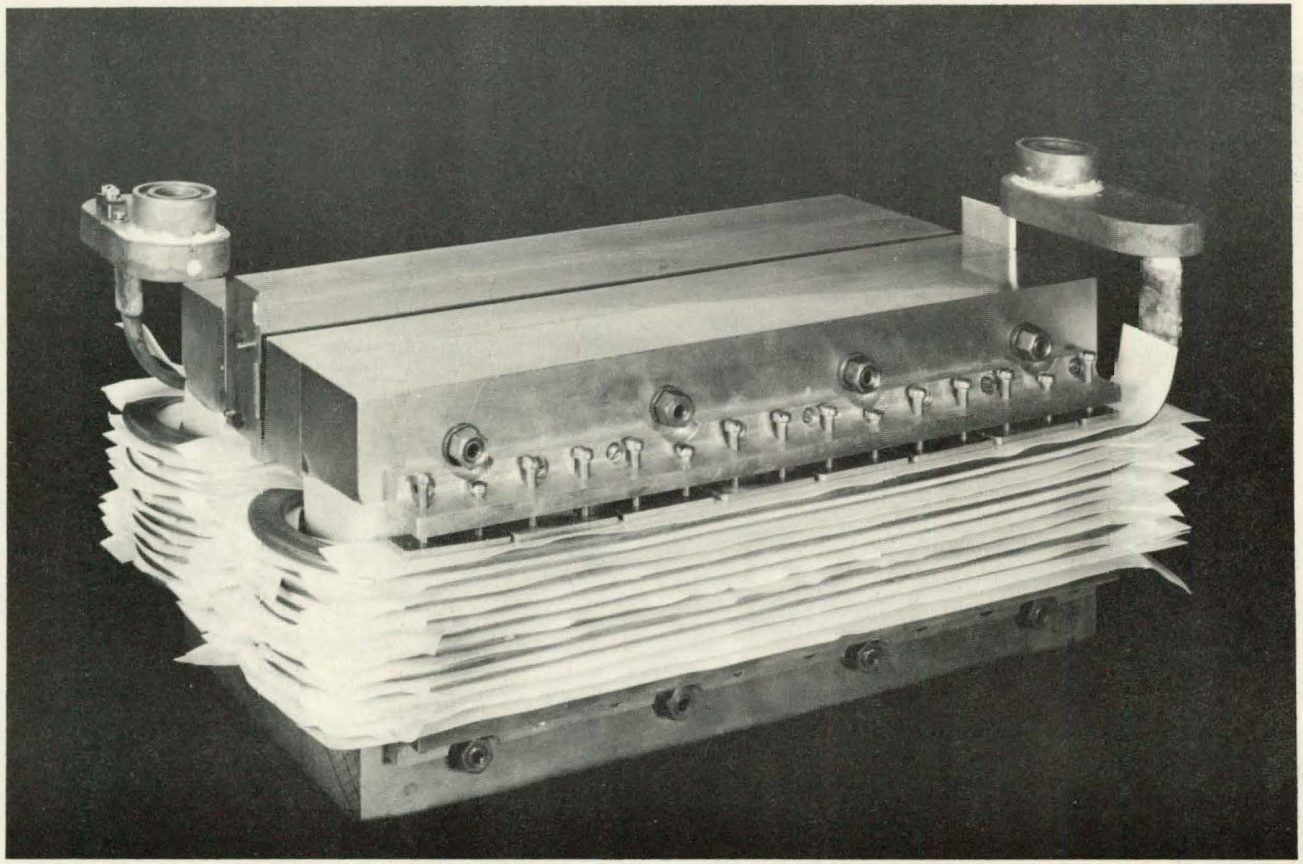

ZN-2381

Fig. 11. Over-all view of the assembled C magnet.

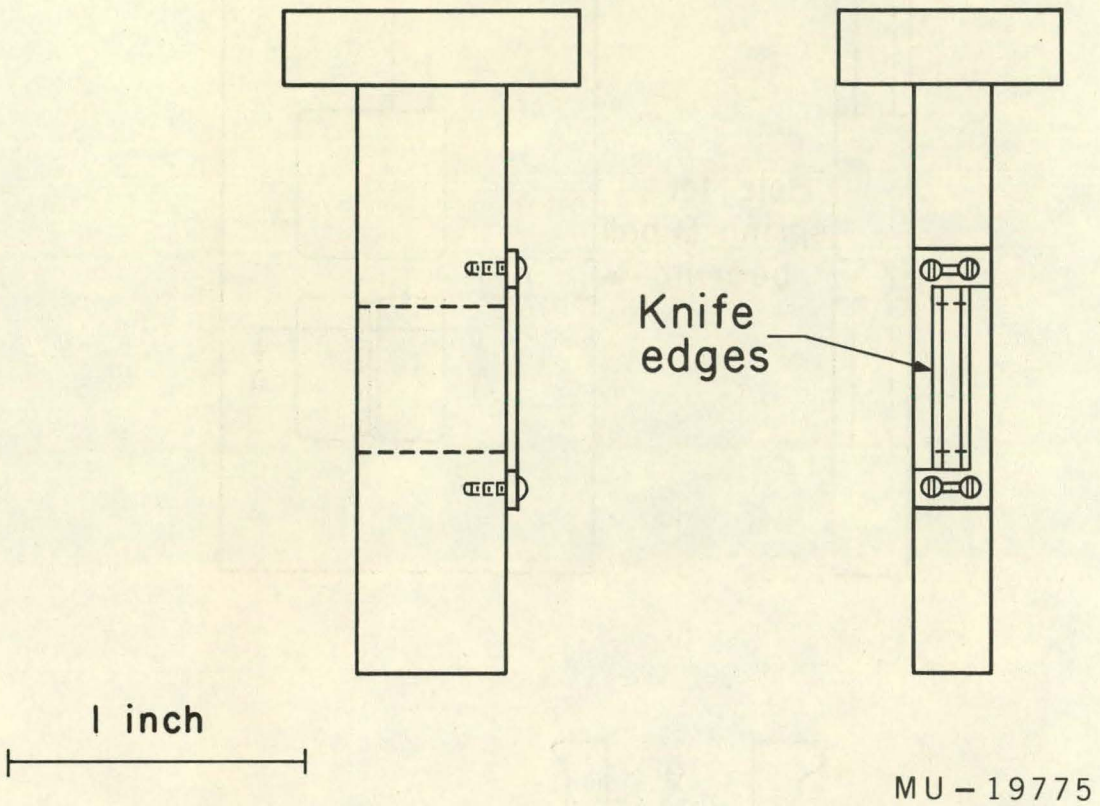

Fig. 12. Collimator assembly.

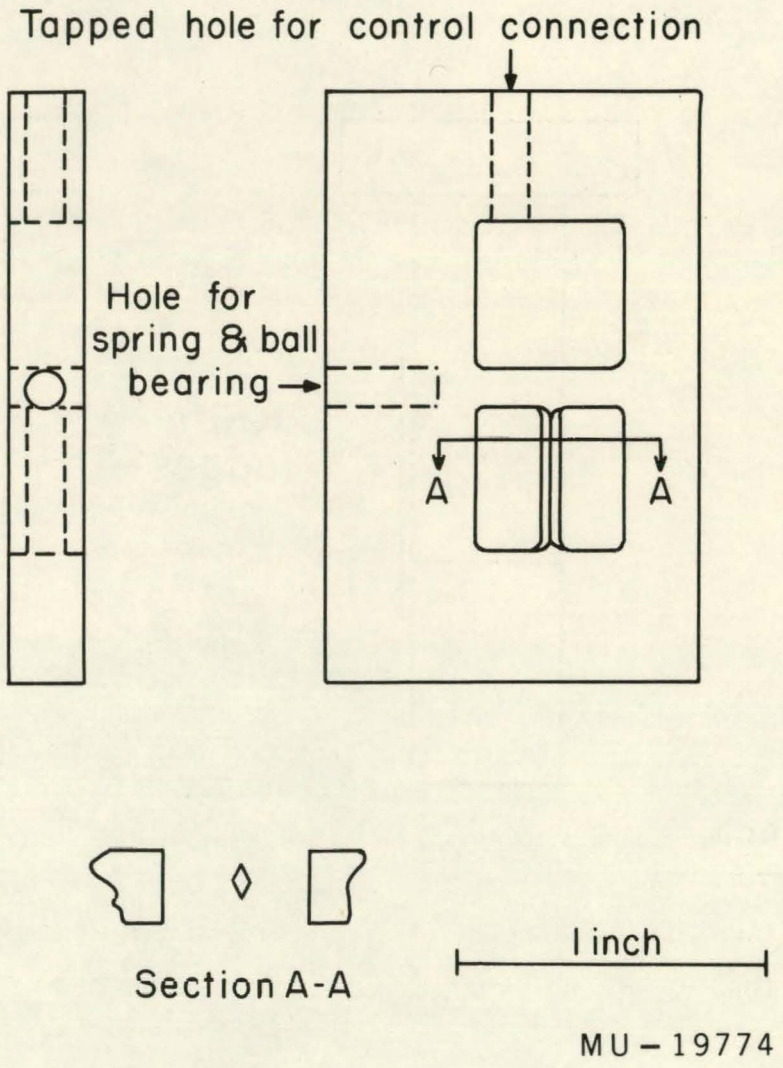

Fig. 13. Shape of the stop-wire housing.

plate B, a plunger and rocker-arm arrangement allows the stop wire to be placed in the beam (up position) or out of the beam (down position).

Each magnet carries a pair of knife edges, as can be seen in Fig. 10, to facilitate initial alignment by optical methods. The three magnets sit on a flat plate positioned in the can before the magnets were placed on it. Four adjusting screws for each magnet, near the ends of the yoke, allow fine translational adjustment of the magnets and serve to lock the magnets in position after adjustment. Each screw is covered by a screw-on vacuum seal fitted with an O ring.

Each end of a magnet's coil is brought out of the vacuum can by a current seal through a top port cover plate. Figure 14 shows the construction of this seal. Both A magnet leads are in plate A, both B magnet seals are in plate B. The C magnet leads are at either extremity with one lead out of top plate C_1, the other one out of plate C_2. This allows maximum access to the center of the C magnet through the rf port.

The A and B magnet windings are connected in series and fed by a bank of 12 2-v 10,000-amp hr submarine batteries connected to give 350 amp at 4 v. A push button controls a large relay mounted outside in a weatherproof box which turns the deflecting magnets on or off. No other adjustment is needed.

The C magnet current is controlled by a rather novel arrangement. Since the value of the static field is one of the critical parameters of this experiment, it must remain stable for long periods of time. Submarine batteries exhibit a long-time drift which is unsatisfactory for precision work. The magnetic field of the C magnet is not homogeneous enough or large enough to use standard NMR probes to lock the field to a proton resonance. In this machine, a transition is observed in the easily detectable stable carrier isotope in the beam, and the field is electronically locked to the peak of this resonance at the frequency corresponding to the magnetic field desired. Long-time stability of about one part in ten thousand of the static C field can be obtained in this manner. The system is described in detail in Appendix C.

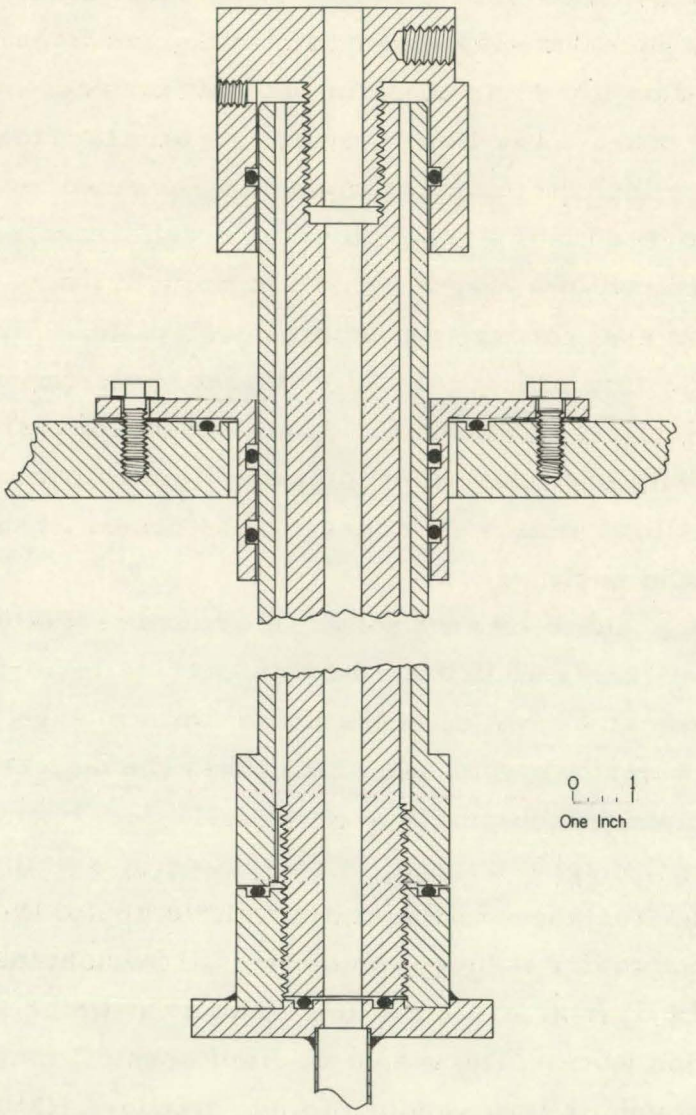

Fig. 14. Magnet-current seal.

No attempt has been made to provide magnetic shielding of the C magnet from the fringing fields of the deflecting magnets, since any pulling of the C field is compensated by the locking system mentioned above. The over-all homogeneity of the C field is certainly affected, limiting the use of the C magnet gap to the central few inches, but this restriction has already beem imposed because of the inherent lack of quality of this magnetic field. Owing to space limitations in the can, it was not practical to mount larger pole faces.

E. The Radio-Frequency System

To induce an atom in the beam to change its orientation in the static C field, a rotating magnetic field of the proper frequency, orientation, and strength must be superimposed on the C field. An elaborate signal generator with its associated equipment has been assembled to perform this function. Figure 15 is a picture of part of the assembled radio-frequency equipment. The rest of the rf gear, together with the machine controls, C magnet locking system, and electrometer is shown in Fig. 16.

The heart of this equipment is a Gertsch Products, Inc. AM-1 VHF Interpolator and FM-4 Microwave Frequency Multiplier. There are two sets of these, one for search and one for exciting the resonance to which the C field is locked. These are phase-locked oscillators operating in the ranges 20 to 40 Mc and 500 to 1,000 Mc respectively, and are capable of producing a continuously tunable signal with a stability of 1 part in 10^8 if the 100-kc standard frequency which must be fed in is equally stable. In the early stages of this work the 100-kc internal crystal oscillator of a Hewlett-Packard HP 524B Frequency Counter was used, but its drift rate of several parts in 10^7 per hour was excessive for observation of very narrow lines. The primary frequency standard is a National Company "Atomicron," a cesium atomic-beam machine which locks an oscillator to the peak of the field-independent Zeeman transition in Cs^{133} at 9192.631840 Mc. This provides a series of output frequencies with an accuracy of better than

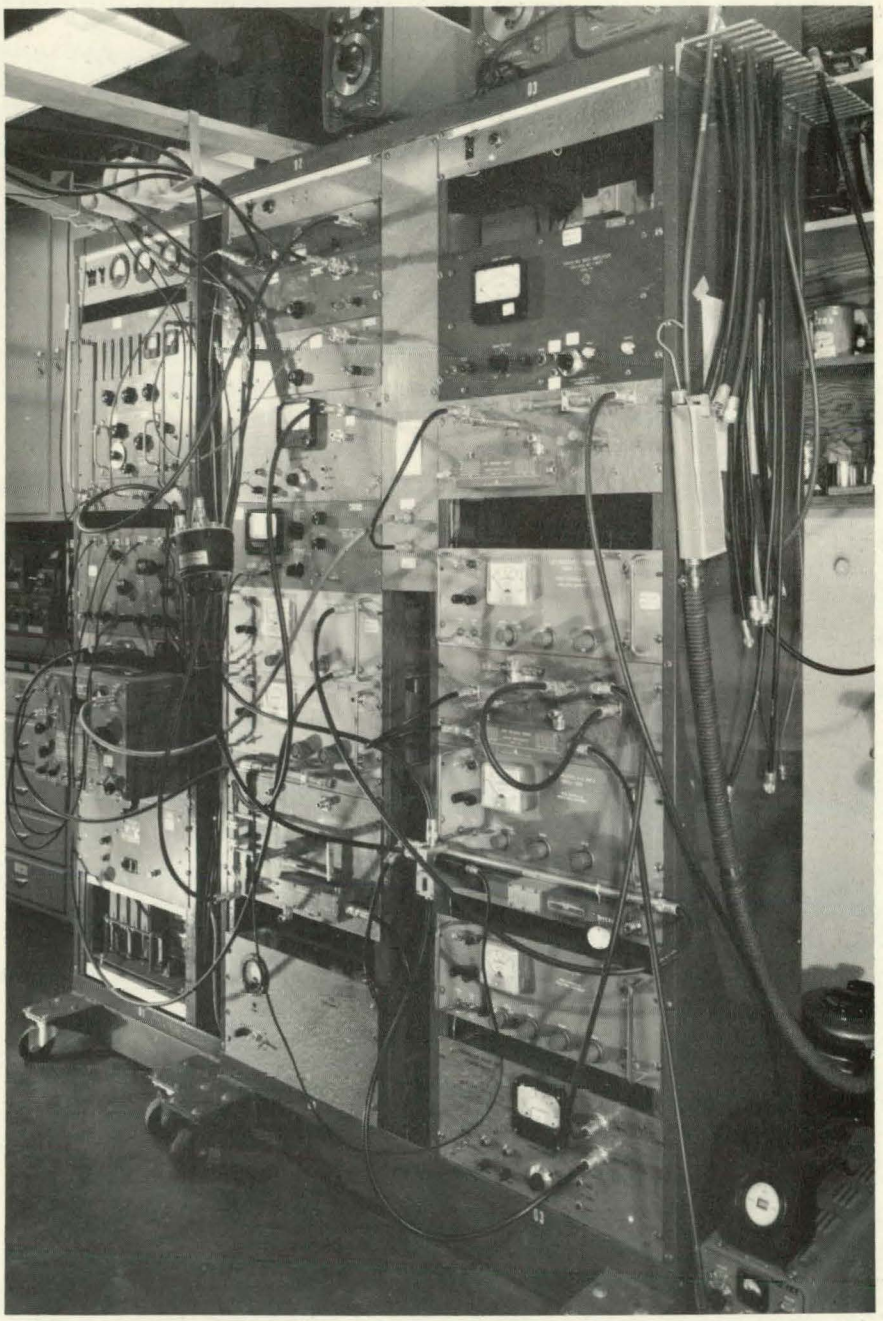

ZN-2382

Fig. 15. Part of the radio-frequency system, showing search oscillators and all amplifiers.

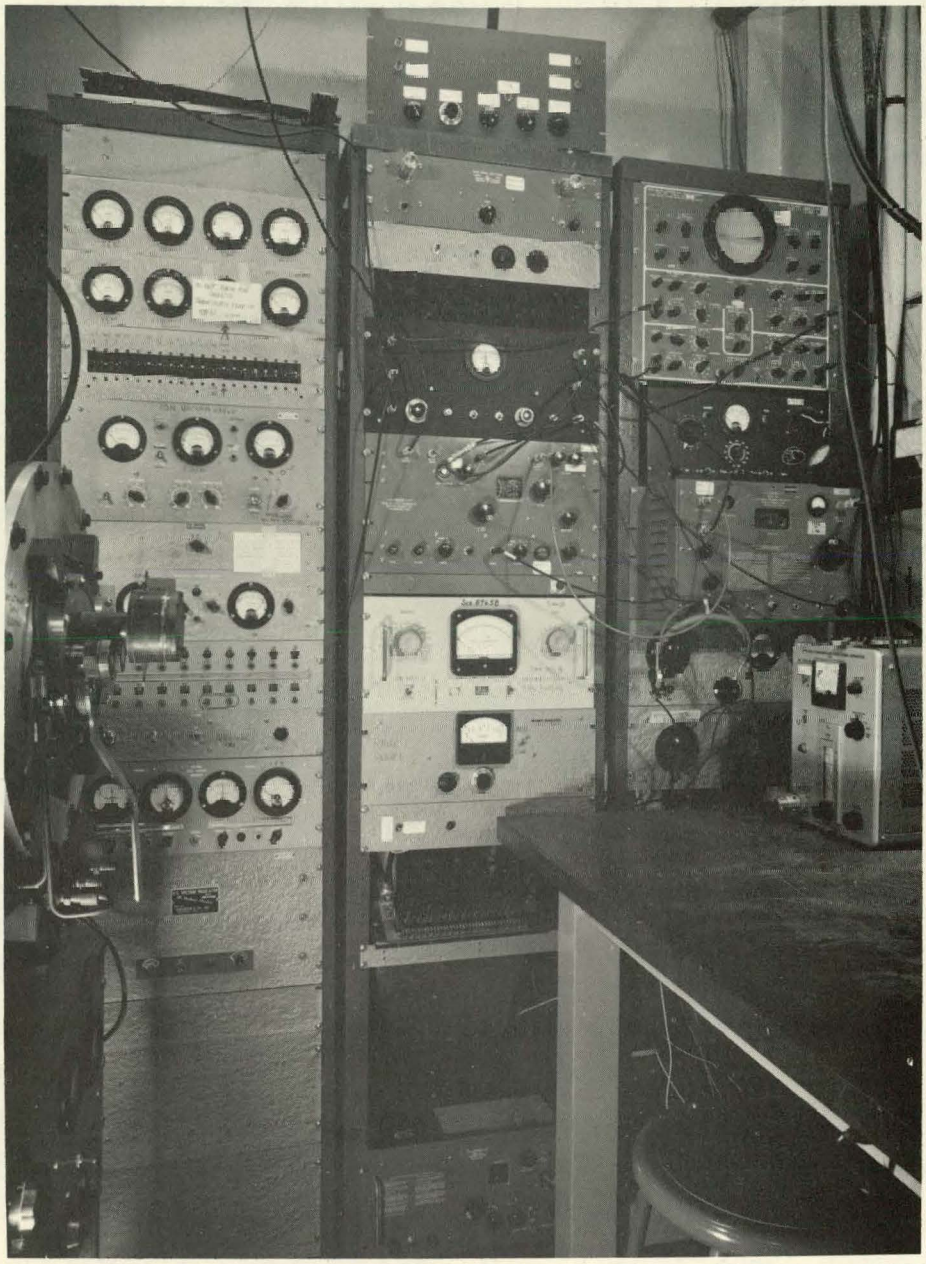

ZN-2383

Fig. 16. Racks containing apparatus controls, magnet-locking system, and locking oscillators.

$1:10^9$ and stability $1:10^{10}$. It was possible, by comparing on an oscilloscope the 100-kc output from the Atomicron with the HP 524B internal oscillator and by manually adjusting the latter, to keep the two within a few parts in 10^8. It should be noted that it was not possible to use the Atomicron's 100 kc directly into the Gertsch equipment, as this signal had some spurious phase modulation which prevented the phase-locked oscillators from performing reliably. This constant comparison with the primary standard was putting excessive operating time on the Atomicron beam tube, so a James Knight Co. JKFS-1100 secondary frequency standard was installed. This is a 1-Mc quartz-crystal oscillator in a temperature-regulated double oven which has a stability of $5:10^{10}$/day. A frequency-divider circuit provides a 100-kc signal with the same stability. It is necessary only to compare this oscillator once a week with the Atomicron. There was some harmonic content in the 100-kc output, which was easily filtered out. Now both sets of Gertsch oscillators and the HP 524B Frequency Counters use this output as their frequency-standard input.

The AM-1 multiplies the 100 kc to 10 Mc and then by a variable multiplier increases this to 19 to 38 Mc. This signal is mixed with a free-running 1- to 2-Mc internal oscillator whose output is monitored by a frequency counter. The upper side band of the mixer output is fed to a buffer amplifier which locks a 20- to 40-Mc oscillator to this frequency. This higher-level signal is fed to a crystal diode which produced harmonics up to several thousand megacycles. The drift of the 1- to 2-Mc oscillator is about $2:10^6$/hr, or about $1:10^7$/hr on the output. This is easily corrected manually, since the frequency is continuously monitored.

The AM-1 output with its high harmonic content is fed to the FM-4. Its internal oscillator (500 to 1000 Mc) mixes with a selected harmonic from the AM-1 to give a 10-Mc IF signal. This is phase-compared with a 10-Mc signal for the AM-1. Any phase difference produces a dc voltage which is impressed across a crystal diode in

the plate cavity of the 500-1000-Mc oscillator whose effective capacity is a function of this impressed dc voltage. A closed loop is formed so that the oscillator's frequency is adjusted to maintain exactly the 10 Mc intermediate frequency with respect to the harmonic of the AM-1.

To obtain higher frequencies, a series of coaxially mounted harmonic generators is available, together with traveling-wave-tube (TWT) amplifiers for reasonably high output power. The total complement of rf equipment is listed in Table I. Depending on the output power required, the output frequency above 1000 Mc may require one or more stages of frequency multiplication. One stage is usually the amplifier, a directional coupler followed by a harmonic generator with double stub tuner and a cavity filter to pass only the desired harmonic to feed the next stage. At 3900 Mc, for instance, 300 mw can be obtained in one stage by taking the fourth harmonic of 975 Mc. More power at the frequency requires the frequency multiplication to be done in two stages with intermediate amplification.

The traveling-wave tube is an inherently broad-band device which achieves amplification by interaction of the slowed-down electromagnetic wave with an electron beam. Band widths of two octaves can be obtained and some gain can be squeezed out far beyond that by careful tuning of the helix and collector voltages. These tubes with their associated high-voltage power supplied are not yet reliable. The tubes are expensive and their cathode life is only a few hundred hours. They are easily damaged by excessive currents and the power supplies must be extensively interlocked. The commercial power supplies originally purchased were poorly designed and had to be modified. Solenoids are required to provide an axial magnetic field for focusing the electron beam. These are heavy and raise the ambient temperature of the device. Some Sylvania tubes with permanent-magnet focusing were used with power supplies designed and built in the laboratory. Figure 17 shows one of these tubes in its power supply.

Table I

Radio-Frequency Equipment

	Number	Item	Frequency range	Remarks
Standards				
	1	National Co. Atomicron	0.1, 1, 5, 10, 100 Mc	Primary standard
	1	James Knights Co. JKFS 1100	0.1, 1 Mc	Secondary standard
Oscillators				
	2	Gertsch AM-1	20–40 Mc	
	2	Gertsch FM-4	500–1000 Mc	
	1	Gertsch FM-5	0.200–20 Mc	
	1	Tektronix 190A	0.5–50 Mc	
	1	Hewlett Packard 608A	10–500 Mc	
	1	Hewlett Packard 670SM(klystron)	2.6–4 kMc	with HP 707 A power supply
	1	Hewlett Packard 670GM(klystron)	4–6 kMc	with HP 707 A power supply
	1	Hewlett Packard 670MM(klystron)	6–8 kMc	with HP 707 A power supply
Amplifiers				
	2	Hewlett Packard 460A	0.200–200 Mc	
	2	Hewlett Packard 460B	0.200–200 Mc	
	1	Instruments for Industry Inc. 500	0.200–200 Mc	
	2	Wave Particle Co. (Sperry TWT)	0.5–1 kMc	tends to oscillate
	1	(Modified)Clegg Co. (Sylvania TWT)	1–2 kMc	
	1	Our own make (Sylvania TWT)	1–2 kMc	
	1	Our own make (Sylvania TWT)	2–4 kMc	
	1	Hewlett Packard 491A (Huggins TWT)	2–4 kMc	
	1	Wave Particle Co. (Huggins TWT)	2–4 kMc	
	1	Wave Particle Co. (Huggins TWT)	4–8 kMc	
	1	Wave Particle Co. (Huggins TWT)	8–12 kMc	
Measuring Equipment				
	2	Hewlett-Packard 524B Frequency Counters with plug-in frequency converters		
	1	Hewlett Packard 540B Transfer Oscillator		
	1	Hewlett Packard 430C Power Meter		
	1	Marconi wavemeter	0.5–1 kMc	
	1	Marconi wavemeter	1–2 kMc	
	1	Marconi wavemeter	2–4 kMc	
	1	Wayne Kerr wavemeter	3–8 kMc	
	1	Wayne Kerr wavemeter	7–13 kMc	

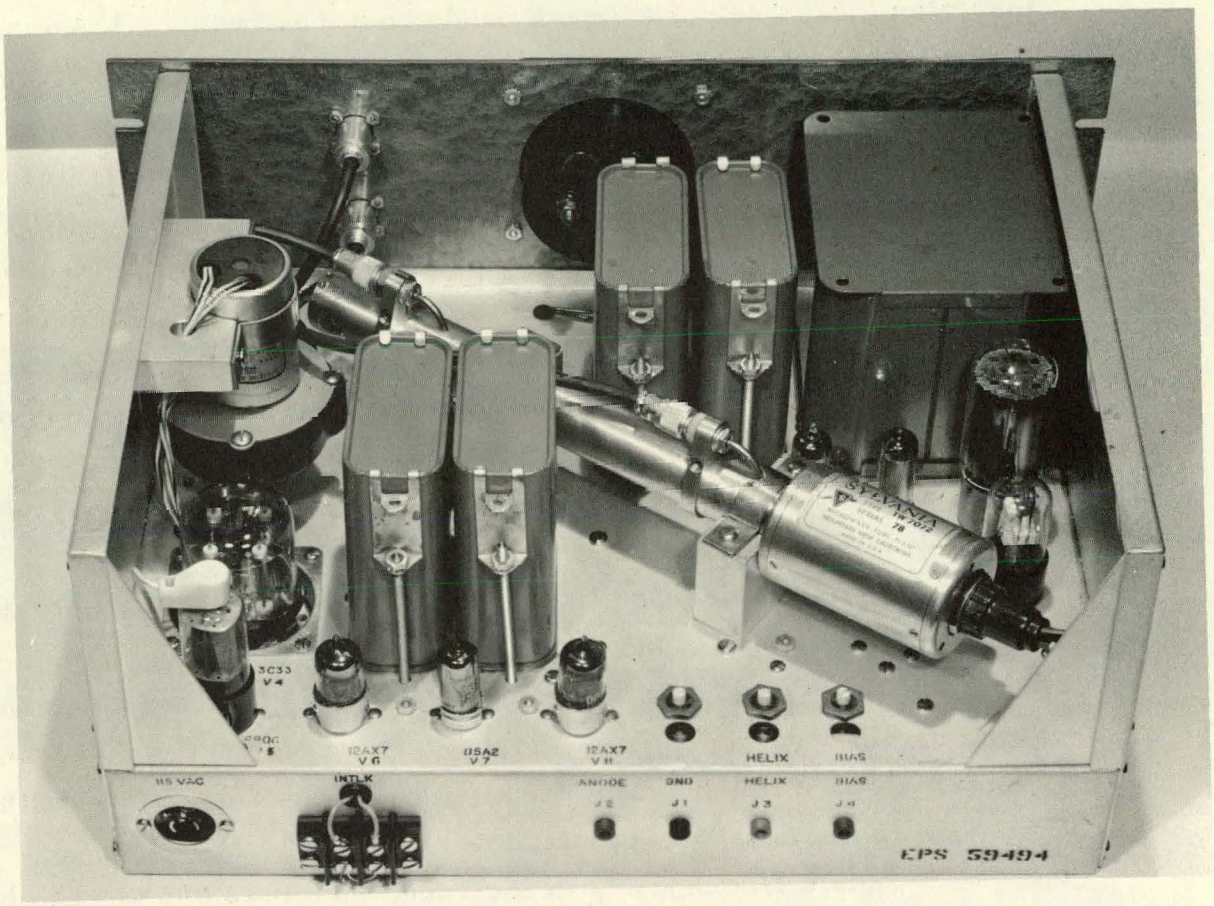

ZN-2378

Fig. 17. Traveling-wave-tube amplifier mounted in its power supply.

Coaxial tunable cavities act as band-pass filters with an insertion loss < 2db and a pass band about 2 Mc wide. These are used to suppress unwanted harmonics and, after being calibrated, serve as rough checks on the frequency. In the 0.5 to 1-kMc amplifier, the cavity filters out the inherent oscillation present at high power level. The calibration curves were obtained by standard methods (KIN 52, GIN 57), and are accurate to a megacycle or two. Calibrated wavemeters are available to verify the frequency settings and check the absence of spurious frequencies.

The Power Meter consists of a thermistor element in one arm of a Wheatstone bridge. Microwave power impinging on this element heats it and its resulting change of resistance unbalances the bridge. The power level is read directly.

The Transfer Oscillator contains a stable 100- to 220-Mc oscillator, a mixer, video amplifier, and oscilloscope. The frequency of an unknown signal is determined by beating it against a harmonic of the oscillator, whose frequency can be read directly on a frequency counter. For frequencies in the kilomegacycle range, this method is accurate to about $1:10^6$.

Thus a frequency f_0 in the range 500 to 12,000 Mc can be generated according to the relations

$$\begin{aligned} f_0 &= nf, \\ f_1 &= mf_2 \pm 10 \text{ Mc}, \\ f_2 &= p(1 \text{ mc}) + f_3, \end{aligned} \qquad \text{(IV. 1)}$$

where f_1 is in the range 500 to 1000 Mc, f_2 is in the range 20 to 40 Mc, f_3 is in the range 1 to 2 Mc, and n, m, and p are integers corresponding to the harmonic number used. The frequency is then checked to $1:10^6$ by

(a) filter cavity settings of multiplier stages,

(b) wave meter on output,

(c) transfer oscillator.

The accurate value is then read from f_3 as displayed on the Frequency Counter.

For lower frequencies and for field calibration where line widths are larger and measurement time short, standard manually tuned signal generators are satisfactory. Instruments listed in Table I are used for this purpose. Owing to lack of suitable amplifiers, power levels greater than 50 mw cannot be obtained in the region 200 to 400 Mc. Fortunately no frequencies in this range are needed for this work.

The signal f_0 must be fed from the final amplifier into the vacuum system to the "hairpin" which conveys the radio frequency to the vicinity of the beam. RG-8/U coaxial cable with standard UG series conductors are used with the outer rubber coat stripped off the cable for use inside the vacuum. Because of the extremely broad frequency band covered, a design for the coaxial vacuum feed-through is subject to compromise. A rather simple design was tried, details of which are shown in Fig. 18, which exhibited essentially zero db insertion loss to 1000 Mc and only 3 db at 8000 Mc. A box was built covering the rf flange, as shown in Fig. 19, carrying five of the feed-throughs to allow for flexibility and possible future complexity. This replaced an older design in which two coaxial leads were fed through a flush port cover in much the same manner as the magnet-current seals. The later design is less lossy and eases the problem of access to the C magnet gap, since all electrical connections can be made before the top plate is closed.

Getting the rf to the vicinity of the beam is more of a problem, aggravated by a rather small C-magnet gap (0.250 in.) and lack of space inside the can above the magnet gap.

Torry (TOR 41) has shown that the width of a resonance line for the value of a single oscillatory field corresponding to an optimum perturbation is

$$\delta\nu = 1.07 \frac{a}{\ell} , \qquad \text{(IV. 2)}$$

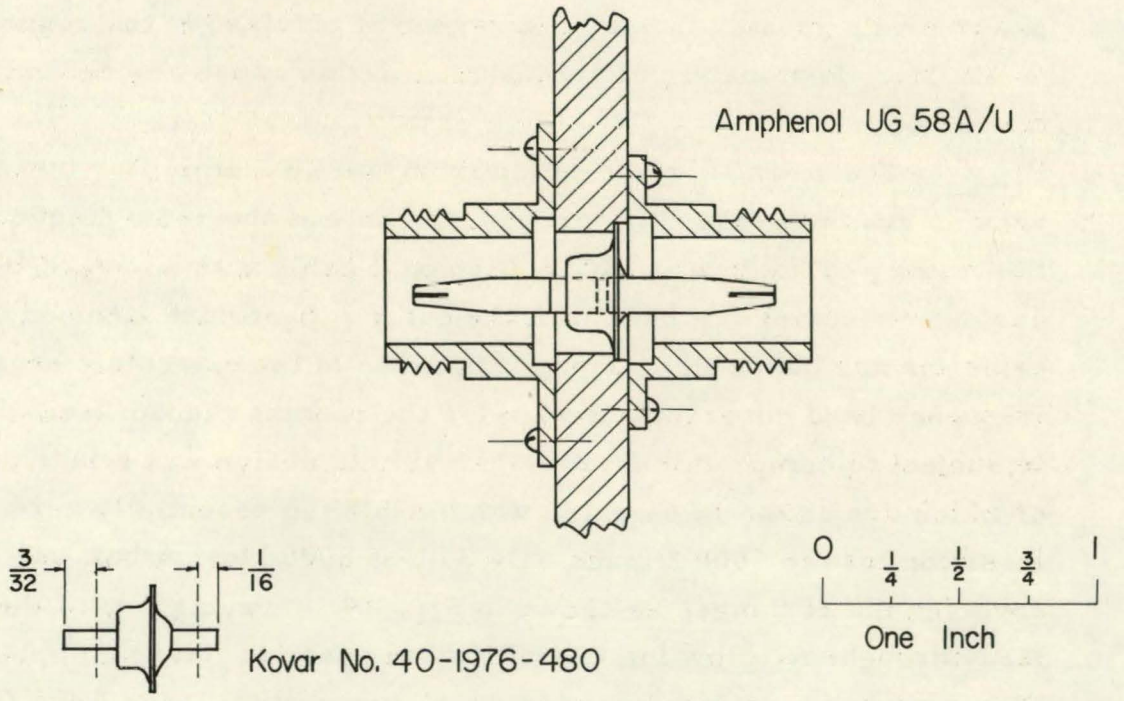

Fig. 18. Detail of the coaxial vacuum feed-through.

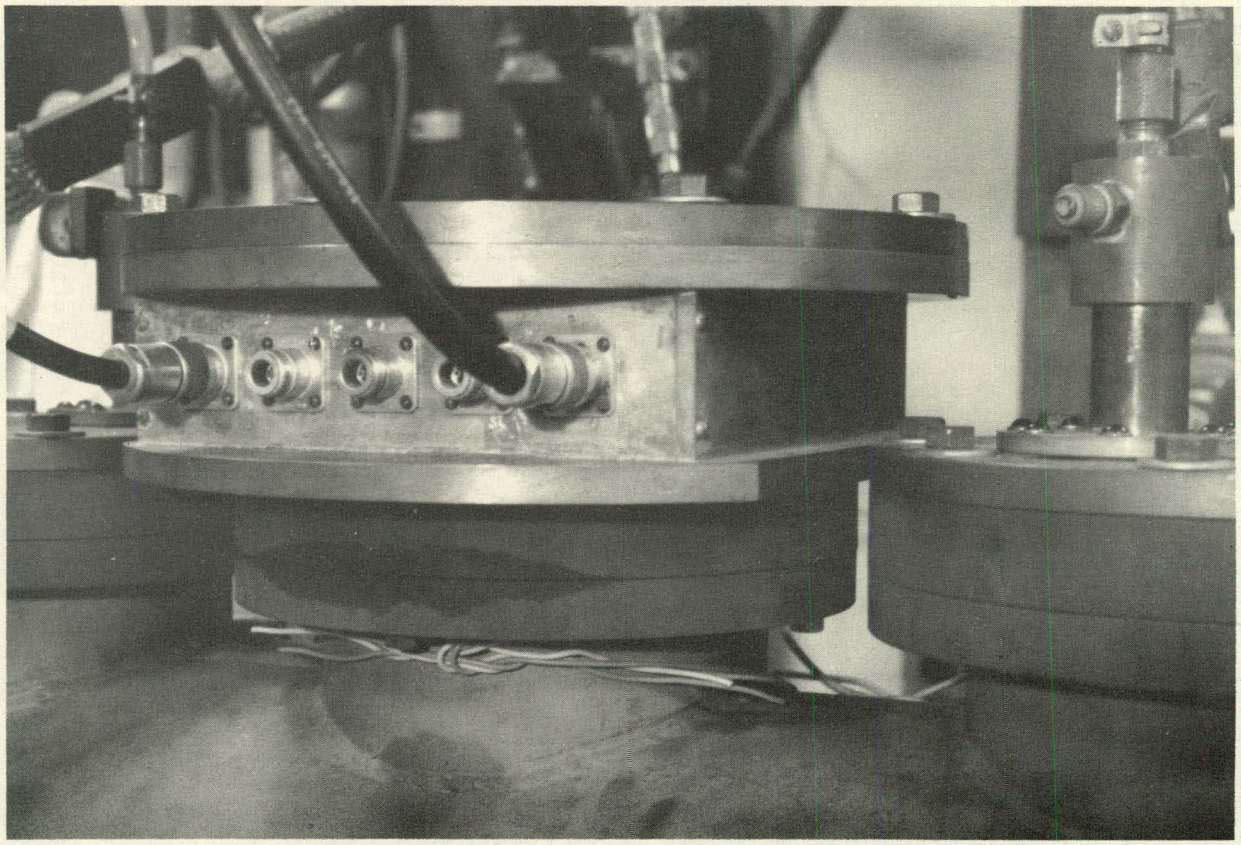

ZN-2390

Fig. 19. New cover box over the rf port, showing coaxial feed-throughs.

where a is the most probable velocity of the atom and ℓ is the length of the oscillatory field along the beam. For separated oscillatory fields of length ℓ, Ramsey (RAM 50) showed that if the two fields are fed in phase and the C field is sufficiently homogeneous so that the two individual patterns overlap, there is a sharp central interference peak at a frequency corresponding to the spatial average value of the field in the region between the rf fields. The width of this central peak is given by

$$\delta\nu = 0.65 \frac{a}{L} , \qquad \text{(IV. 3)}$$

where L is the distance between the rf fields. The line widths used in this sense are the full widths at half full resonance height.

The width, Eq. (IV. 2), is the minimum obtainable, and is seen only for transitions that are field-independent. Usually field inhomogeneities broaden the line to many times this value. Ramsey patterns for separated oscillatory fields wash out completely if the transition is field-dependent and one single line, also broadened, is seen. Care must be taken in analyzing a resonance, since distortions may be present (RAM 56) that shift the observed peak from the true transition frequency. Examples of such effects are shown in the following sections.

Selection rules for magnetic dipole radiation require that the oscillatory magnetic field be parallel to the static field for $\Delta m = 0$ (σ) transitions and perpendicular to the static field for $\Delta m = \pm 1$ (π) transitions. An arrangement of conductors is needed that will fit in the magnet gap, displaying a reasonable electrical impedance while orienting the rf magnetic field to excite the desired type of transition. Various configurations are described in the literature (RAM 56, KUS 59). For microwave frequencies, waveguides and cavities are attractive for use as hairpins (LUR 56, FRI 59). For the relatively long microwaves used in this experiment such designs were not practical because of space limitations in the gap. Again, with a large bandwidth to consider, compromises must be made. The simplest design is a strap bent in the form of a U and placed in the magnet gap but insulated from the pole

faces. This is a shorted parallel-plate transmission line whose impedance is given (RAM 44) by

$$Z_0 = 120\pi \frac{a}{b}, \qquad \text{for } a \ll b,$$

where a is the separation of conductor and b is the length along the beam. For straps about an inch long, the mismatch to a 50-ohm coaxial line should not be serious, provided that the coaxial-to-plate transition is efficient. Examples of such hairpins, which were insulated from the pole faces by thin strips of teflon, are shown in Fig. 20. Of course, the impedance is modified because the structure is placed in the gap and the fact that the hairpin is shorted makes useful impedance measurements almost impossible, but the strap does carry a TEM mode which has a magnetic field oscillating parallel to the beam and it does work as a hairpin and seems to be efficient. Being unshielded, these straps radiate, so that there is considerable fringing field in the gap, making it difficult to estimate what the effective length of the oscillatory field really is and--more seriously--what configuration it has. Examples are shown in Section V of resonances distorted by this distribution of mode structure along the beam. Furthermore, when the wavelength is of the order of the size of the vacuum can, unshielded hairpins can excite cavity oscillations in the can. It was found, in the excitation of a strap with a frequency-modulated 500-Mc signal for locking the C field, that the modulation apparently reached the detector by this means, masking the signal obtained from the beam itself. Installing a conducting reflector (aluminum foil) between the B magnet and detectors with only a small beam hole did alleviate the problem. A better solution would be to use a shielded structure in which all rf fields are confined to the insides of the conductors.

The obvious shielded structure is a coaxial line with a slot cut for the beam to pass through, and with the line terminated in a short beneath the beam path. If the axis of the coaxial line coincides with the beam line the rf magnetic field is perpendicular to the beam if the TEM mode (RAM 44) is propagated, but is in two out-of-phase patches

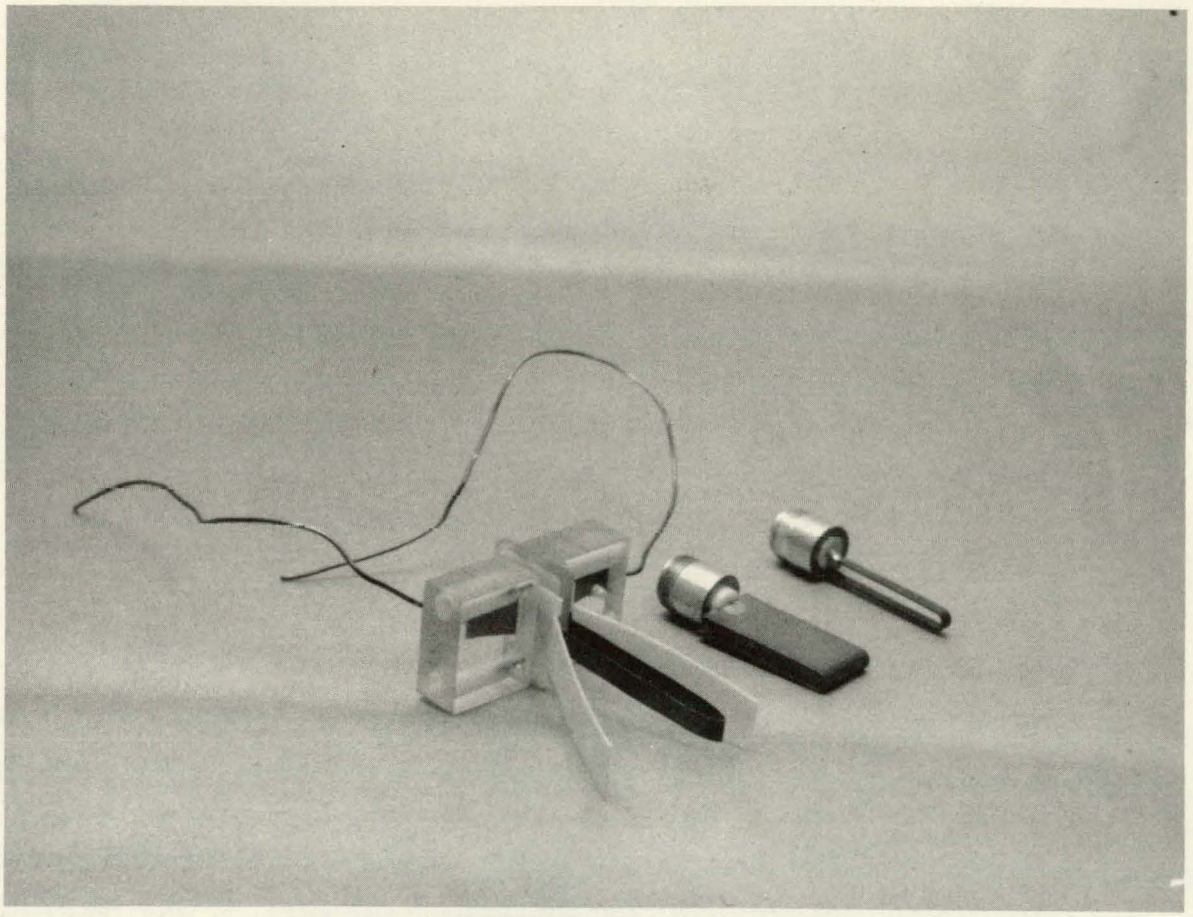

ZN-2385

Fig. 20. Typical strap hairpins of early and later design.

separated by the inner conductor. If the static field is homogeneous, a Ramsey interference pattern for oscillatory fields 90 deg out of phase can be observed (WOO 56) on σ transitions. If the axis of the coaxial line is to one side of the beam line the rf magnetic field is mostly parallel to the beam and π transitions can be observed. The magnet gap in this machine is too small to allow insertion of a coaxial line of reasonable impedance offset so as to observe π transitions, but an "eccentric" coaxial line with the center conductor off center was built which, while sacrificing some power owing to impedance mismatch, allows both π and σ transitions to be observed (without moving the hairpin).

Originally this design was incorporated into separate structures designed to be placed about 12 in. apart in the gap so as to give very narrow Ramsey patterns for π transitions, but again owing to field inhomogeneities, no interference patterns were observed. These hairpins are shown in Fig. 21.

The use of short-circuited hairpins presents difficulties in the microwave region because of the high standing-wave ratio present in the transmission line. Although these hairpins are not good short circuits, having a high reactive component, the reflection coefficient due to their presence as a line termination is high enough to make it difficult to match out with stubs or line stretchers. Furthermore, this large reflection from the end tends to mask out reflections from the coaxial vacuum feed-through and the coaxial-hairpin connection, so that it is difficult to say, without actually observing transitions in the beam, whether the rf power is actually getting to the beam vicinity or is being mostly reflected by the other discontinuities. The presence of high standing waves at high frequencies requires some form of isolation, usually an amplifier, for the oscillator; otherwise frequency pulling can be expected.

Power is usually measured by means of a directional coupler in the line. If the VSWR is high, as it is for a shorted hairpin, the power reading of the transmitted (forward) wave has only a relative

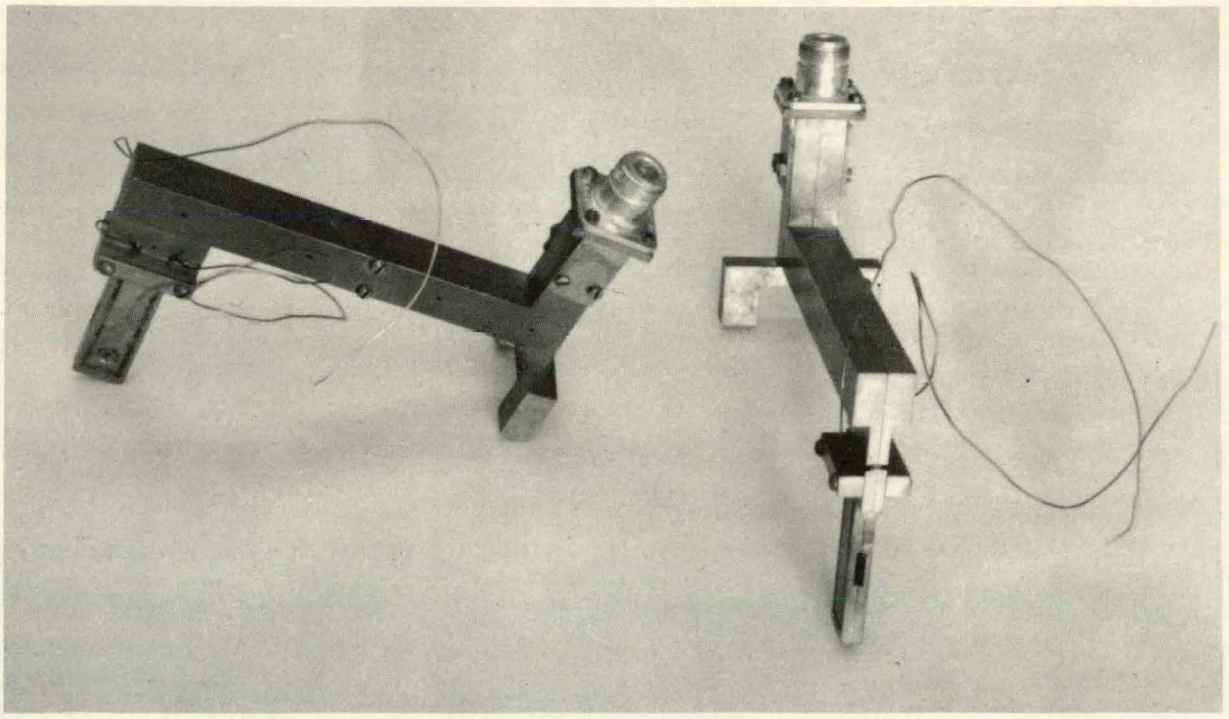

ZN-2392

Fig. 21. Original configuration of coaxial hairpins.

meaning (KIN 52), but it is still useful to specify this reading, since the level required for optimum perturbation must be experimentally determined for each hairpin as a function of frequency by observations of resonances in beams of stable isotopes.

If a hairpin is unshielded, a small coupling probe located near by can give a relative indication of power reaching the end. Such probes have been used (STR 57, KUS 59) for some time in atomic beam work and one was used for a short time in this experiment to check the efficiency of the coaxial feed-through and the coaxial-parallel-plate transition. A small loop about 1/8 in. in diameter was fashioned by bending the center conductor of a piece of RG-58/U cable in a circle and soldering it to the outer conductor of the cable. The outer conductor was soldered to the underside of a strap hairpin so that the loop was in a vertical plane normal to the beam line. The voltage induced in the coaxial line is proportional to the rf current at the hairpin short. A coaxially mounted crystal detector is attached so that the rectified crystal current is proportional to the rf power at the shorted strap which is close to the beam.

In an attempt to produce a Ramsey pattern, a strap 1-1/4 in. long, looking like an inverted U (see Fig. 22) was constructed to see if it would produce two patches of inphase rf field, but it was found that the two ends were not really isolated, owing to the radiated field from the coaxial-hairpin transition, and this hairpin acted like a single strap, giving a 10-kc resonance width on field-independent lines. Another strap 2 in. long was constructed to try to reduce the line width (see Eq. (IV. 2)), but in the light of possible distortions (RAM 56) due to Doppler shift and possible non-TEM-mode structure, the resonances obtained with this strap cannot be considered reliable. Section V of this thesis shows the poor quality of resonances obtained with this hairpin.

In a further attempt to see Ramsey patterns, the previously mentioned eccentric coaxial hairpins (Fig. 21) were cut and soldered carefully together to make a fixed, rigid structure as shown in Fig. 23.

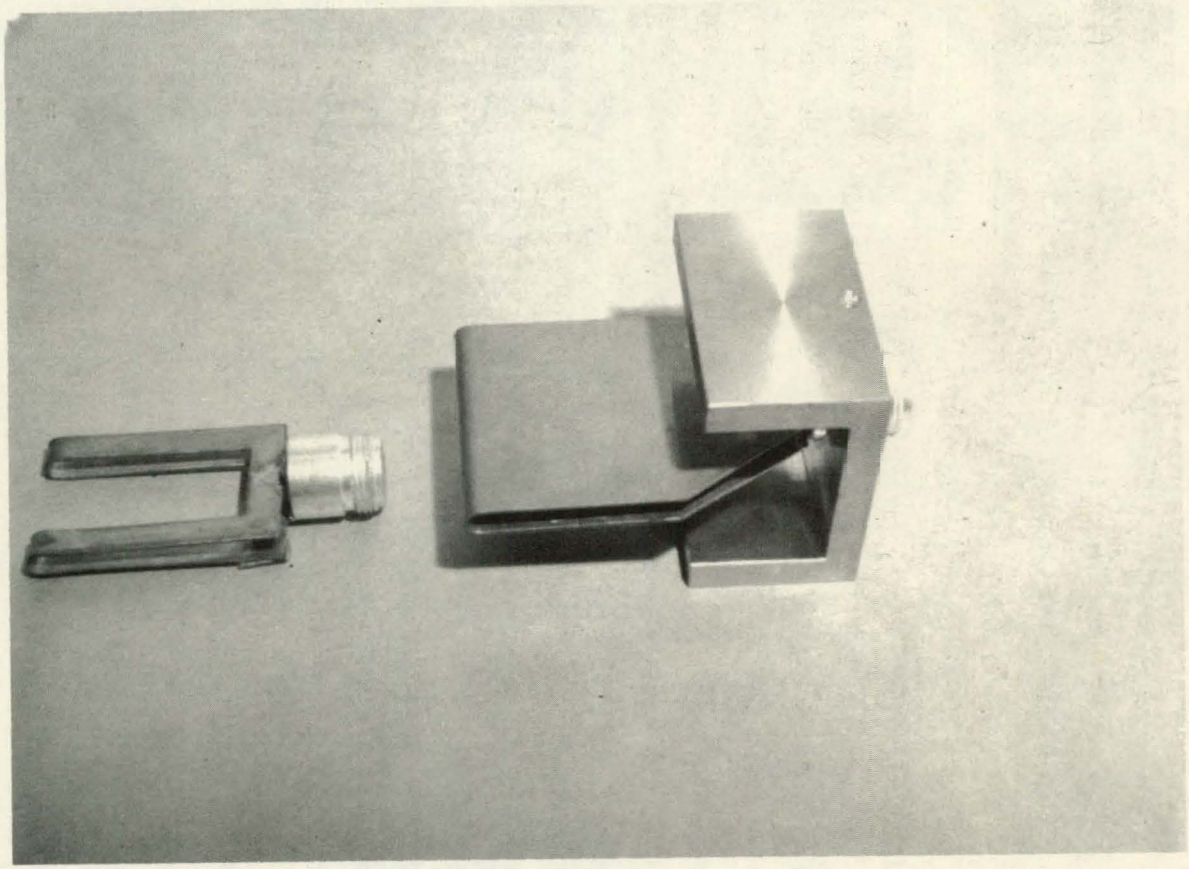

ZN-2386

Fig. 22. Larger strap hairpins, one of which is shown in its mounting bracket.

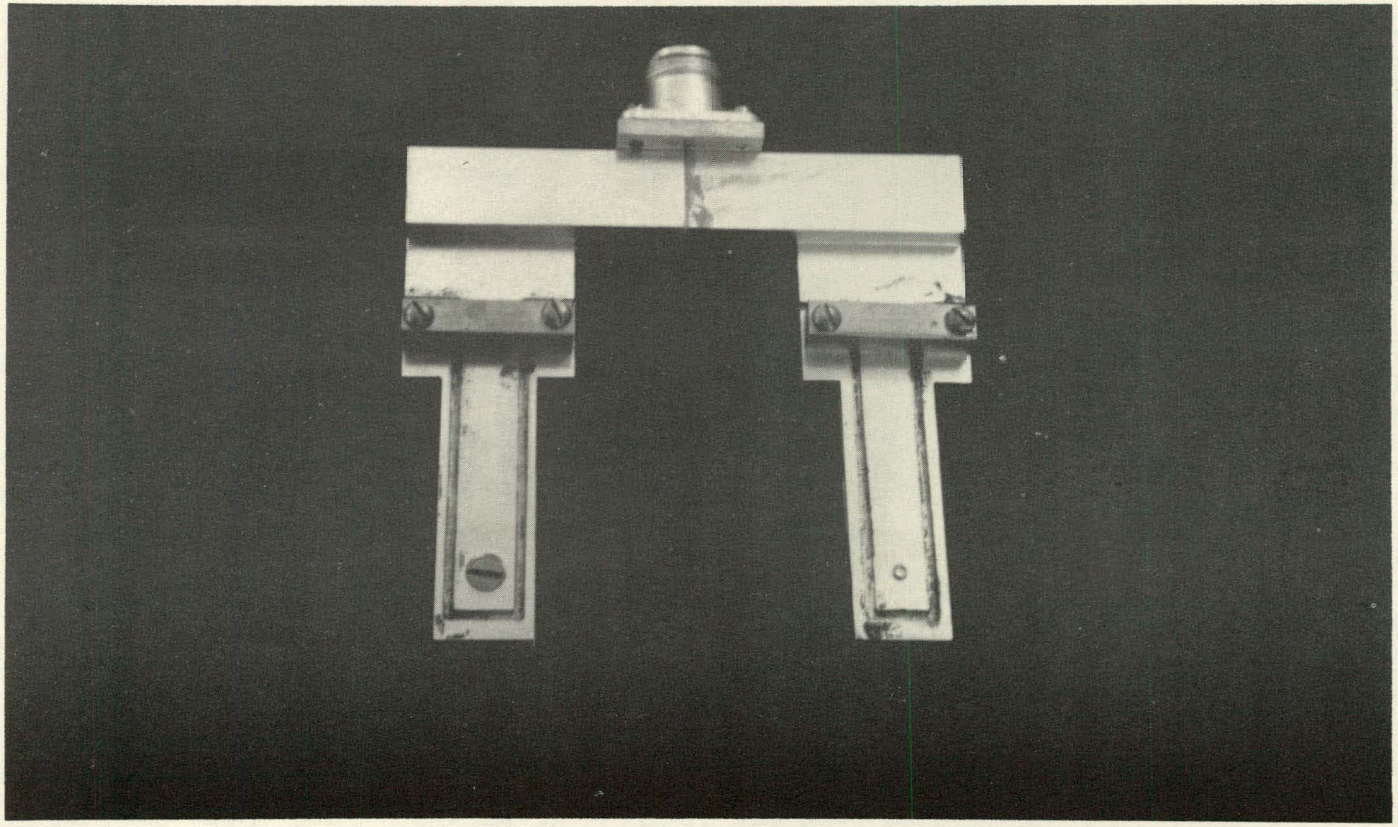

ZN-2389

Fig. 23. The Ramsey structure.

Figure 24 shows details of its construction. This gave sufficient isolation of the two rf fields, and satisfactory Ramsey patterns were obtained (see Section V). However, by fixing the length from the shorted end to the junction of the two lines, the frequency band over which the hairpin is useful is reduced. The input impedance of two shorted stubs is $\frac{1}{2} Z_0 \tan(2\pi \ell/\lambda)$, where Z_0 is the characteristic impedance of the line (approx 50 ohms) and ℓ is the length of the stub; whenever the tangent takes on the value 0 or ∞ (which is pretty often in the microwave region for $\ell \approx 10$ cm as used in this hairpin), all input power is reflected from the junction and no rf reaches the beam. The usual way around this difficulty is to bring both arms of the hairpin out of the vacuum and connect a trombone structure so that the stub length ℓ can be varied simultaneously for both. This necessarily means that the arms would be several wavelengths long, and can lead to phase shifts due to slight differences in length between the two arms which are almost impossible to measure electrically in this configuration. It was decided that a fixed length was easier to use, and that some idea of the possible phase shift present could be obtained by observing resonances in each of the two orientations of the structure. The possible phase shift between the two separated fields is probably the most serious distortion of the Ramsey pattern and can easily shift the resonance peak up to half a line width from the Bohr frequency.

A traveling-wave hairpin is very attractive if the magnet gap is wide enough to permit mounting a coaxial line with its axis off the beam line. In this case the line is terminated in a matched load, which can be a thermistor mount so that transmitted power can be read directly. The atoms see the traveling wave as an oscillating field, as before, and now all the matching and reflection problems are eliminated. This should be tried in future experiments, especially for the locking hairpins in which the modulation must be prevented from leaking to the detector.

Also tried were hairpins of shorted strip transmission line (PAC 57). These had the slight advantage of needing no insulation from

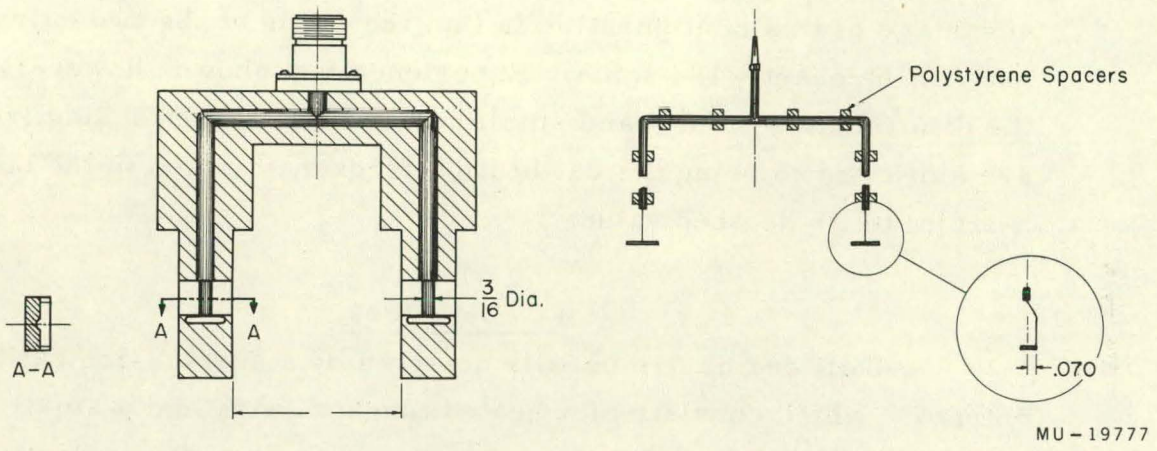

Fig. 24. Details of the Ramsey structure.

the magnet pole tips, but higher-order modes were found to be present above 3000 Mc, causing nonuniform distribution of the oscillatory field along the beam, therefore these structures were discarded.

Two hairpins are used in these experiments, one carrying the locking frequency and the other carrying either the field calibration or search frequency. Mutual interference problems make the connection of both oscillators to one hairpin impractical, so for effective isolation two hairpins are used, separated by less than 1 in. The only disadvantage of this configuration is that the fields at the two hairpins may not be exactly the same. Experience has shown, however, that the difference is small, and small corrections of the locking frequency are sufficient to bring the calibration frequency (taken in the other hairpin) to its desired value.

F. Detectors

Alkali beams are usually detected by a surface-ionization detector, which consists of a heated tungsten wire and a small collector plate. Since the work function of tungsten exceeds the ionization potential of the alkalis, essentially every alkali atom that strikes the heated wire comes off as a positive ion. These ions can be attracted by a few volts negative potential to the small plate and the ion current measured with a good electrometer. It is possible to cause these ions to pass through a mass spectrometer so that only those ions of a desired mass are detected. With such a combination K^{40} beam intensities have been measured, although this isotope is only one part in 10^4 of the total in beams of natural potassium (EIS 52). Radioactive cesium isotopes have also been observed with mass spectrometers (STR 57). Jhan M. Khan (at this Laboratory) is constructing such a spectrometer, which will be attached to this apparatus for detecting radioactive beams.

The method of detecting radioisotopes used in this Laboratory is to expose a sulfur surface to the beam for a fixed time and to count the collected activity on some suitable low-background counter (NIE 57). The sulfur is packed into a slot in a small brass "button" of

standardized dimensions. A rotary button loader with vacuum lock is mounted on the rear end plate of the can, which allows these buttons to be inserted from the outside, exposed at the machine focus, and withdrawn for counting. This structure can be seen in Fig. 3.

Three hot-wire ionization detectors are provided in this machine. The first is a 0.010-in. K-free tungsten wire mounted vertically in the center of and 1/4 in. behind the exit slit of the apparatus. This exit slit, 0.065 in. $\times$1 cm, is in the center of the exit plate that hangs from the port cover of top port D; provision is made for translational motion of the exit plate with the attached detector in a plane normal to the beam line. A micrometer screw and dial position indicator are provided for accurate positioning. The purpose of the exit plate is to prevent deflected and scattered radioactive atoms from reaching the focal point at the button loader and contributing to the machine background. The assembled detector is shown in Fig. 25. A 1$\times$1-cm copper plate serves as the ion collector which is connected through a re-entrant kovar seal to the inner conductor of an external female type-N connector on the top plate. The filament is at ground potential and the plate at -45 v. Ion current is read by a Beckman Model 5 Micro-microammeter, a vibrating-capacitor electrometer. This detector serves to monitor the beam as it is brought to operating level, to line up the oven with respect to the collimator and stop wire, and to detect the C magnet locking resonance. When used as part of the locking system, it is connected to the phase detector (see Appendix C) through a small preamplifier mounted on its output connector. With a filament current of 0.9 amp, background ion current is 1×10^{-12} amp; a typical full beam reads 2×10^{-10} amp and a resonance in a stable isotope is about 1×10^{-11} amp.

A second ionization detector is mounted in a brass cylinder on the rotary button loader, as can be seen in Fig. 3. It consists of a .070-in. K-free tungsten ribbon mounted vertically (when in position) with a small copper plate to one side acting as collector. The detector serves to calibrate the static C field at the search hairpin by observing

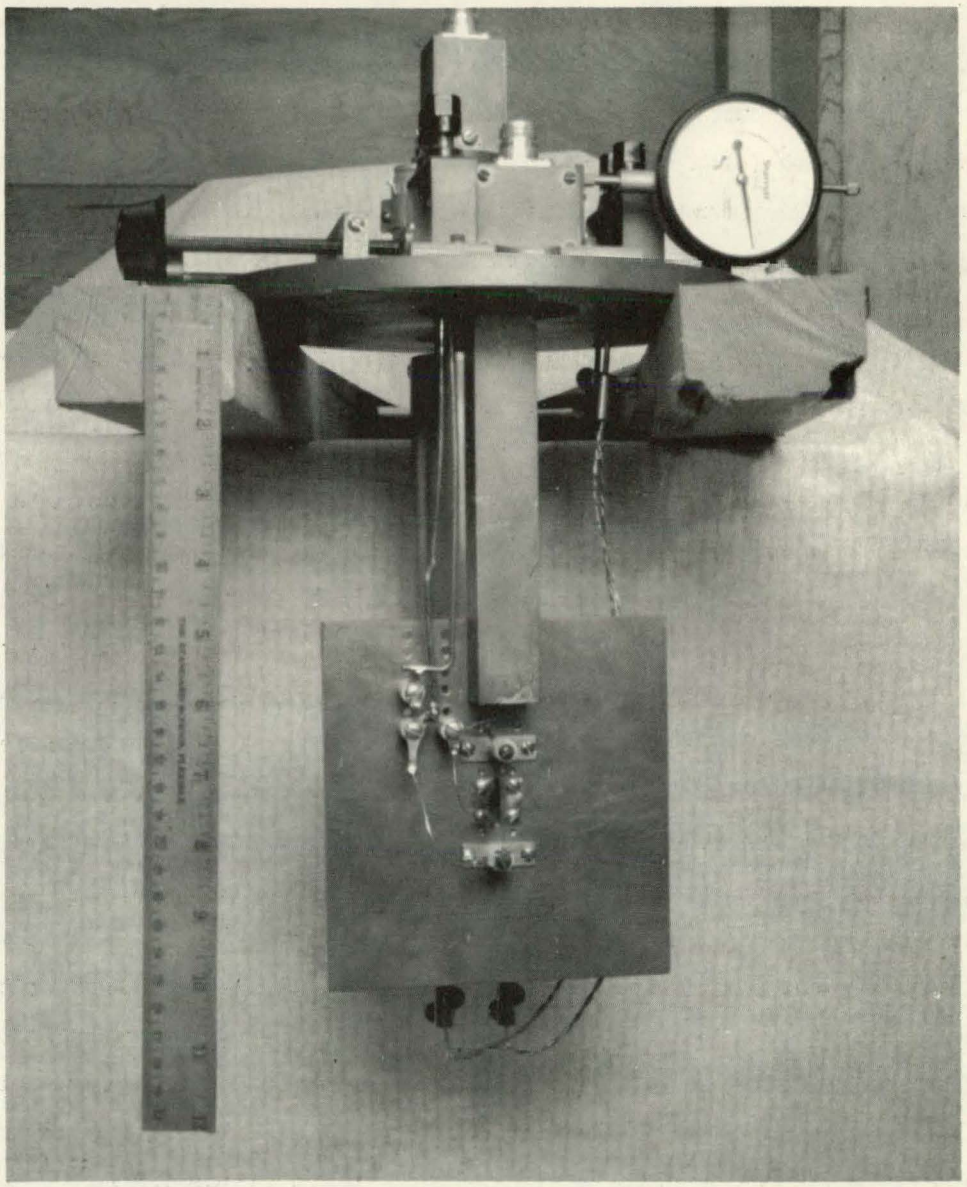

ZN-2387

Fig. 25. Rear view of the detector assembly, showing the exit slit in the exit plate.

resonances in the stable carrier. Since the locking and search hairpins are at slightly different positions in the magnet, this step is necessary to measure the actual field at the search hairpin. When calibration has been accomplished, the electrometer and filament connections are removed so that the button loader may be freely rotated during button exposures. The loader has a window position opposite the detector position between the two button locks so that the cold filament need not be exposed to the beam during a run. With a filament current of 6 amp, background ion current is about 1×10^{-11} amp.

A third hot-wire ionization detector, also 0.010-in. K-free tungsten wire, is mounted in front of the exit slit inside a mu-metal cylinder in which holes have been cut to allow free passage of the beam. This structure can be seen in Fig. 26. This detector sits to one side of the beam axis and monitors the flopped-out beam as described in Section II. C. With the electrometer connected to this detector during button exposures, any changes of the full beam intensity during a run can be monitored and the counting rates of individual buttons normalized to a constant full-beam level. The procedure used is to take a reading of the full beam on the exit-slit detector, turn on the deflecting fields, and raise the stop wire into place. The monitor detector is moved laterally until it sits on the peak of the flopped-out beam, and the reading at that point is taken. This establishes the monitor calibration for that run. At the end of the run the monitor is again read, the deflecting fields turned off, the stop wire lowered, and the calibration checked by reading the full beam again on the exit-slit detector. Experience shows that the calibration is linear and that the two points lie on a line intercepting the origin of a plot of the full-beam reading against monitor reading. That the use of this detector for normalization gives consistent results, together with observations of the linearity of the monitor despite small changes of deflecting fields and oven temperature, indicates that the method is quite satisfactory.

Originally a surface-ionization detector was placed in the buffer chamber to look directly at the beam emerging from the oven

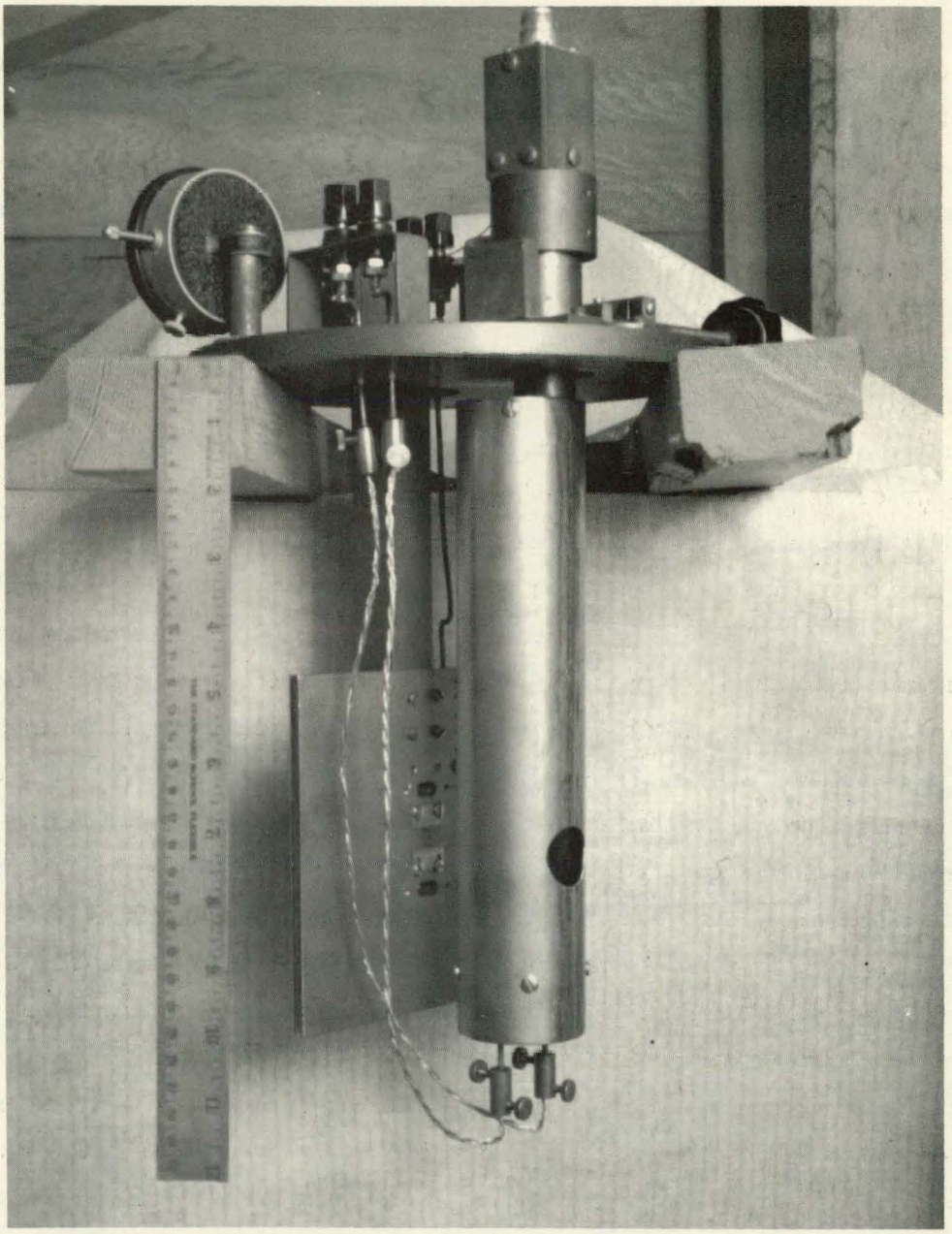

ZN-2388

Fig. 26. Side view of the detector assembly, showing the monitor detector housing.

before any deflections take place. Heating of the oven by electron bombardment caused the operation to become erratic. This condition could not be remedied, so the detector was abandoned and the method used as described above.

G. The Counting System

Figure 27 shows a button used to collect the beam activity, and the scintillation counter assembly used for counting the activity. The counter is a very thin NaI(Tl) crystal (approx 2 mm) backed by a phototube whose output is fed to a single-channel pulse-height analyzer and scaler. A ball bearing in the counter housing fits into a slot on the button, so that a constant counting geometry is maintained for all buttons. The sulfur surface of exposed buttons is covered with a single layer of Scotch tape before being brought to the counting area, to prevent any accidental brushing off of activity. Four of these counters are used in conjunction with this machine, each of which is mounted in a thick lead pig to keep background to a minimum. The counting arrangement is shown in Fig. 28.

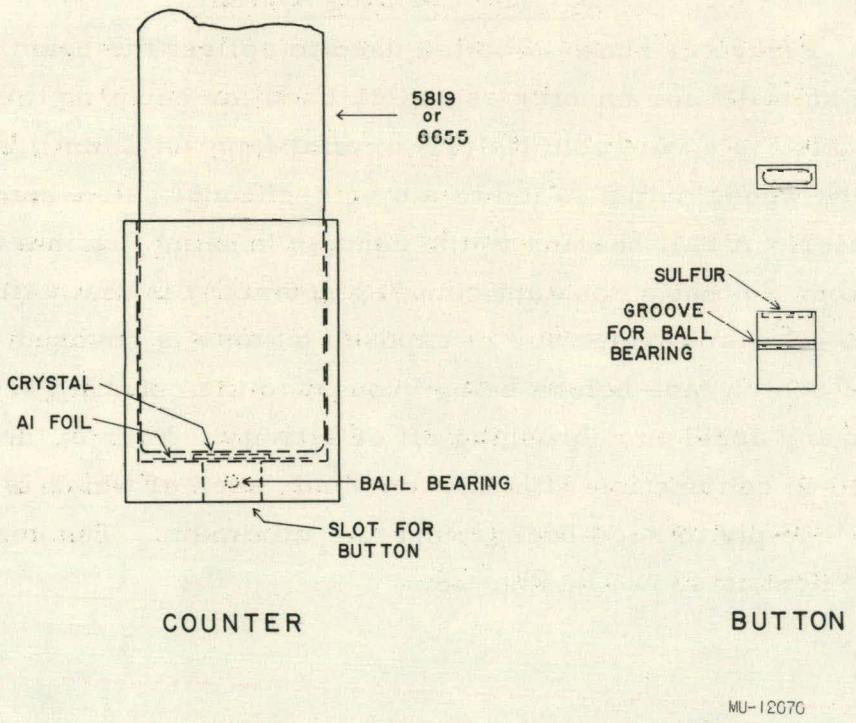

Fig. 27. Scintillation counter and button.

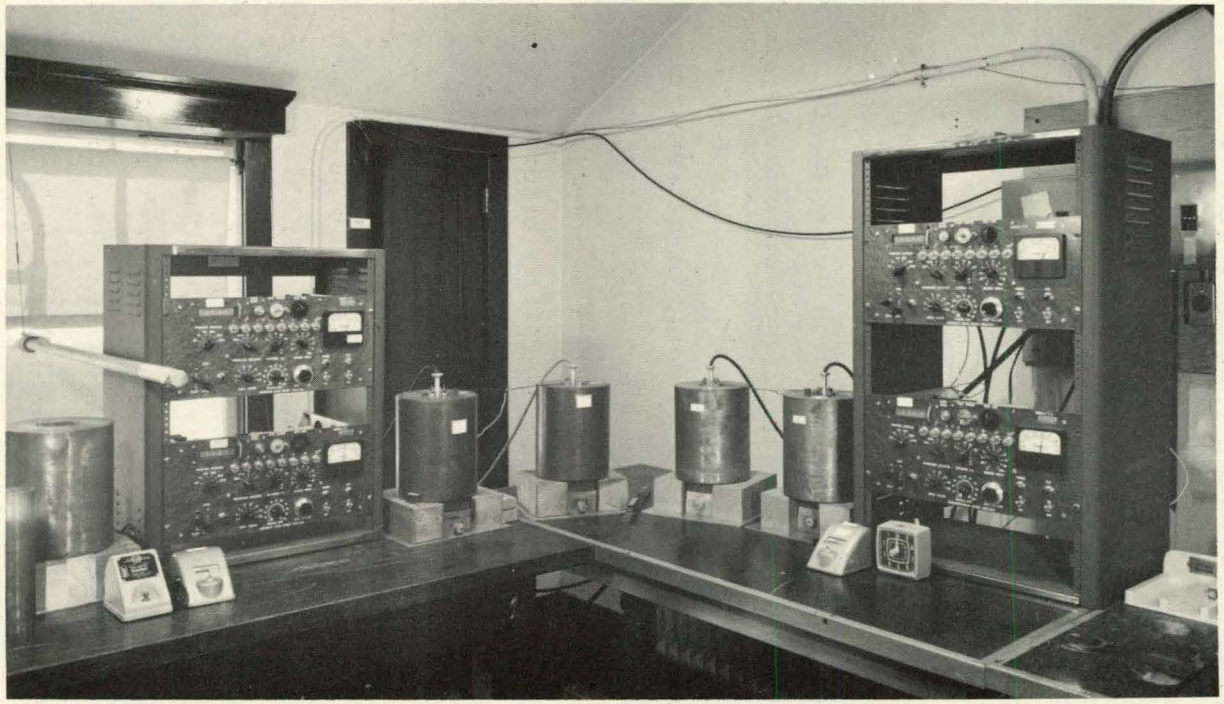

ZN-2384

Fig. 28. Counting facilities, showing the four scintillation counters in lead pigs, and associated scalers.

V. EXPERIMENTS ON STABLE ISOTOPES

This section includes the initial line-up of the apparatus, early results, and measurements on stable isotopes whose $\Delta\nu$ and g_I are already known, with the purpose of checking the proposed experimental technique for radioactive isotopes.

A. Machine Line-Up and Early Resonances

After the magnets had been placed in the can on their base plate the magnets were made level by adjusting screws on the three support points of the can. Cross hairs were installed at either end of the open can and, with the help of a telescope, the magnets were aligned optically by using the knife edges mounted for that purpose (see Fig. 10). Since a beam of atoms is deflected more than a beam of molecules, because of the much larger effective magnetic moment, the line-up is not as critical as it would be for a molecular machine. When the alignment was as good as could be determined, the collimator and stop wire were inserted; these actually define the centerline for the beam. They were found to be 0.0057 and 0.0066 in., respectively, from the optical centerline. This was satisfactory for an atomic beam. The magnets were locked in place with the adjusting screws and the rest of the machine was assembled.

The initial beam line-up was done with stable potassium. Resonances were found by using a crude strap hairpin and later the coaxial hairpins (Fig. 21) were installed. At this time adjustment of the C magnet current was very crude, consisting of a large rheostat and a pair of stainless steel tubes with an adjustable jumper. Some feeling was developed for the optimum rf power required for resonances by using the various hairpin arrangements, and the dependence of the resonance width on the various parameters was studied.

B. Double Resonance

As explained in Section II. C, $\Delta F = 0$, $\Delta m = \pm 1$ transitions are not refocusable in this machine. In analogy to the work of Feher (FEH 56, FEH 58) in the solid state, an attempt was made to see these transitions by observing their effect on simultaneously excited $\Delta F = \pm 1$ transitions. Three hairpins are used, the outer two (in this case the coaxial type) connected together and fed in phase, and the central one (a strap type) used to excite the $\Delta F = 0$ transition. Consider now a K^{39} atom in a magnetic field corresponding to the Zeeman region of hyperfine structure where the F, m_F representation can be used. Figure 29 shows the position of the energy levels in strong field to indicate that an atom must undergo a change of state from the bottom group to the top group or vice versa to be refocused. If, for example, an atom starts in the state 1, 0, the first hairpin carrying ν_1 flops the atom into the state 2, 0. If ν_4 is present in the middle hairpin, the atom is flopped into the state 2, 1. As the atom passes through hairpin No. 3, also carrying ν_1, it undergoes no transition, since selection rules forbid $\Delta F = 1$ transitions from this state with the frequency ν_1. Thus the atom has moved into the group having opposite sign of effective moment and is refocused. If ν_4 is not present, hairpin No. 3 will flop the atom back into state 1, 0 and the atom is not refocused. Actually, because of the transition probabilities involved, some atoms are left in the state 2, 0, which increases the refocused background. With ν_1 fixed, an oscillator sweeping over ν_4 traces out the $2, 0 \leftrightarrow 2, 1$ transition superimposed on the higher background owing to the $1, 0 \leftrightarrow 2, 0$ transition, provided the rf power associated with ν_1 is properly fixed. Figure 30 shows the variation of the intensity of the ν_1 transition as a function of rf power for hairpin No. 1 alone and with hairpins No. 1 and No. 3 connected. As expected, the optimum perturbation power for one hairpin should give the maximum cancellation for two. With ν_1 set at this optimum power, maximum flop from ν_4 is obtained. These resonances were seen in this apparatus (BRI 58) with all three hairpins in the same field. The same effect

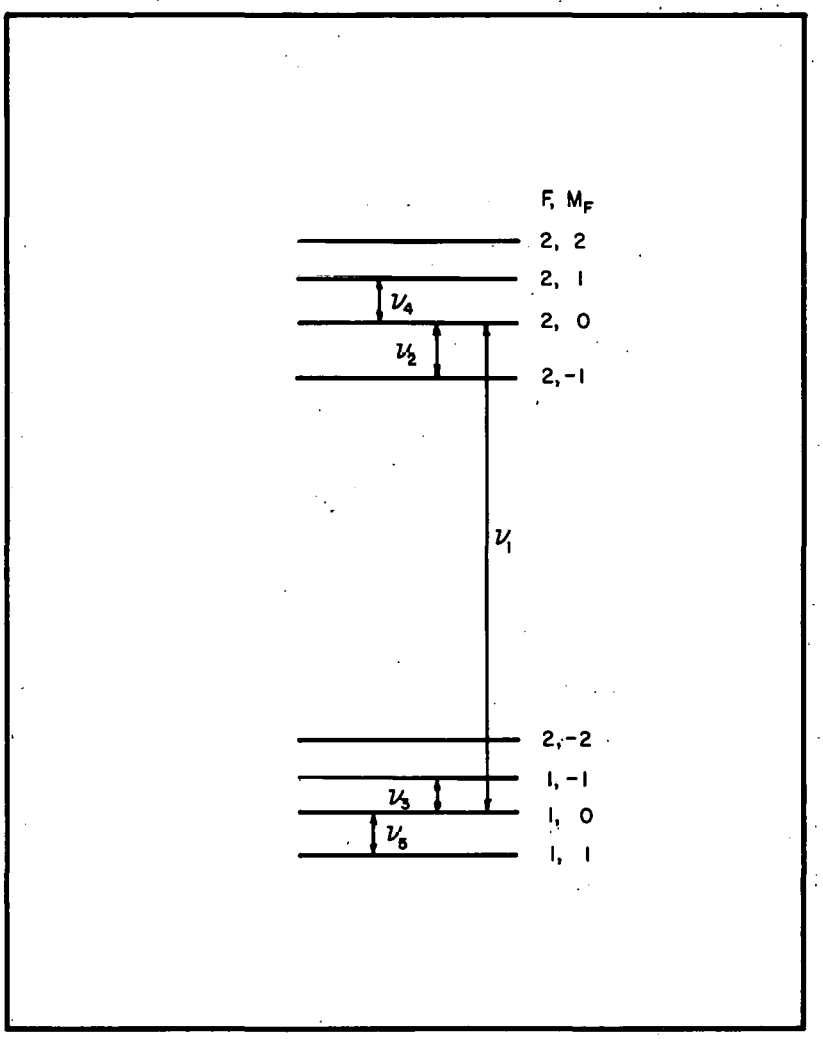

Fig. 29. Energy levels of K^{39} in a strong field; ν_2, ν_3, ν_4, and ν_5 are observable with ν_1 in the outer hairpins.

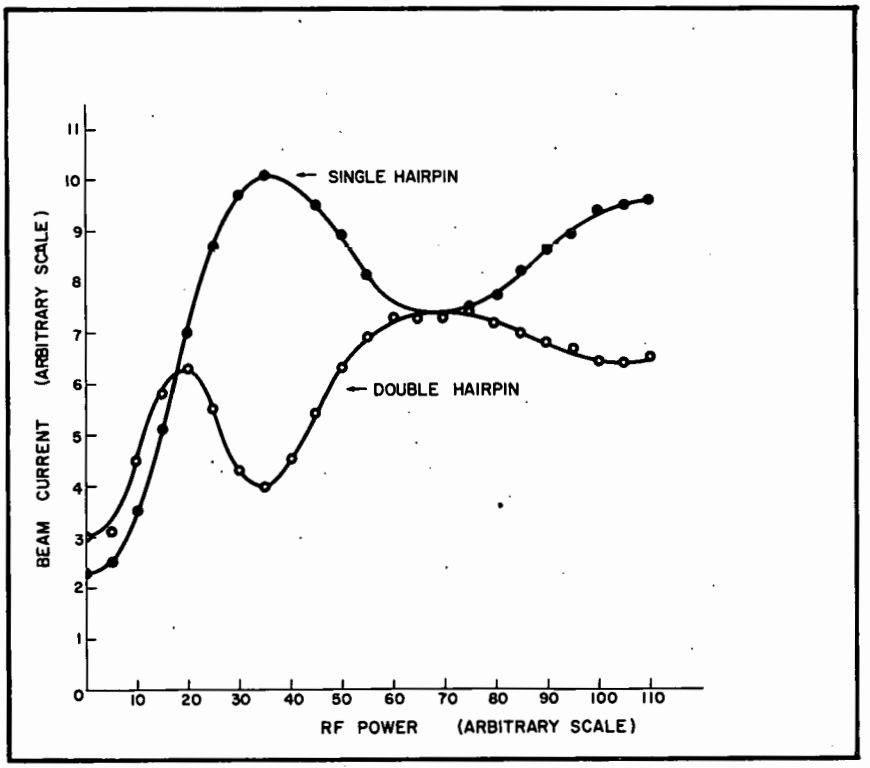

MU-15030

Fig. 30. Flop intensity as a function of rf power for K^{39}; rf ≈ 8 Mc.

was seen independently by Woodgate and Sandars at Oxford (WOO 58) with the outer hairpins placed in the fringing fields between the C magnet and the deflecting magnets. It is, of course, not necessary that the fields be the same, so long as the frequencies are adjusted for transitions between proper levels. In fact, for the obvious application of this method for measuring g_I, it would be advantageous for the $\Delta F = 1$ transitions to take place in the Zeeman region, where these lines are reasonably field-independent, and for the $\Delta F = 0$ transition to take place in high field, where the transitions go through a broad field-independent region and the separation $2g_I\mu_0 H/h$ is as large as possible. This technique was used by Sandars (SAN 59) to measure the nuclear moment of Eu^{151}.

It should be noted that when ν_1 is the frequency of an unresolved doublet, as indicated in Fig. 31, certain $\Delta F = 0$ transitions, ν_2 and ν_3, between states involved in the doublet transitions are obviously not observable, whereas ν_4 and ν_5 would be observable. However, if an adjacent $\Delta F = 1$ transition is chosen, ν_2 and ν_3 can be seen. All possible $\Delta F = 0$, $\Delta m = \pm 1$ transitions were observed in this apparatus by choosing proper $\Delta F = 1$ frequencies in the outer hairpins.

Nothing further was done with this effect, as it was not practical to modify the interior of the apparatus. Attempting to operate all three hairpins in high field would not be satisfactory because the desired $\Delta F = 1$ transitions are very broad and the signal from the $\Delta F = 0$ line would be too small to see.

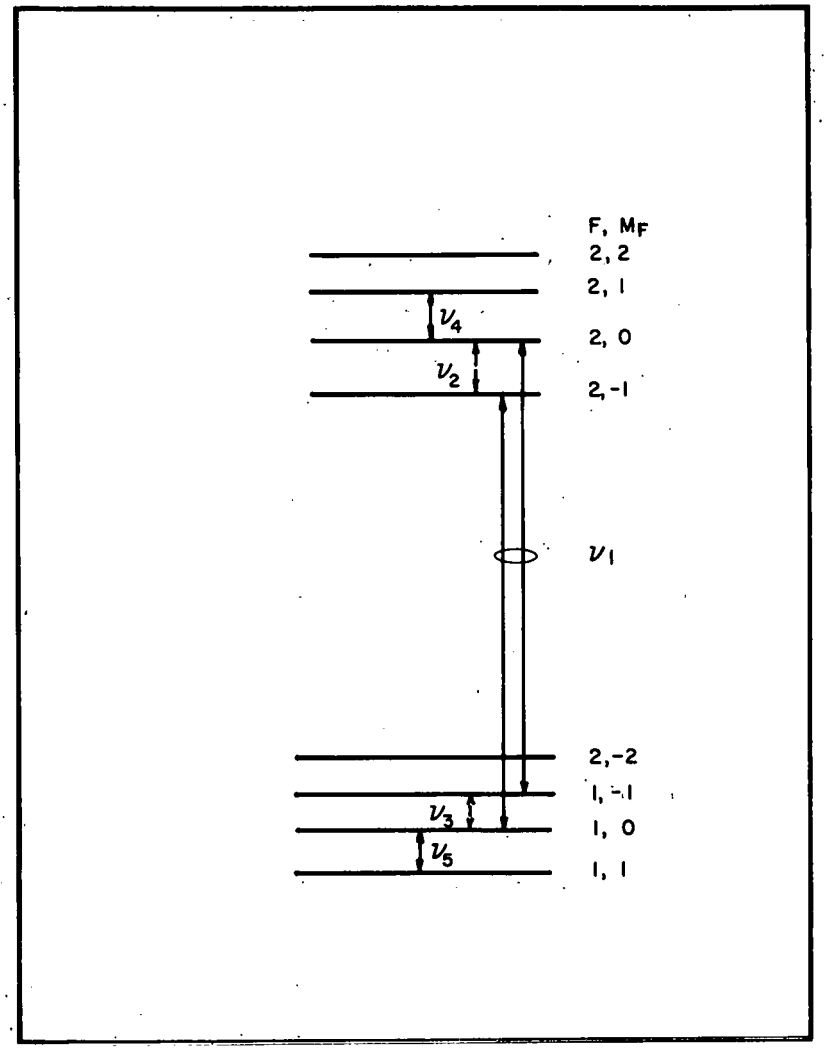

Fig. 31. Energy levels of K^{39} in a strong field; ν_1 is an unresolved doublet; ν_2 and ν_3 are not observable with ν_1 in the outer hairpins.

C. Measurements on Rb^{85}

As expected, the resonances observed by using both strap and coaxial hairpins broadened considerably owing to inhomogeneity of the C field, but widths were reasonably close to the expected values (Eq. (IV. 2)) for field-independent lines. Typical values for a 3/4-in. strap are: on field-independent lines, 20 kc; field-dependent Zeeman lines, 50 to 400 kc; the $\Delta F = 0$ refocusable transition in the region 10 to 600 gauss, 100 kc to 1 Mc.

When the 2-in. strap was installed, it was immediately used for investigation of radioisotopes. When stable Rb^{85} was investigated in the region where the nuclear moment is measured, very poor quality resonances were observed, an example of which is shown in Fig. 32. Instead of a single resonance peak 8 kc wide, somewhat broader lines having more than one peak were observed. This distortion is probably caused by a combination of Doppler shift, stray fields from the coax-hairpin transition, and radiation fields in the gap. Because of this poor shape, the uncertainty in the value of the difference of the doublet was too large to obtain a usable value of g_I, and it became imperative to use some sort of shielded structure, preferably one using the method of separated fields.

As was mentioned in Section IV. E, the coaxial hairpins were spliced together so that the separation of the fields would be of the order of 2 in., since work with straps indicated that the field would be homogeneous enough over this region; the separation was actually set by the requirement that the arm lengths be such that the input impedance in the 3,000- to 4,000-Mc range be approx 50 ohms. With a separation of 2-1/4 in., an interference pattern with a central peak about 3 kc wide was expected. As shown in Fig. 33, a satisfactory reasonably symmetrical Ramsey pattern was indeed seen with the central peak 3 kc wide.

Although the hairpin structure was carefully machined to keep the two arms of equal length, the slight asymmetry indicated that there probably was some phase shift. Other distortions (RAM 56) should be

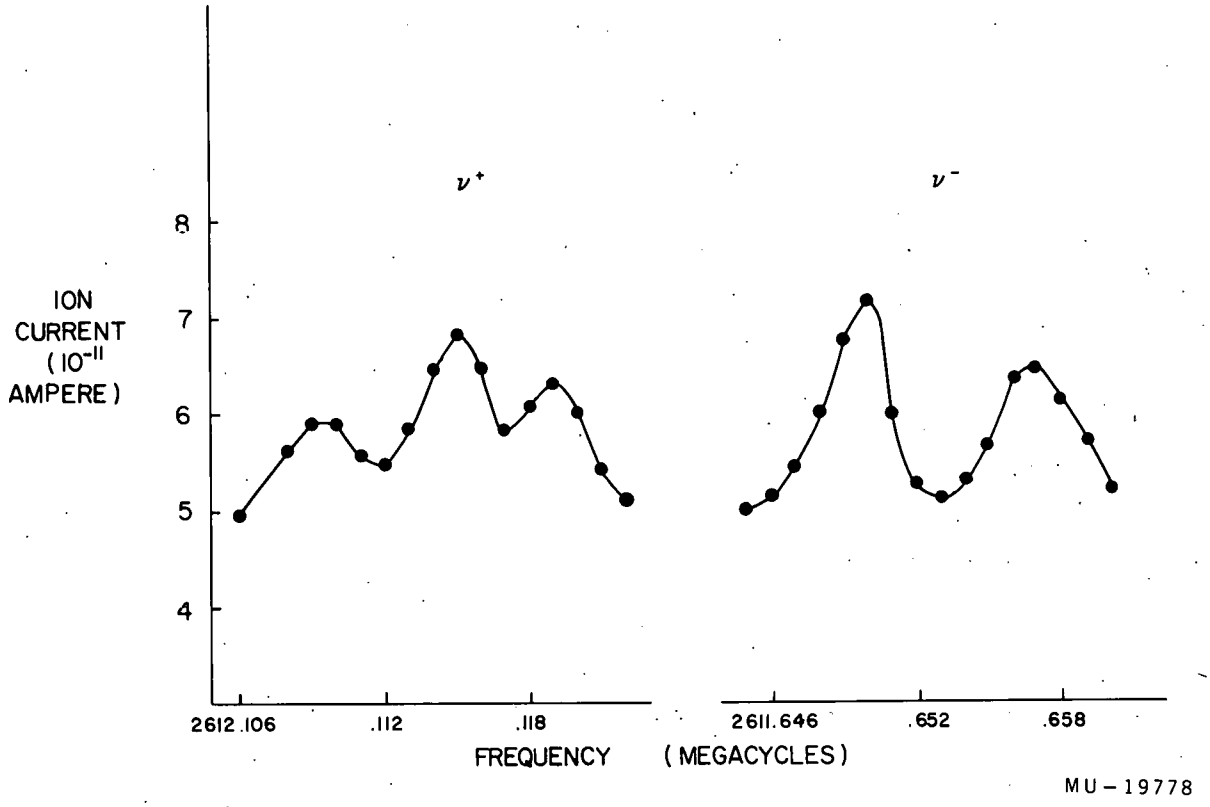

Fig. 32. Rb^{85} lines observed with 2-in. strap hairpin, showing distortion.

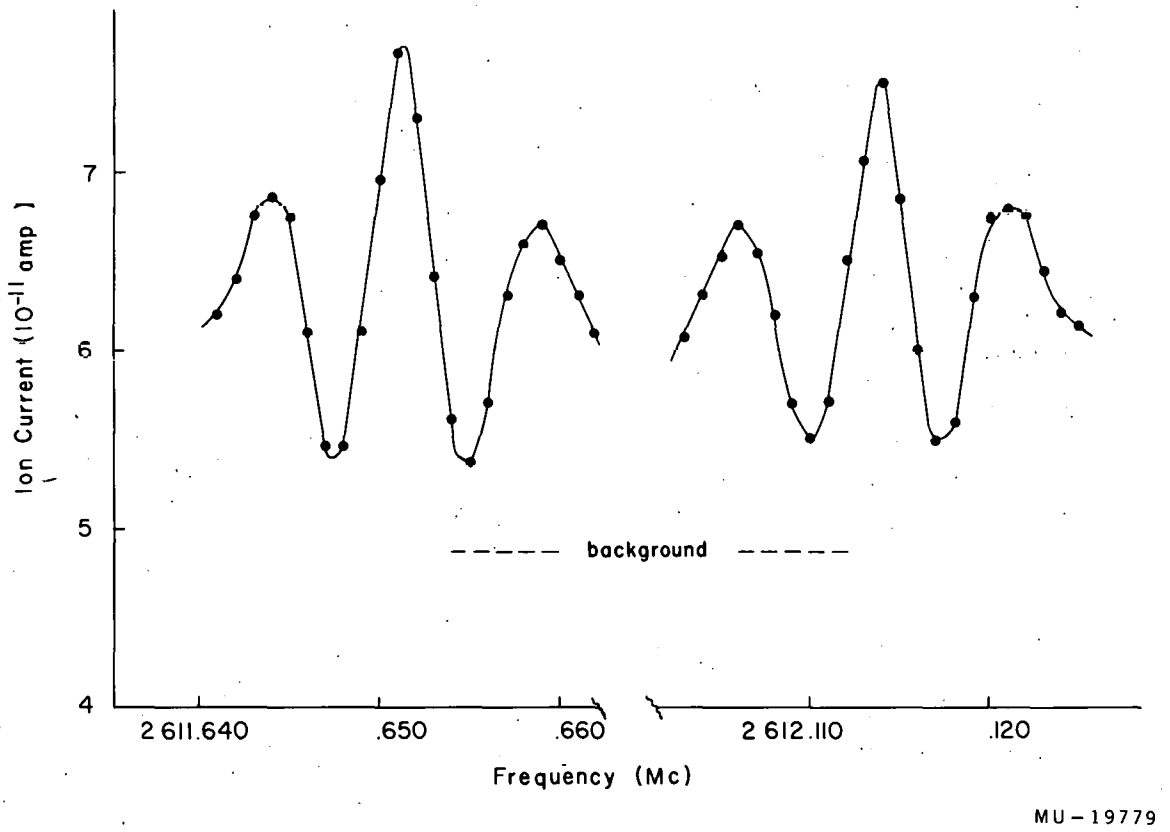

Fig. 33. Ramsey patterns observed on the Rb^{85} doublet.

negligible. Estimates of the shift of the peak (HOL 59) indicated that it should be of the order of 0.1 kc. The hairpin was reversed in the magnet and the resonances of Fig. 33 were observed again at the same field and within the uncertainty of the position of the peak, ±.2 kc, no shift was seen, indicating that the analysis developed in the reference above for the Atomicron beam tube probably gives a general idea of the size of shift to be expected in this apparatus (HOL 60). Even if a phase shift is present it is not likely that it is so frequency-sensitive that a change of 0.5 Mc out of 2,600 Mc will affect it, therefore the moment calculated from the difference of the two peaks should be insensitive to this distortion.

Because of field broadening, field-dependent lines excited with this hairpin show no interference effect and the observed line is essentially a superposition of the broadened lines of the two separated fields. The line is symmetrical, as shown in Fig. 34, so that it is possible to observe calibrating resonances with this structure. The uncertainty of the value of H in this region due to the uncertainty in the placing of the peak of this relatively broad line is certainly greater than the actual variation of field in the region, for otherwise no interference patterns could be seen.

As mentioned before, an out-of-phase Ramsey pattern can be seen on σ transitions from each coaxial hairpin, since the eccentric position of the center conductor produces components of the oscillating field parallel to the C field. Since the transition probability on resonance is zero for this pattern, there is no interference pattern between two sets of these patches, and the single patterns overlap if the fields are the same. Observation of the field-independent Zeeman line $3, 0 \leftrightarrow 2, 0$ in Rb^{85} (Fig. 35), shows the shape of the observed transition by using the Ramsey structure. The width of the central minimum depends on the separation of the two patches, and because this is quite small the minimum is broad. It is too broad to be of much use here, but some new hairpins based on this idea are being constructed that should give narrow minima and allow odd-A $\Delta\nu$'s to be measured with precision.

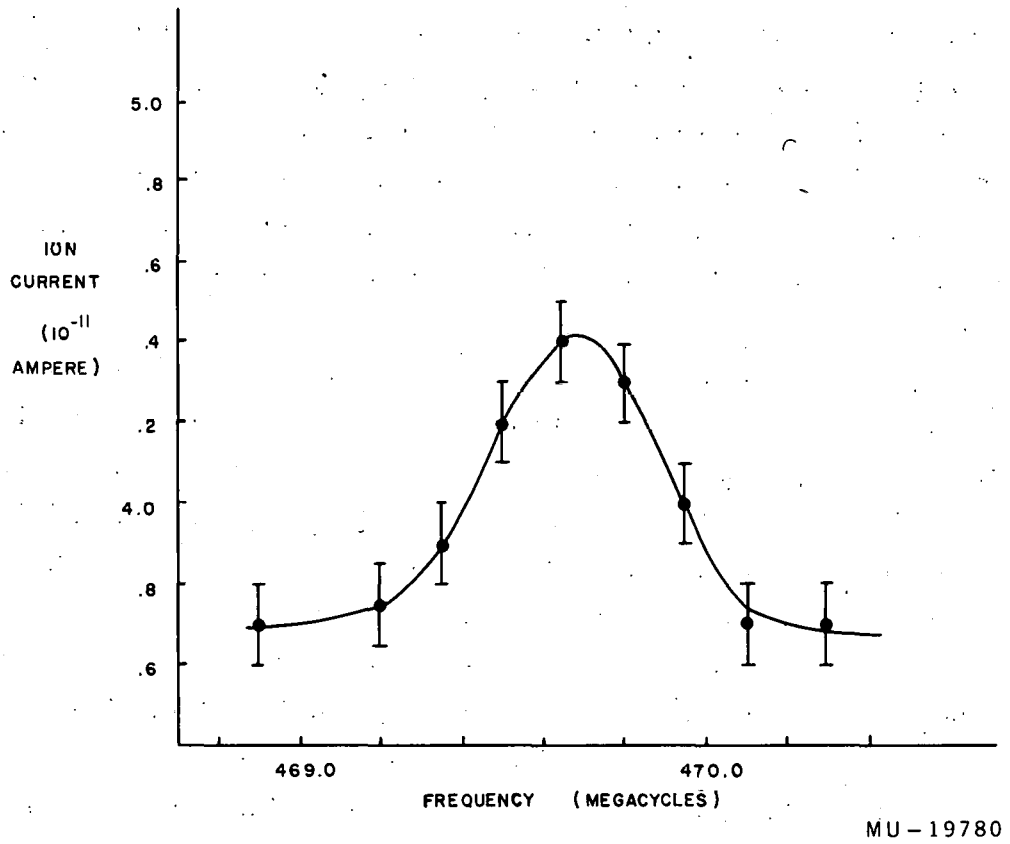

Fig. 34. Typical calibrating resonance; $\Delta F = 0$ flop-in line of Rb^{85}.

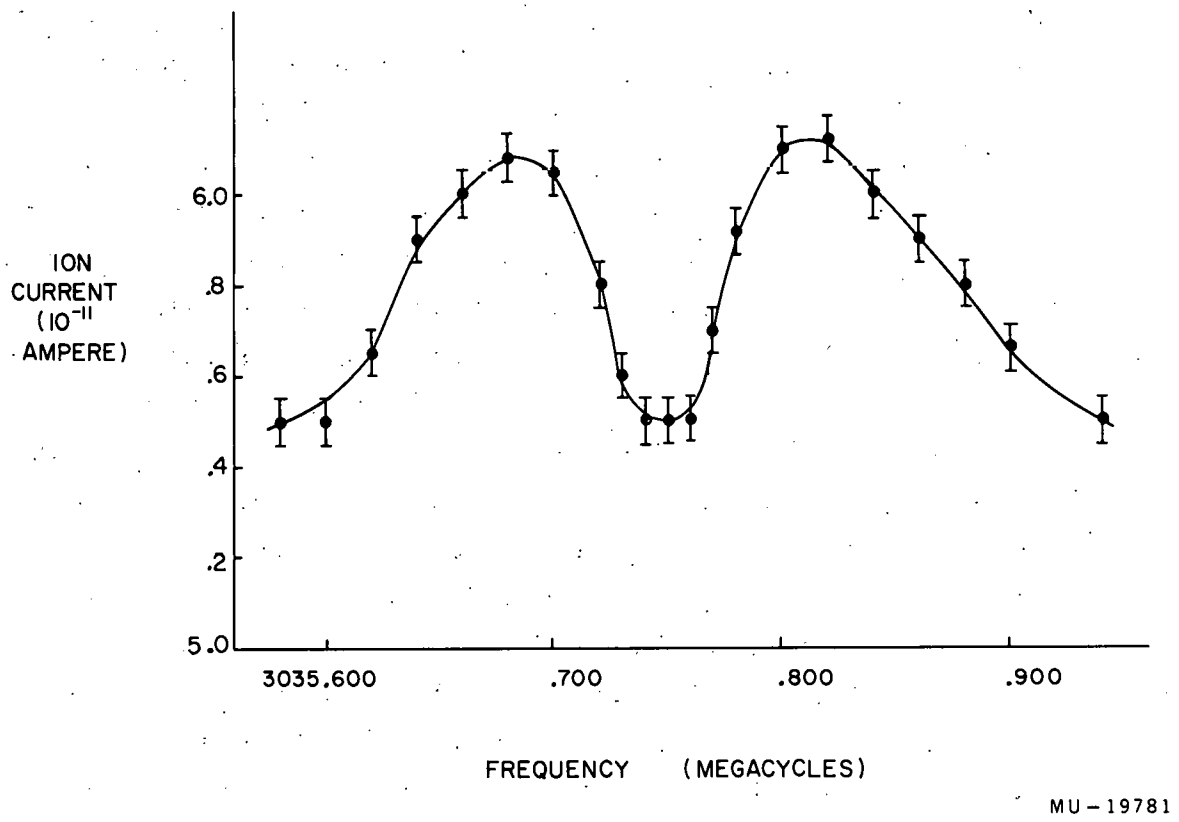

Fig. 35. Out-of-phase Ramsey pattern observed on the field-independent Zeeman line of Rb^{85}.

D. hfs Separation and Nuclear Moment of Rb^{85}

By using the Ramsey structure, the doublet 3, -1 ↔ 2, -2 and 3, -2 ↔ 2, -1 in Rb^{85} was observed in the field where its mean value is a minimum. Details of the calculations involved are given in Appendix B. The C field at 562.6 gauss was locked to the 3, 3 ↔ 2, 2 Rb^{85} transition at 4431 Mc. It was necessary to lock to a $\Delta F = 1$ transition because the $\Delta F = 0$ flop-in transitions for both Rb^{85} and Rb^{87}, the stable components of the beam, were in the range 420 to 470 Mc, which the locking system was not designed to cover. Actually it was found to be advantageous to use this highest-frequency π line because (a) it is a singlet, and is the first transition observed at this frequency as H_0 is increased from zero after degaussing, so that the identification problem is eased, and (b) large frequency deviation is obtained at these harmonics of the FM-4 frequency, which allows better control of the locking performance without the danger that excessive deviation may pull one of the oscillators off its phase lock. The field was calibrated by observing the Rb^{87} $\Delta F = 0$ flop-in transition at 469.8 Mc. The Gertsch equipment was operated at the settings shown in Table II. Optimum rf power was 500 mw for Ramsey patterns, 300 mw for locking, and 200 mw for calibration. Observations of the doublet were made at several values of H_0 near the minimum point, and results are summarized in Table III and are shown in Fig. 36 superimposed on plots of Breit-Rabi transition frequencies for the doublet calculated with the $\Delta\nu$ and g_I obtained by best fit of the data. The results are, for Rb^{85} in the $^2S_{1/2}$ state,

$$\Delta\nu = 3035.7327(7) \text{ Mc},$$

$$g_I = 2.938(2) \times 10^{-4},$$

to be compared to the published values (BED 52, YAS 51)

$$\Delta\nu = 3035.735(2) \text{ Mc},$$

$$g_I = 2.93704 \times 10^{-4}.$$

Table II

Radio-frequency oscillator settings, Rb^{85} moment search
(Symbols defined by Eq. (IV. 1))

	Locking system	Search system
f_3	1.2847 Mc	1.6849 to 1.6903 Mc
P	23	27
f_2	24.2847 Mc	28.6849 to 28.6903 Mc
m	30	30
f_1	738.542 Mc	870.5 to 870.7 Mc
n	6	3
f_0	4431.2 Mc	2611.64 to 2612.12 Mc

Table III

Rb^{85} Results

Observation	ν_{87} (Mc)	H_0 (gauss)	ν^- (Mc)	ν^+ (Mc)	$\frac{\nu^+ + \nu^-}{2}$ (Mc)	$\nu^+ - \nu^-$ (Mc)	g_I
1	469.41(8)	562.18(8)	2611.6514(3)	2612.1138(3)	2611.8826(5)	0.4624(5)	$2.938(2)\times10^{-4}$
2	469.65(8)	562.41(8)	2611.6512(3)	2612.1136(3)	2611.8824(5)	0.4624(5)	$2.937(2)\times10^{-4}$
3	469.83(8)	562.60(8)	2611.6510(3)	2612.1139(3)	2611.8824(5)	0.4629(5)	$2.939(2)\times10^{-4}$
4	469.95(8)	562.72(8)	2611.6514(3)	2612.1142(3)	2611.8828(5)	0.4628(5)	$2.938(2)\times10^{-4}$
5	470.25(8)	563.03(8)	2611.6575(3)	2612.1145(3)	2611.8830(5)	0.4630(5)	$2.938(2)\times10^{-4}$

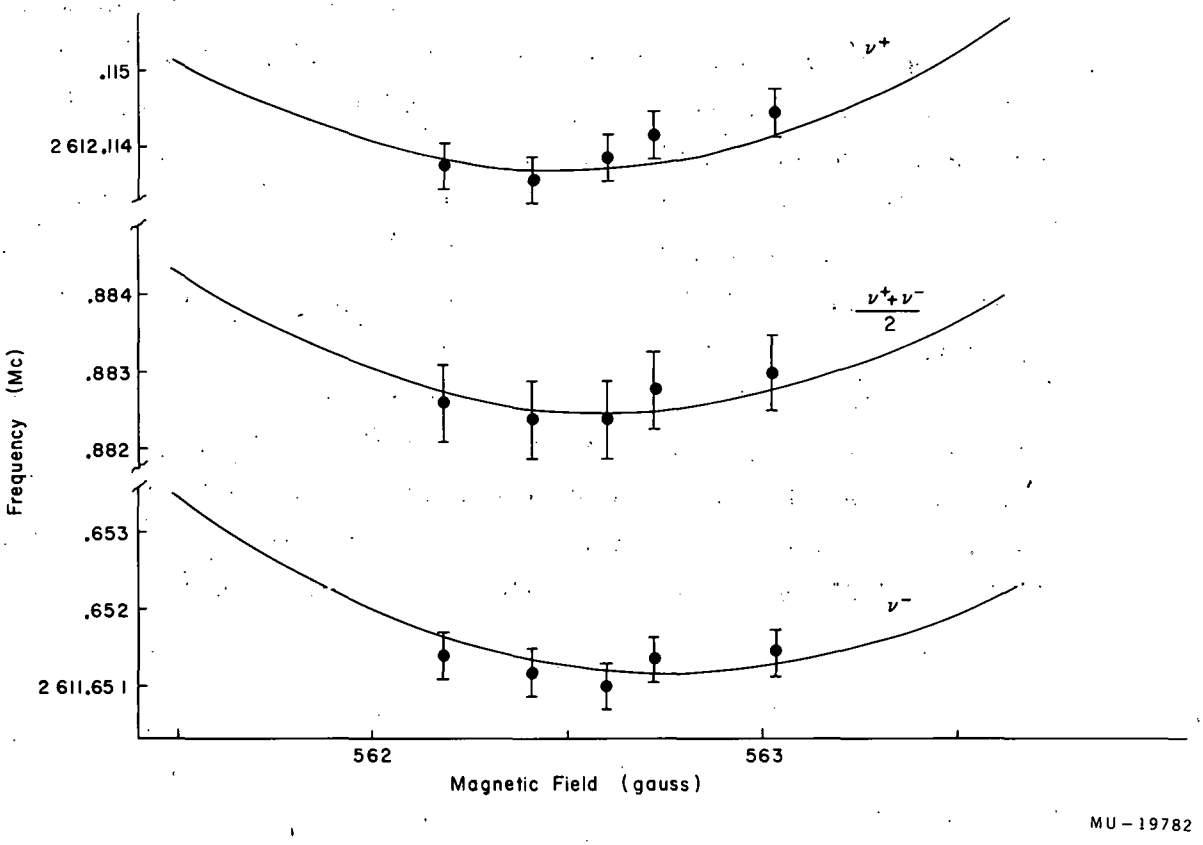

Fig. 36. Experimental observations on Rb^{85} superimposed on a plot of Breit-Rabi transition frequencies.

The Breit-Rabi transition frequencies were obtained by using an IBM 704 routine written by Dr. W. Bruce Ewbank of this Laboratory, using the values of the pertinent physical constants as given in Appendix A.

On the basis of the experimentally determined constants above and the corresponding published values for Rb^{87}, the hfs anomaly Rb^{85} - Rb^{87} has the value 0.31(7)%, which is to be compared to the more accurate value (BED 52) of 0.3513(6)%.

This result indicates that the method used here should be capable of measuring the moment of Rb^{86} with comparable accuracy and should give the Rb^{85} - Rb^{86} hfs anomaly with an experimental uncertainty of about 0.1%.

It is not likely that the Zeeman-region $\Delta\nu$ measurement of Rb^{85} by Bederson and Jaccarino (BED 52) can be improved significantly with this apparatus, even with new hairpins. It might be interesting to see a measurement of this value made by methods of optical pumping (KAS 50, ARD 58, BEN 58) to be compared with the value obtained here.

VI. EXPERIMENTS ON RUBIDIUM-86

Because Rb^{86} is the most readily available and cheapest radioactive alkali of reasonable half-life whose moment had not been measured directly, it was decided to make the first measurements by radioactive detection on this isotope although the theoretical difficulties of matching theory with experiment for a member of the odd-odd group (see Section VII) make the determination of hfs anomalies involving this isotope less useful than one of the odd-A isotopes. The techniques developed in this work are applicable for all the alkalis, and measurements on both odd- and even-mass number rubidium and cesium isotopes are now under way.

A. Chemistry

The isotope was obtained from Oak Ridge National Laboratory in the form of RbCl in an HCl solution in shipments of 300 millicuries, with specific activities ranging from 300 mC/g to 12,000 mC/g. The isotope is produced by the reaction Rb^{85} (n, γ) Rb^{86}, so that the target material cannot be separated chemically from the reaction product; thus fixing the proportion of carrier isotope to radioactive isotope in the beam material unless one wants to decrease the specific activity. This is usually not desired, since as high a counting rate as can be obtained is needed for good signal-to-noise levels and good counting statistics with reasonable exposure and counting times.

All chemistry was done in a standard cave box, an airtight inner box surrounded by a lead shield; handling of objects inside the cave was from outside by remotely controlable tongs. The only "chemistry" required was to obtain RbCl powder from the 10 to 20 ml of solution after it had been removed from the shipping bottle. Originally ammonium hydroxide was added to neutralize the acid solution, but since HCl comes off as a gas during evaporation, this was not needed. By use of hot nitrogen gas blowing from above, the solution was evaporated to dryness in a 40-ml centrifuge cone. The powder was scraped from the walls and put directly into an oven.

Freshly filed calcium chips were added and the oven cap pressed into place. The oven was passed out of the cave box and inserted into the oven loader.

B. Production and Detection of the Beam

About half an hour was required for the oven loader to be brought through the successive pumpouts into position and for the oven chamber pressure to fall to about 2×10^{-6} mm Hg. The oven filament current was then slowly increased to the operating point and, when the pressure fell back to its previous value, several watts of electron power was applied. Power was slowly increased, keeping the pressure about 5×10^{-6} mm, to about 15 watts. In about 10 minutes the beam would become detectable and would rapidly rise to a level of 2 to 3×10^{-10} amp of ion current at the exit-slit detector. During the course of the run the power had to be gradually increased to maintain a constant beam level as recorded by the monitor detector. The practical limit was 60 to 70 watts; at any higher power arcing was observed between the oven and oven loader, and oven pressure rose to the point at which scattering of the beam was appreciable. The stable components of the beam, Rb^{85} and Rb^{87}, were detected with the hot-wire ionization detectors as described in Section IV. F, and the Rb^{86} was detected by the counting of the sulfur carrying buttons after exposure to the beam. The decay scheme of Rb^{86} (SEA 58) is shown in Fig. 37. The 1-Mev gamma ray is not completely absorbed in the thin counting crystal so the counting efficiency is low. Most of the decay is by beta emission and the passage of the emitted electron through the electronic cloud of the atom has a small probability of producing the characteristic x rays of the atom by "internal ionization" (EVA 55). The counting rate in the thin crystal counters due to this radiation was quite satisfactory; the pulse-height analyzer settings for the peak of this radiation were very close to those for optimum counting of the K x-ray from the neutron-deficient rubidium isotopes, as would be expected if the counting rate were primarily due to the internal ionization.

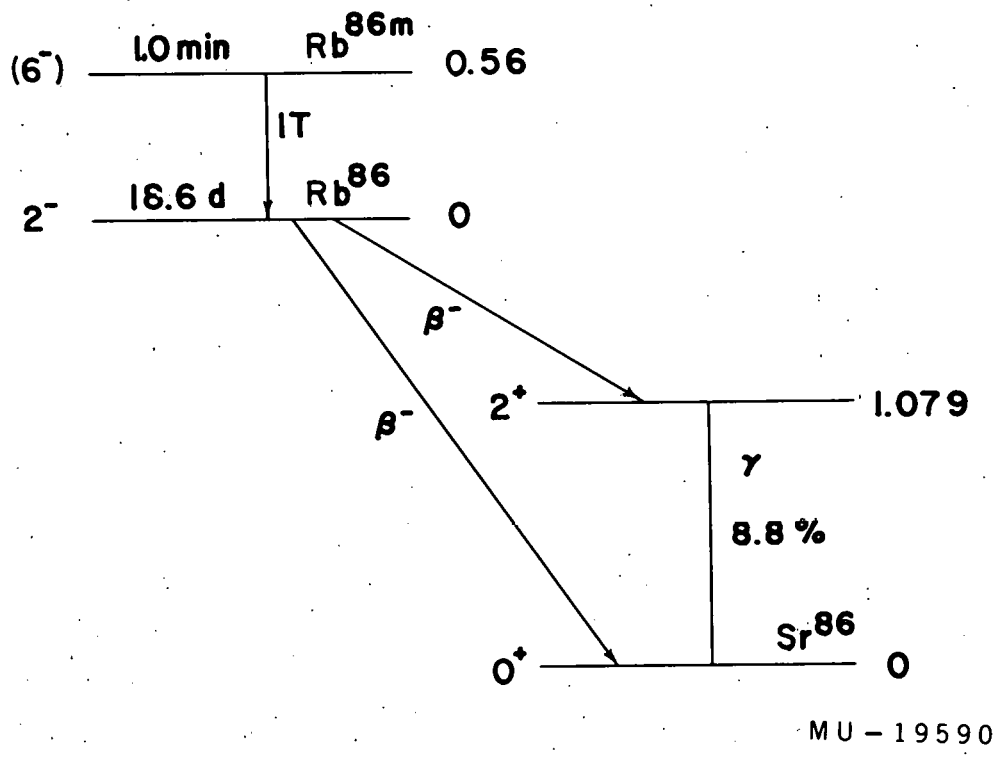

Fig. 37. Decay scheme of Rb^{86}.

Typical counter background is 1.5 counts per minute with settings for optimum detection of Rb^{86}. Identification of the isotope is simplified because it has the only observable activity resulting from the neutron bombardment, all others being of such short half-life that they have decayed during shipment. Checks were made, however, by decay of both the chemistry and the resonance peak buttons and observation of their gamma spectrum by using a 2×2-in. NaI(Tl) crystal and the Laboratory's RCL 256-channel pulse-height analyzer.

C. Experimental Procedure

When the beam reached about 10^{-10} amp the oven and exit slit were aligned with the collimator and stop wire by the following procedure: The beam was observed while the oven loader was moved until a maximum reading was obtained. The stop wire was raised and the exit slit moved to either side to observe on the exit-slit detector that small part of the full beam that is not shadowed by the stop wire, and the oven loader was slightly adjusted until this profile was symmetrical. Figure 38 shows the beam profile as seen at the exit-slit detector, showing the shape with the stop wire in place and with the stop wire removed. The oven, collimator, and stop wire were then aligned. With the stop wire out the full beam was observed on the button loader detector and the exit slit laterally moved to check that the profile was symmetrical, then moved to the peak. Figure 39 shows the beam profile measured at the button loader detector. The apparatus was then aligned.

When the beam reached a steady value, a button was exposed to this full beam for a fixed time, usually 5 minutes. From the counting rate of this button the expected counting rate for a resonance could be estimated and adjustment of exposure time or beam level could be made, if necessary, to get a counting rate at least several counts per minute above background. Resonances in Rb^{86} ranged from 6 to 40 cpm above counter background, with an apparatus background of about 2 cpm.

The full beam was read then with the exit-slit detector, the A and B magnet current was turned on and the stop wire put into place,

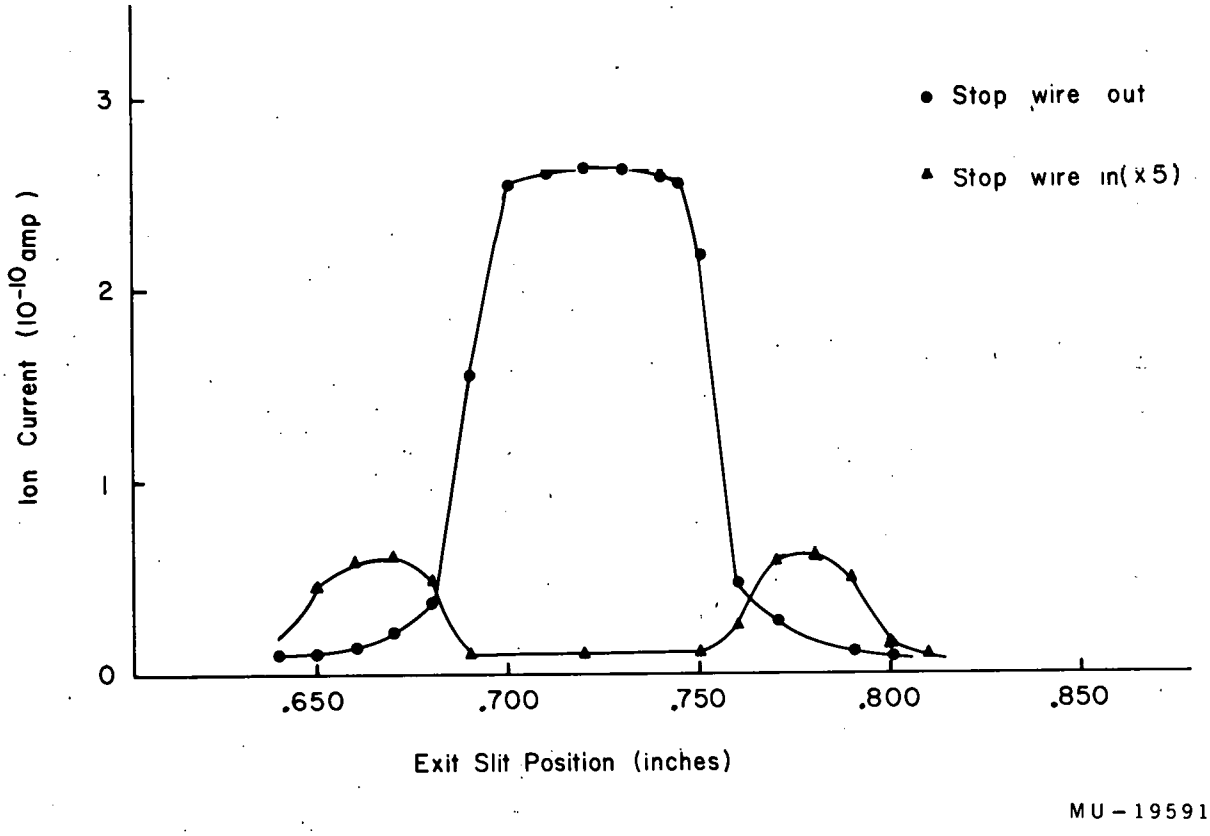

Fig. 38. Beam profile observed on the exit-slit detector.

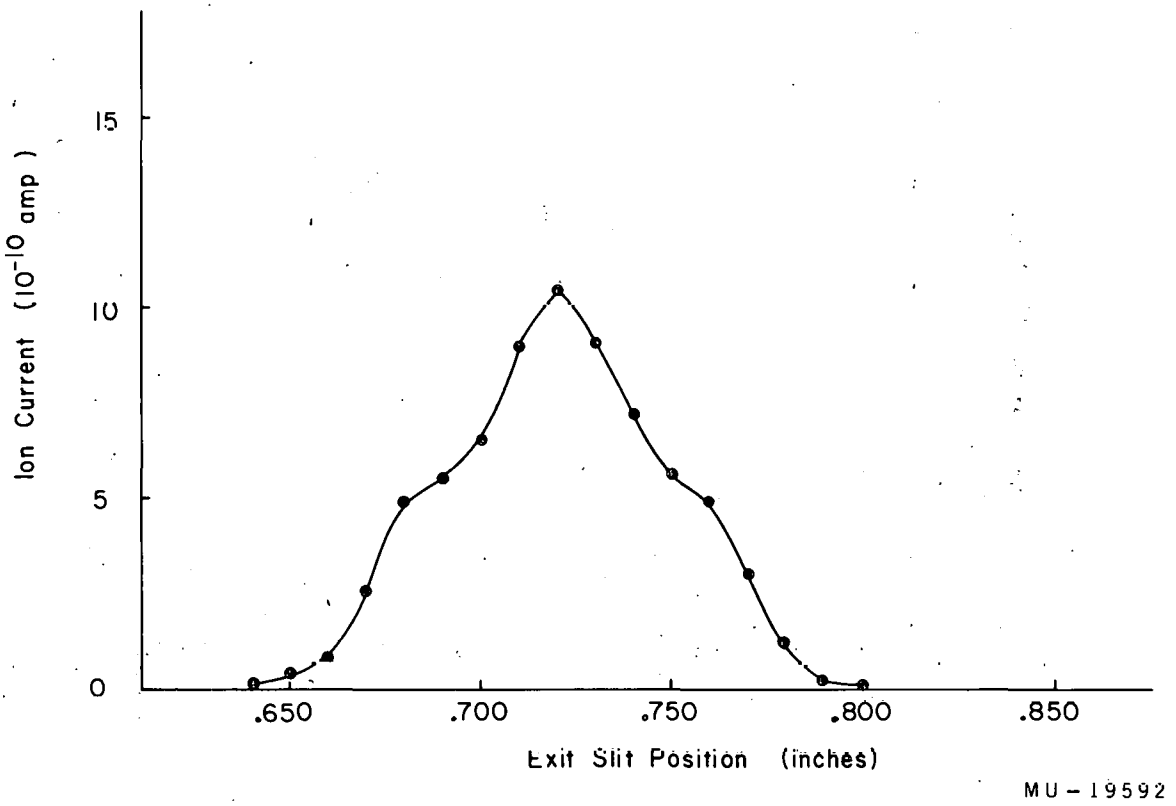

Fig. 39. Beam profile observed on the button-loader detector.

the monitor detector moved to the peak of the flopped-out beam, and the reading taken at that point. Figure 40 is a beam profile for this detector made for a full beam, deflected beam with stop wire out, and deflected beam with stop wire in place. The C magnet was then degaussed by putting maximum current in the C-magnet windings and slowly decreasing this current to zero while alternately reversing the current direction. The Majorana flop at zero field (see Section II. C.) was observed with the button loader detector. The locking rf signal was then introduced and the C-magnet current increased until the resonance was focused. The phase lock of the magnet-regulator system (Appendix C) was turned on and minor adjustments of modulation index, gain, and rf power were made to obtain optimum locking conditions. The calibrating frequency was then introduced in the search hairpin and the calibrating resonance observed by using the button loader detector. If the position of the calibration indicated that the field was not locked close enough to the desired value, slight adjustments of the locking frequency could be made without pulling either the oscillators or the magnet off lock. Several readings of the peak of the calibrating resonance were made and exposure of buttons begun. The first search frequency was introduced and the button exposed, during which time it was necessary to monitor the error signal and oscilloscope display of the field-locking system, the beam monitor, the search frequency as displayed on a frequency counter, the phase lock on both AM-1's and FM-4's if used, the beat note of the search frequency f_0 in the transfer oscillator, its power level, the power level of the locking signal, and the oven chamber pressure. At the end of an exposure, the button loader was rotated to the window position, the search frequency changed, and the button loader rotated to the next exposure position, after which the previously exposed button could be removed through the vacuum lock and a fresh one inserted for the next exposure. The search system is summarized in Table IV. After several buttons had been exposed the button loader was rotated to place the hot-wire detector in the focus and the peak

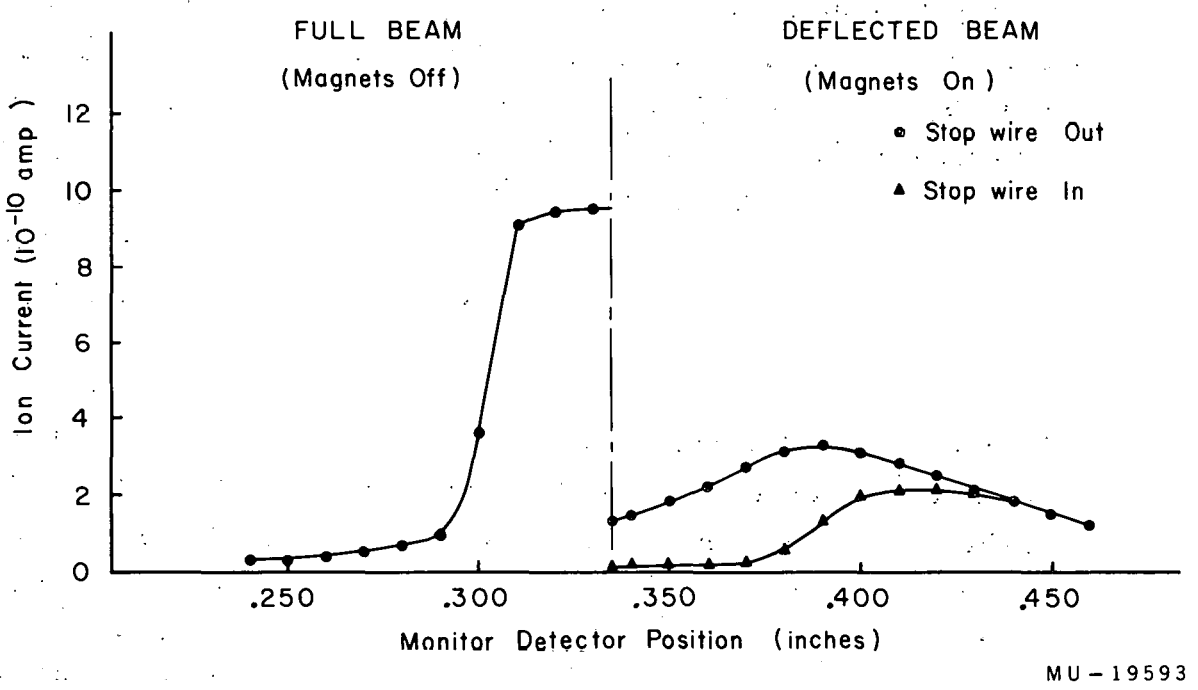

Fig. 40. Beam profile observed on the monitor detector.

of the calibration flop was read again to check the field lock. Sometimes lock was lost during an exposure; the detector would be immediately rotated into place, the lock restored, and the field recalibrated before another button was exposed. Exposing a button with the search frequency off served to determine the apparatus background for a particular run.

At the end of a run the monitor reading was made just before the deflecting magnets were turned off. Then the full beam with stop wire removed was read with the exit-slit detector. The exposed buttons were then counted, background subtracted, and correction made for beam normalization, using the monitor detector readings. The individual button counting rates were then plotted against their exposure frequency and a resonance curve (if there was one there) was fitted both by eye and by the OMNIBUS computer routine (SHU 57), using an IBM 650 digital computer, which fits a bell-shaped curve by the method of least squares.

Table IV

Radio-frequency oscillator settings for Rb^{86} $\Delta\nu$ search
(Symbols defined by Eq. (IV. 1))

	Locking system	Search system
f_3	1.3 - 1.8 Mc	1.0688 - 1.0691 Mc
P		38
f_2		39.0688 - 39.0691 Mc
m		25
f_1		986.7 Mc
n		4
f_0		3946.87 - 3946.92 Mc

D. Measurement of $\Delta\nu$

The spin (BEL 51) and rough value of $\Delta\nu$ and sign of the moment (BEL 53) for Rb^{86} were measured by Bellamy and Smith at Cambridge University as

$$I = 2$$
$$\Delta\nu = 3960 \pm 20 \text{ Mc},$$
$$g_I \text{ negative}$$

by observation of the $\Delta F = 0$ flop-in transition in fields of 4 to 163 gauss and using Eqs. (II. 23)–(II. 25). It was necessary to reduce the uncertainty in $\Delta\nu$ before a direct $\Delta F = \pm 1$ transition search could be undertaken, therefore further observations were made of this transition at fields of 184, 271, and 630 gauss. Typical arrangement of radio-frequency equipment is as shown in Fig. 41. The resonances obtained are shown in Figs. 42 through 44 and lead to the result that the $\Delta\nu$ was in the 4-Mc region, centered around 3948.7 Mc.

A search was then started for direct transitions in the Zeeman region (3 to 4 gauss). The observable Zeeman spectrum of an isotope with spin 2 consists of four π lines separated by $4/5\ \mu_0 H_0/h$ (see Section II.D). All except the highest-frequency line are doublets, so the search was begun for the upper frequency doublet since it is field-dependent and was expected to be greater than 100 kc wide, making it relatively easy to spot. Several runs were made in the region 3950 to 3960 Mc, but no resonances were seen. Analysis of these runs in the light of the more accurate value of $\Delta\nu$ obtained later on indicated there were indeed no resonances in the region searched. Exposures were made in 50-kc steps to reduce the possibility of missing a narrow line. This proved to be expensive in time and activity. It was decided to try exposing buttons while sweeping the AM-1's low-frequency oscillator with an electric motor connected to its control knob, thus integrating the exposure over 150 kc at 3950 Mc. Signal-to-noise ratio was, of course, reduced, but the speeding up of the search was considerable. A button was found with a counting rate three times the average, and

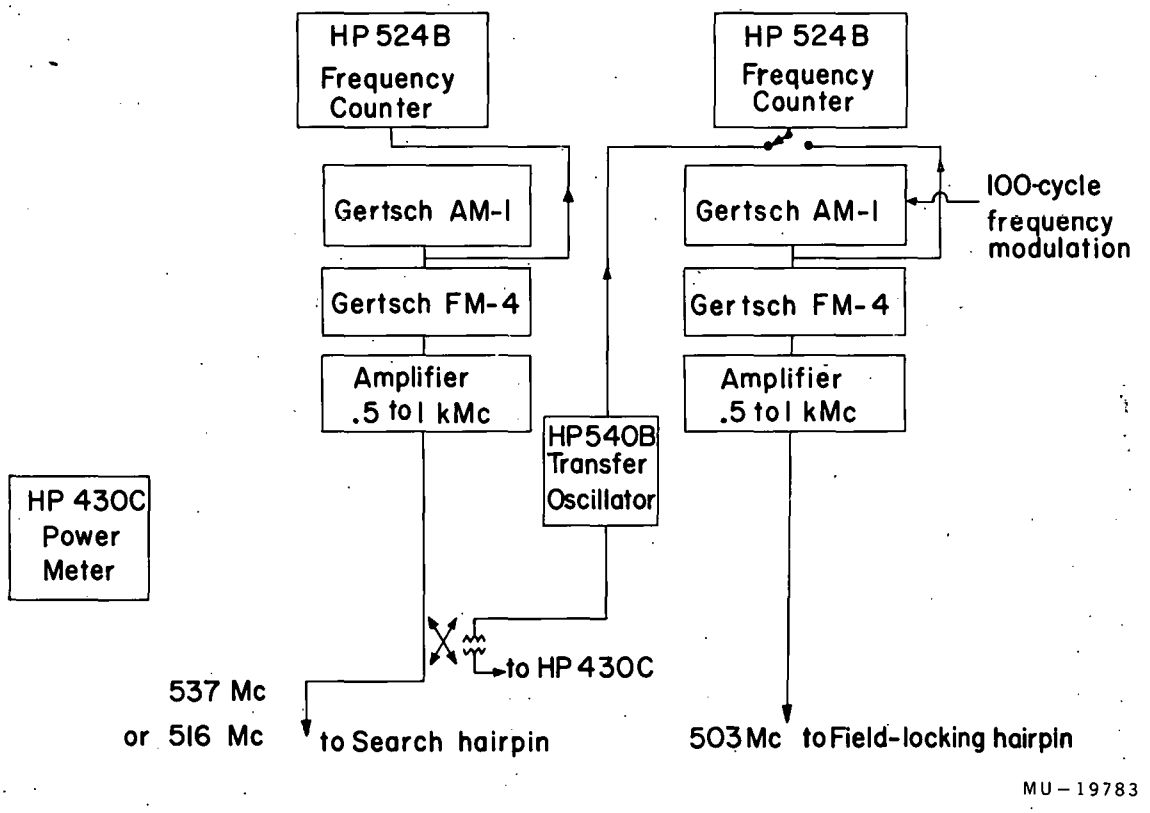

Fig. 41. rf Block diagram for high-field $\Delta F = 0$ search in Rb^{86}.

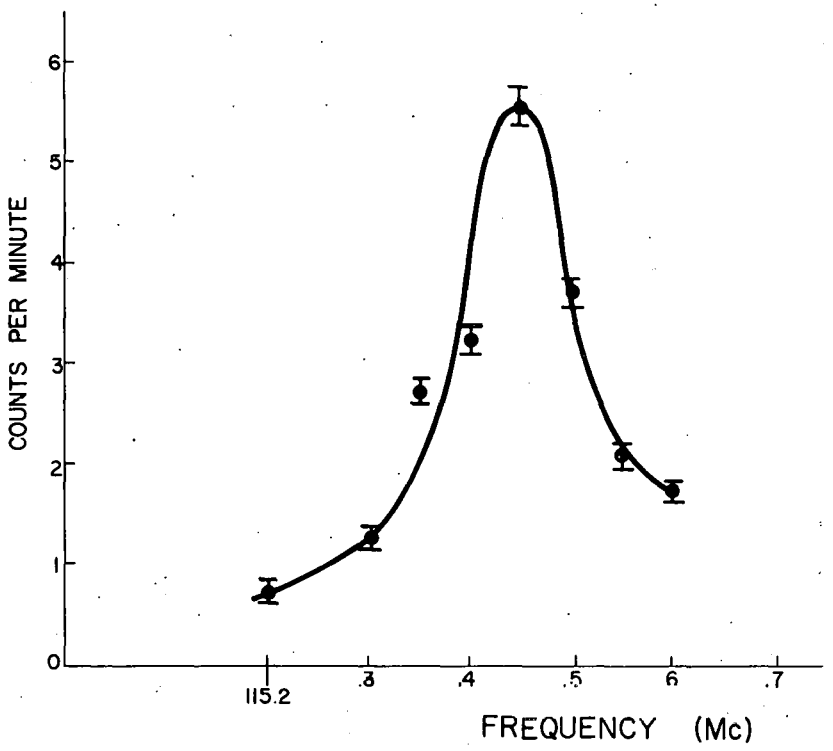

MU-16135

Fig. 42. Observed resonance of $\Delta F = 0$ transition at 184 gauss.

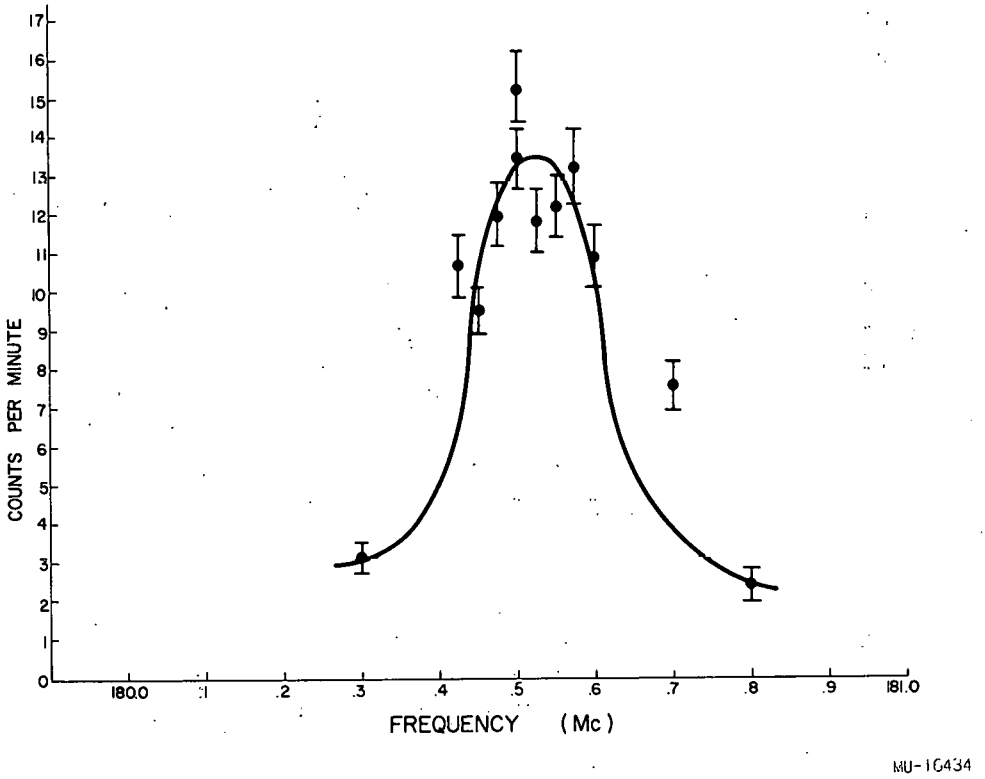

Fig. 43. Observed resonance of $\Delta F = 0$ transition at 274 gauss.

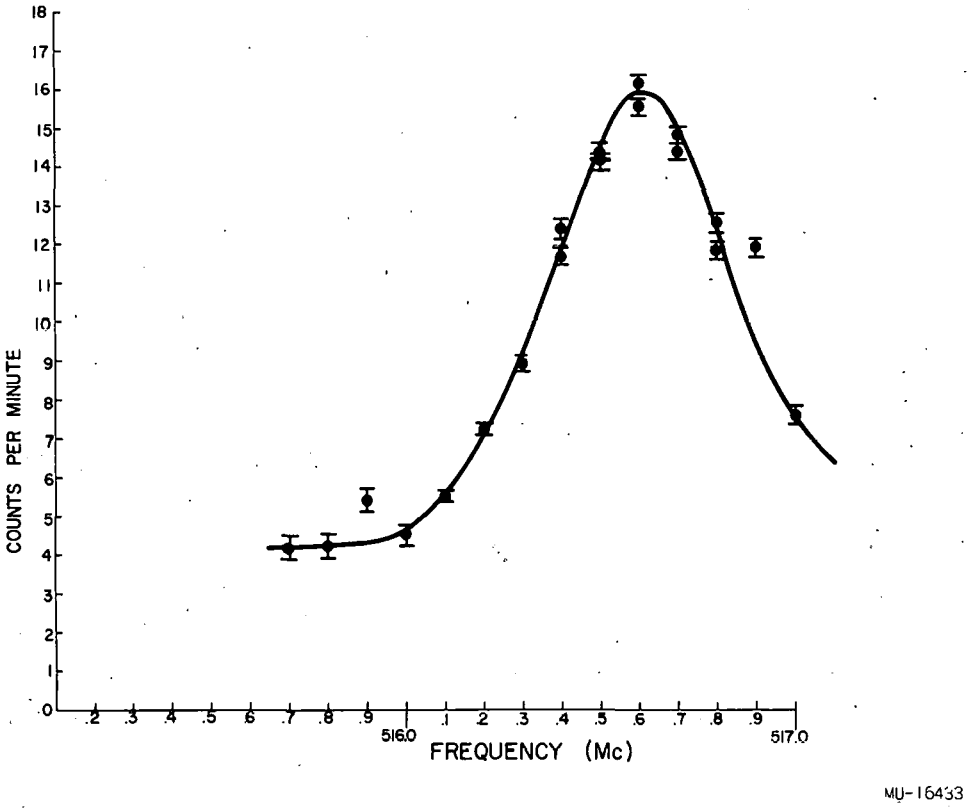

Fig. 44. Observed resonance of $\Delta F = 0$ transition at 630 gauss.

upon searching that region in discrete steps, a resonance was found having a width of 400 kc. A broad line was expected, since excessive rf power was being applied for that purpose. The field was shifted slightly and another set of buttons was exposed. From the shift of the resonance peak the line was identified as the high-frequency doublet. Unfortunately, the field was not shifted far enough to make good identification, and in the excitement of the moment this point was overlooked. As was found later that this was the adjacent singlet. The line $4/5\ \mu_0\ H_0/h$ lower was found, but always disappeared when the field was shifted, indicating that it was not the field-independent doublet near $\Delta\nu$. All observable π lines were then seen and positive identification of the proper field-independent line was made. Several observations were made of this line at various fields with the 3/4-in. and 1-1/4-in. straps. Figure 45 shows some of these resonances. The results are listed in Table V. For these observations the C field was locked to the Rb^{87} flop-in transition near 1.5 Mc and the field calibrated by using the corresponding Rb^{87} transition. A block diagram of the rf equipment is shown in Fig. 46 with the Gertsch equipment settings as shown in Table IV. From these resonances, the hfs separation was determined to be 3946.883(3) Mc.

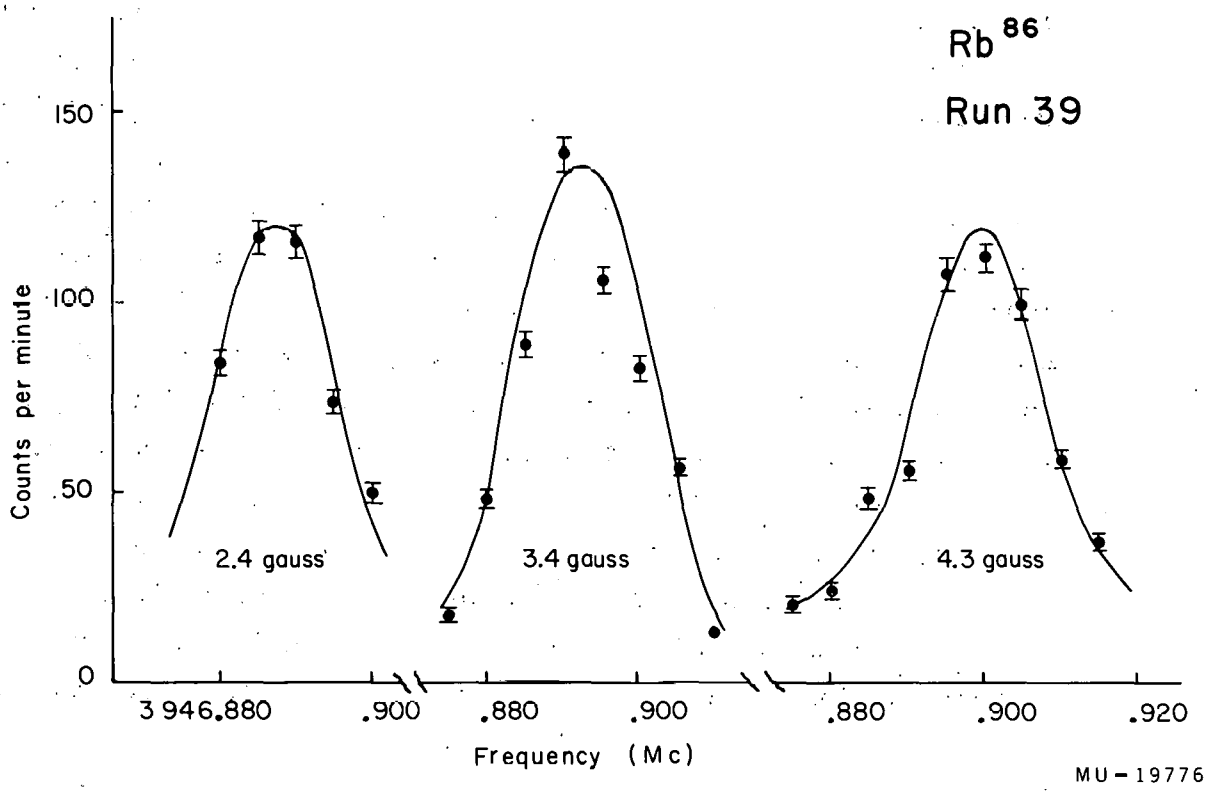

Fig. 45. Observed resonances of $\Delta F = \pm 1$ transition in low field.

Table V

Measurement of $\Delta\nu$ for Rb^{86}

$m_F = \pm 1/2 \leftrightarrow m_F = \mp 1/2$ Zeeman transition

Run	ν (Mc)	$\nu(Rb^{87})$ (Mc)	$\Delta\nu$ (Mc)	Remarks
33	3946.891(5)	1.52	3946.886(5)	3/4 in. strap
39	3946.900(4)	2.98	3946.883(4)	1-1/4 in. strap
	3946.893(4)	2.37	3946.882(4)	
	3946.887(4)	1.66	3946.882(4)	
63	3946.894(4)	2.24	3946.884(3)	2 in. strap
78	3946.898(4)	2.66	3946.884(3)	
79	3946.894(4)	2.28	3946.884(3)	

Intermediate-field doublet

Hairpin position	$\bar{\nu}$ (Mc)	Average $\bar{\nu}$ (Mc)	$\Delta\nu$ (Mc)
Original	3599.9340(5)		
		3599.9345(8)	3946.883(1)
Reversed	3599.9350(5)		

Hairpin position	$\bar{\nu}^+$ (Mc)	$\bar{\nu}^-$ (Mc)	$\frac{\bar{\nu}^+ + \bar{\nu}^-}{2}$ (Mc)	$\Delta\nu$ (Mc)
Both	3600.3147(5)	3599.5542(5)	3599.9345(8)	3946.883(1)

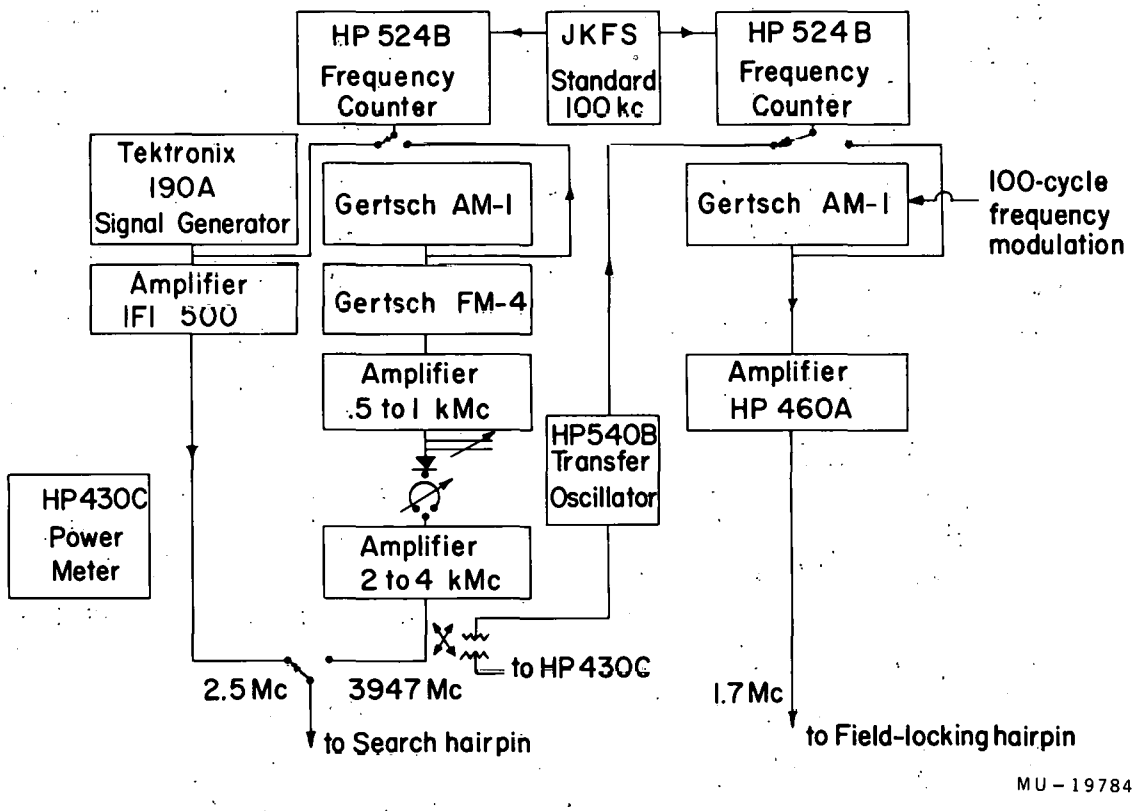

Fig. 46. rf Block diagram for Zeeman $\Delta\nu$ search in Rb^{86}.

E. Measurement of the Nuclear Moment

A search was made for the doublet used to measure g_I on the basis of the value of $\Delta\nu$ found above. Resonances about 10 kc wide were found, but were much too wide to permit measurement of their difference frequency with sufficient accuracy.

At this point the 2-in. strap was introduced as a hairpin and several pairs of resonances were observed, an example of which is shown in Fig. 47. The shape and consistency of the experimental values of the peak frequency were not good enough to yield a reliable value of the nuclear moment. Furthermore, the discrepancy between the low-field $\Delta\nu$ determination (Section VI. D) and the $\Delta\nu$ determined from the minimum value of the mean frequency of this doublet was 4 kc, which was too large to be comfortably ascribed to experimental error. This apparent shift was thought to be due to distortion caused mostly by Doppler shift, and observation on Rb^{85} (Section V. C) confirmed this suspicion. A serious move was then made to use a Ramsey hairpin for this determination of g_I. After the operation of the separated-field hairpin on Rb^{85} (Section V. D) had been checked, Ramsey patterns were observed on the Rb^{86} doublet. When the peak of one had been found, the rf power was varied to determine its optimum value, with the result given in Fig. 48. Several sets of resonances were taken with steps of 1 kc between exposures at 3600 Mc. The block diagram of the radio-frequency equipment used is shown in Fig. 49, and the settings of the Gertsch equipment for this experiment shown in Table VI. The magnetic field at 592 gauss was locked to the $3, 3 \leftrightarrow 2, 2$ transition in Rb^{85} at 4508 Mc and calibration made with the $\Delta F = 0$ Rb^{85} flop-in transition at 457.5 Mc. The peak frequencies of these resonances were determined both by eye and by the OMNIBUS curve-fitting routine. These two methods agreed within at most 0.2 kc. Because of the symmetry of the central peak, the agreement of the two methods of finding the peak, and the consistency of data, the criterion set for the uncertainty of the peak was 1/10 of the line width. A typical pair of resonance lines for this doublet is shown in Fig. 50. As was done with Rb^{85},

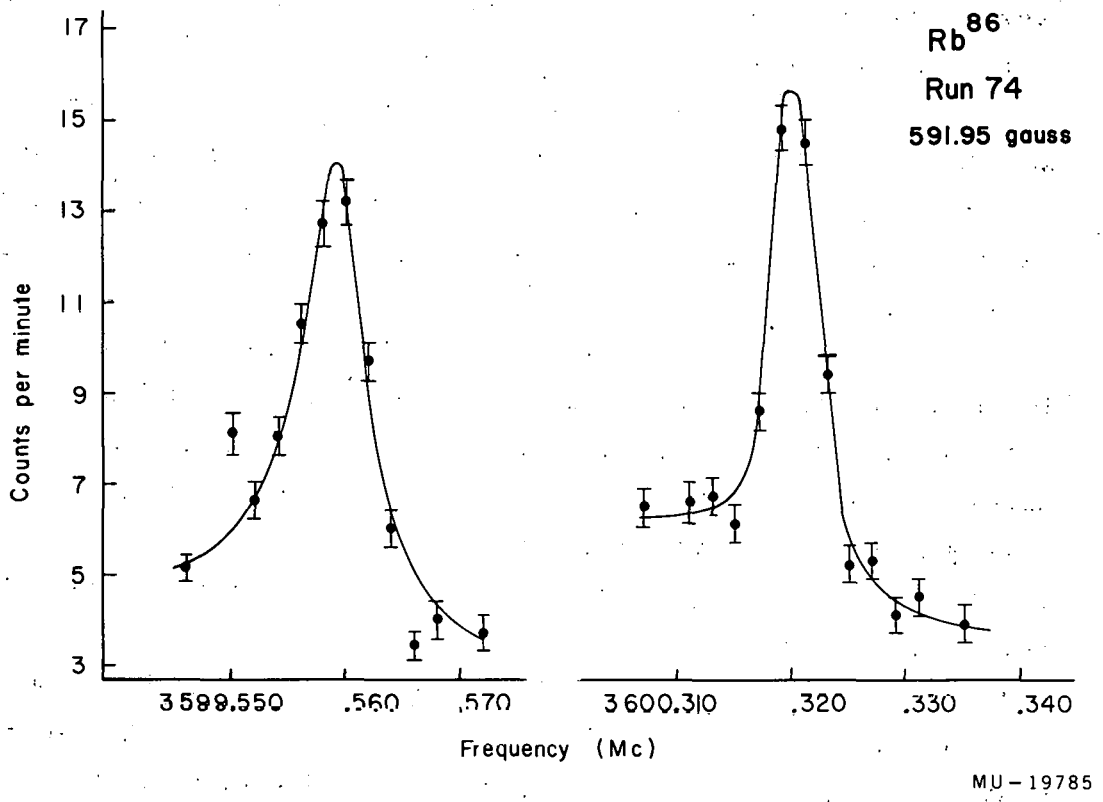

Fig. 47. Typical resonances observed on the Rb^{86} doublet with 2-in. strap hairpin.

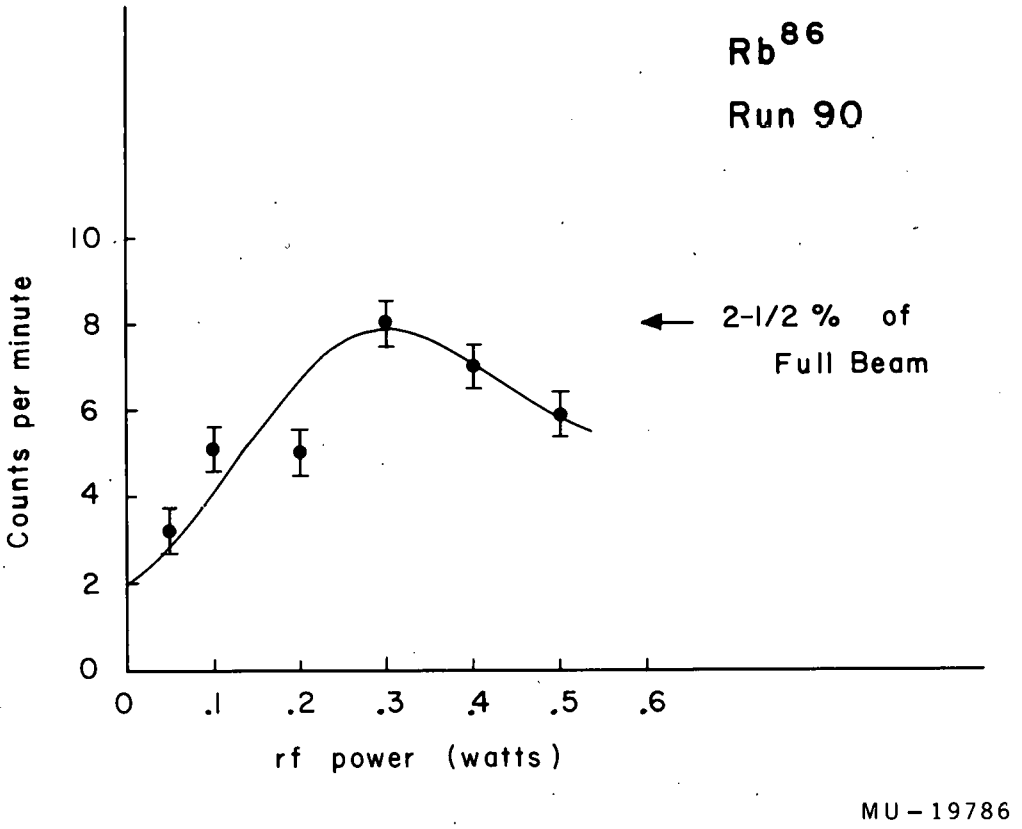

Fig. 48. Dependence of the peak intensity of the Ramsey pattern in Rb^{86} on input rf power.

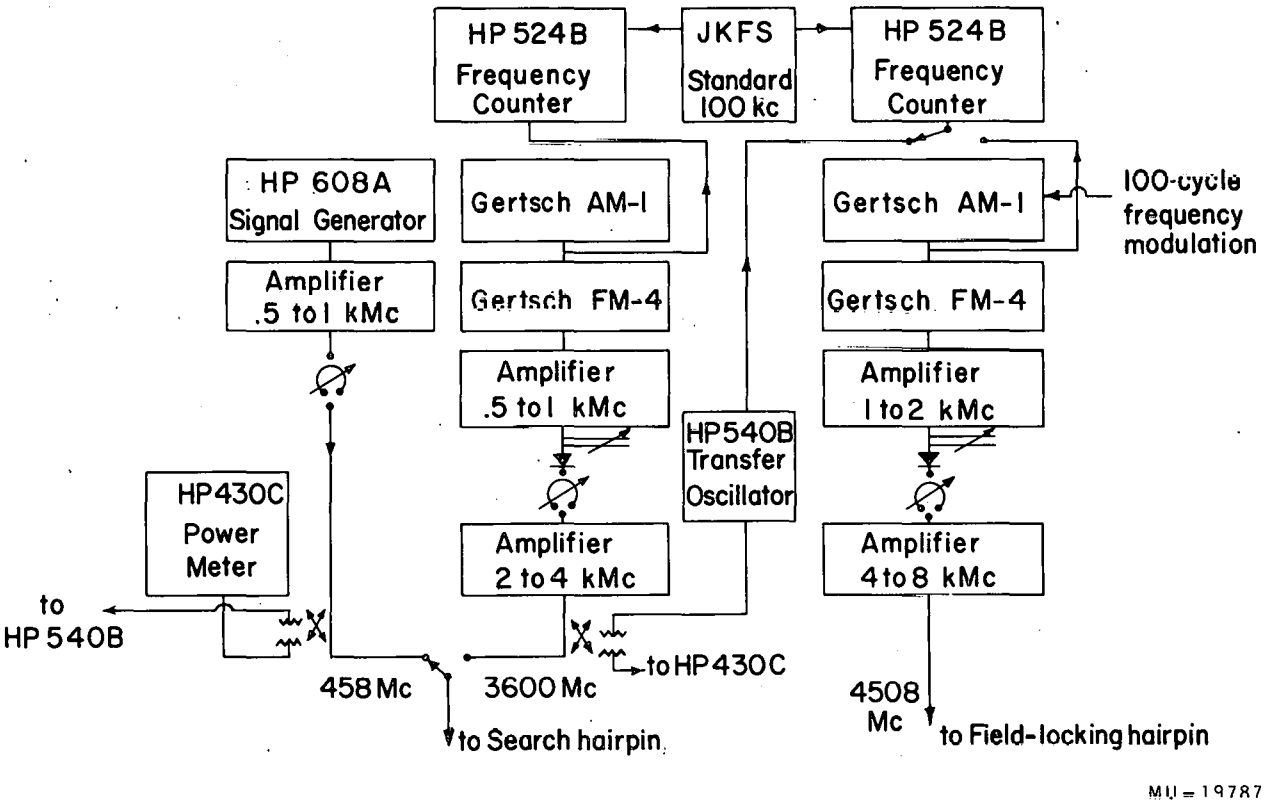

Fig. 49. rf Block diagram for Rb^{86} doublet search.

Table VI

Radio-frequency oscillator settings for Rb^{86} g_I search
(Symbols defined by Eq. (IV. 1))

	Locking system	Search system
f_3	1.7050 Mc	1.595 - 1.604 Mc
P	23	34
f_2	24.7050 Mc	35.595 - 35.604 Mc
m	30	25
f_1	751.15 Mc	899.8 - 900.1 Mc
n	6	4
f_0	4506.9 Mc	3599.54 - 3600.34 Mc

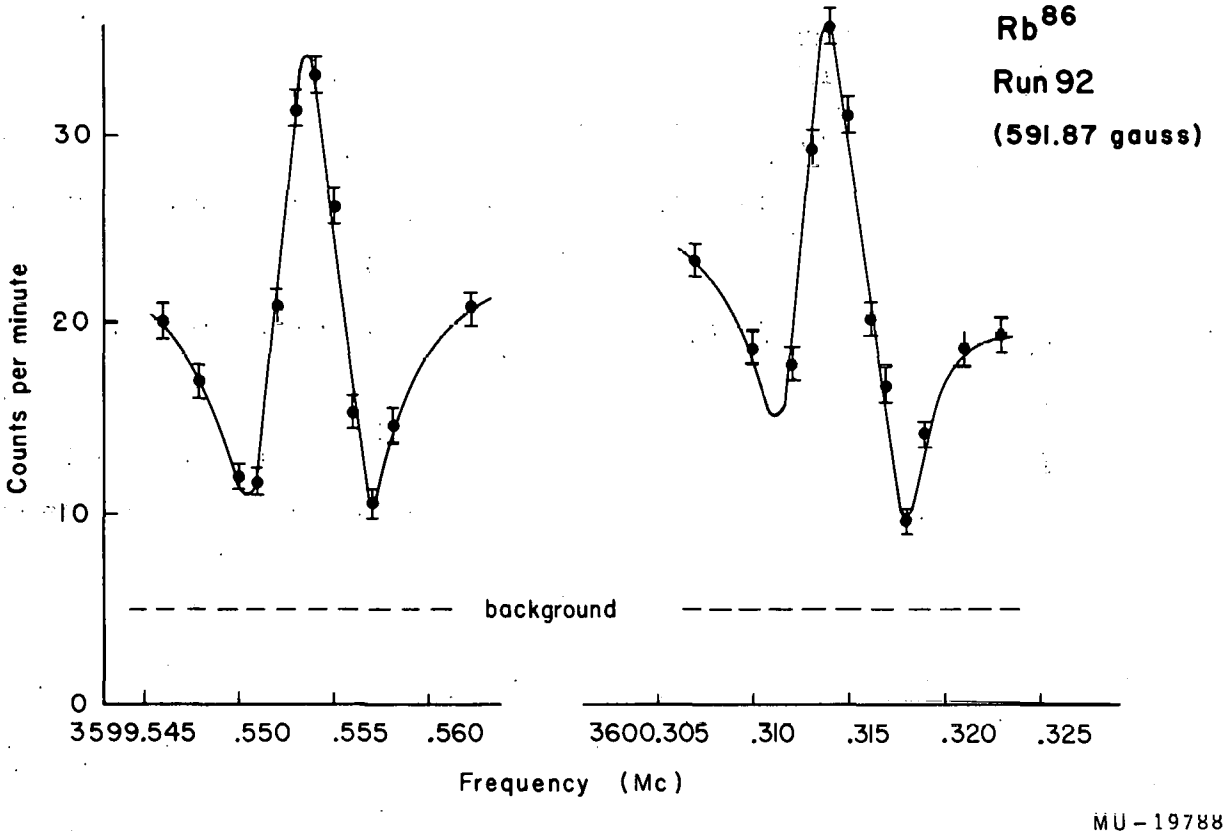

Fig. 50. Typical Ramsey patterns observed on the Rb^{86} doublet.

since the slight asymmetry of these lines indicated a possible frequency shift, the structure was reversed with respect to the beam direction and the doublet again observed. This time a shift of frequency of the lines was found, but the separation of the doublet had the same value as that found with the hairpin in the original (unreversed) position.

The results obtained are consistent with the assumption that there is a phase-shift distortion which shifts the peak of the resonance, but which has the same value for the two lines since their separation is small compared with the frequency. The actual value of the transition frequency can then be found from the mean value of the observed transitions in the two hairpin positions.

It is rather interesting that there is a phase shift in the structure at 3600 Mc and no apparent shift at 2600 Mc. This indicates that the shift is due, not to a difference in physical length of the arms, but probably to the polystyrene spacers in the coaxial structure. It would be worth while rebuilding this hairpin using polyfoam or other material of low dielectric constant as spacer material so that the arms would have the same electrical length in this frequency region.

F. Experimental Results

The nuclear g factor was calculated from the doublet separation by taking the separation of the observed lines with the hairpin in each of its two positions and, for two sets taken near the same value of field in different hairpin positions, the average value of each line was determined and then the difference taken between these average values. Results are given in Table VII.

The final results, allowing for systematic experimental errors not apparent, are, for Rb^{86} in the $^2S_{1/2}$ state

$$\Delta\nu = 3946.883(2)\ \text{Mc},$$

$$g_I = -4.590(4) \times 10^{-4},$$

Table VII

g_I Measurement for Rb^{86}

Run	ν^+ (Mc)	ν^- (Mc)	$\nu^+ - \nu^-$ (Mc)	H_0 (gauss)	g_I
91	3600.3138(6)	3599.5536(6)	0.7602(9)	591.86(10)	$-4.588(6)\times10^{-4}$
	3600.3142(6)	3599.5536(6)	0.7606(9)	591.86(10)	$-4.591(6)\times10^{-4}$
92	3600.3143(3)	3599.5537(3)	0.7606(5)	591.87(10)	$-4.593(3)\times10^{-4}$
93	3600.3142(3)	3599.5537(3)	0.7605(5)	591.70(10)	$-4.591(3)\times10^{-4}$
100[a]	3600.3152(3)	3599.5547(3)	0.7605(5)	592.02(10)	$-4.589(3)\times10^{-4}$
	$\bar{\nu}^+$ (Mc)	$\bar{\nu}^-$ (Mc)	$\bar{\nu}^+ - \bar{\nu}^-$ (Mc)	H_0 (gauss)	g_I
92-100[a]	3600.3147(5)	3599.5542(5)	0.7605(7)	591.9(2)	$-4.590(4)\times10^{-4}$

[a]Indicates hairpin in reversed position. The average values above are averages of each transition for the hairpin structure in both positions.

$$\mu_I = I g_I \left(\frac{M_p}{m_E} \right) = -1.6856(14) \text{ nuclear magnetons,}$$

and, using the corresponding values for Rb^{85} given in Appendix A, for the isotopes Rb^{85} - Rb^{86},

$$\frac{a_1}{a_2} = \frac{\Delta\nu_1}{\Delta\nu_2} \frac{(2I_2 + 1)}{(2I_1 + 1)} = .6409562(6),$$

$$\frac{g_{I_1}}{g_{I_2}} = \frac{2.93704(4)}{4.590(4)} = .63988(56),$$

giving, from Eq. (III. 9),

$$\Delta = 0.17(9)\%.$$

VII. COMPARISON WITH THEORY

A. Nuclear Models of Odd-Proton–Odd-Neutron Isotopes

1. Single-Particle Model

The simplest particle description of an odd-odd nucleus is to attribute the nuclear properties to the odd proton and odd neutron, each in its appropriate shell-model state (MAY 55) with the total angular momentum of these two particles vector-coupled to give the g factor

$$g_I = \frac{\vec{I}_p \cdot \vec{I}}{I(I+1)} g_p + \frac{\vec{I}_n \cdot \vec{I}}{I(I+1)} g_n, \qquad \text{(VII. 1)}$$

where I is the spin of the isotope, I_p and I_n the total angular momentum of the proton and neutron respectively, and g_p and g_n the proton and neutron g factors, which are given for either nucleon by

$$g = \frac{\vec{s} \cdot \vec{j}}{j(j+1)} g_s + \frac{\vec{\ell} \cdot \vec{j}}{j(j+1)} g_\ell, \qquad \text{(VII. 2)}$$

where j is the nucleon's total angular momentum and g_s and g_ℓ are the spin and orbital g factors of the "free" nucleon, as follows (BLI 57):

proton	neutron
$g_\ell = 1$	$g_\ell = 0$
$g_s = 5.59$	$g_s = -3.83$

Note that in this section, for computational convenience, magnetic moments are given in units of nuclear magnetons.

Nordheim (NOR 50) pointed out that the ground-state spin of a number of odd-odd nuclei could be accounted for on the basis of this model plus empirical rules giving the coupling of the odd proton and neutron. These rules can be justified on the assumption that the intrinsic spins of these two odd particles always tend to line up parallel. The rules are

"Strong" Rule:

$$I = j_p + j_n \quad \text{if} \quad j_p = \ell_p \pm 1/2 \quad \text{and} \quad j_n = \ell_n \pm 1/2,$$

$$I = |j_p - j_n| \quad \text{if} \quad j_p = \ell \pm 1/2 \quad \text{and} \quad j_n = \ell \mp 1/2; \tag{VII. 3}$$

and

"Weak" Rule: $$|j_p - j_n| < I \leqq j_p + j_n.$$

Fair agreement with experiment can be obtained for magnetic moments by using this model, but although the approximate agreement is encouraging and indicates that the idea is probably valid, it is not sophisticated enough for one to hope to account for the moments of heavier nuclei. It should be pointed out that the above equations are equally valid for a proton or neutron "hole" in a closed angular-momentum shell.

For nuclei in which the neutron and proton states are different, Schwartz (SCH 53) suggested that Eq. (VII. 1) should still be used to calculate g_I, but that the g_p and g_n should represent empirical g factors, i.e., for the odd-odd nucleus Z, N, the g_p and g_n are the measured g values for the neighboring odd-A nuclei Z, N-1 and Z-1, N, respectively, where Z and N are the proton and neutron numbers of the odd-odd nucleus. This empirical rule, which has been justified by Caine (CAI 56), is more successful than using free-particle g factors. Unfortunately, g factors for these adjacent nuclei are not always known, but Schwartz finds that using g factors of near-by nuclei in the same state gives reasonable agreement.

2. Collective Model

Bohr and Mottelson (BOH 53) consider a system of a single particle and a distorted core which is assumed to be uniformly charged and thus to have a g factor

$$g_R \cong \frac{Z}{A} .$$

Several schemes of coupling the odd particle to the core are considered (BOH 51a, b). For the interesting case in which the total j of the odd particle is coupled to the core, Bohr finds

$$g_I = g_\Omega \frac{I}{I+1} + g_R \frac{1}{I+1} ,$$

where Ω is the component of j along the nuclear symmentry axis. For the ground state it is found that $I = \Omega$. Generalizing to two odd particles, one has

$$g_\Omega = \frac{1}{\Omega} [\Omega_n g_\Omega(n) + \Omega_p g_\Omega(p)] ,$$

where $\Omega = I$ and $g_\Omega(n)$ and $g_\Omega(p)$ are the g factors of the odd neutron and proton moving in an ellipsoidal potential. Since these ellipsoid potential g factors are usually not known, g values for pure j states are used. Agreement with experiment should not be expected to be very good. For nuclei with odd particles close to closed shells, such as Rb^{86}, this model is not really applicable, since the core is expected to be close to spherical (GAL 58).

Gallagher and Moszkowski (GAL 58) have determined general coupling rules analogous to the Nordheim rules, Eq. (VII. 3), for deformed nuclei, making the assumption that the components of the neutron and proton spin along the nuclear symmetry axis always couple parallel. Following Bohr and Mottelson, they give for the nuclear moment

$$\mu = (g_\Omega \Omega + g_R) \frac{I}{I+1},$$

where $g_R \tilde{=} Z/A$, and

$$g_\Omega \Omega = [\pm (\Lambda_p + 5.6\ \Sigma_p) \mp 3.8\ \Sigma_n],$$

where the signs of the two terms are the same as the signs of Ω_p and Ω_n appearing in the coupling rules

$$I = \Omega_p + \Omega_n \quad \text{for} \quad \Omega_p = \Lambda_p \pm 1/2 \quad \text{and} \quad \Omega_n = \Lambda_n \pm 1/2,$$

$$I = |\Omega_p - \Omega_n| \quad \text{for} \quad \Omega_p = \Lambda_p \pm 1/2 \quad \text{and} \quad \Omega_n = \Lambda_n \mp 1/2,$$

where Λ_p is the asymptotic orbital quantum number of the proton, and the signs of the asymptotic spin quantum numbers Σ_p and Σ_n are plus or minus depending on whether the particles' intrinsic spins are up (+) or down (-). This notation was introduced by Nilsson (NIL 55, MOT 55) in classifying single-particle states in deformed nuclei.

3. Configuration Mixing Model

Attempts to account for the deviation of the measured magnetic moments from the Schmidt limits predicted by the single-particle shell model lead to the mixing of different nucleon configurations with the odd single-particle configuration (BLI 53, ARI 54) due to very-short-range internuclear forces. The mixing is assumed to be small, but small admixtures can profoundly affect the expectation value of the magnetic-moment operator. The wave function can be written

$$\psi_j = \chi_j + \sum_i a_i \phi_i^j,$$

where χ_j and ϕ_i^j are the ground state and excited single-particle states respectively and a_i is the fractional percentage coefficient. The magnetic moment is given by

$$\mu_{\text{config. mixing}} = \langle \psi_j | \vec{\mu}_{op} | \psi_j \rangle \text{ II}$$

Since a_i is small, only terms linear in a_i need be retained, and because the magnetic-moment operator is a single-particle operator, χ_j and ϕ_i^j can differ only by a single-particle state and the orbital state may not change. The three possibilities are (BLI 57):

(a) for $j = \ell + 1/2$ nuclei, if there is more than one nucleon in the state, ϕ_i^j can be formed by transferring one nucleon to the state $j = \ell - 1/2$;

(b) for $j = \ell - 1/2$ nuclei, if there is more than one hole in this state, one nucleon can be put into the state $j = \ell - 1/2$ to form ϕ_i^j;

(c) for all nuclei there can be a transfer of one nucleon from a closed $j' = \ell' + 1/2$ subshell to an incomplete $j' = \ell' - 1/2$ subshell.

After determining the strength of the interactions, Arima and Horie (ARI 54) successfully predict the moments of most odd-A nuclei.

Recently the theory has been extended (CAI 56, NOY 58) to include odd-odd nuclei, for which the expectation value of the nuclear moment is given by

$$\langle \mu \rangle = \left\{ \frac{j_p(j_p+1) + I(I+1) - j_n(j_n+1)}{2I+1} \right\} \left\{ \frac{\mu_{sp}(j_p) + \delta\mu(j_p)}{j_p} \right\}$$

$$+ \left\{ \frac{j_n(j_n+1) + I(I+1) - j_p(j_p+1)}{2I+1} \right\} \left\{ \frac{\mu_{sp}(j_n) + \delta\mu(j_n)}{j_n} \right\}$$

$$+ \Delta\mu_p + \Delta\mu_n,$$

where $\mu_{sp}(j_p)$ and $\mu_{sp}(j_n)$ are the Schmidt values of the respective nucleons (Eq. (VII. 2)) and $\delta\mu$ are configuration mixing corrections. The terms $(\mu_{sp} + \delta\mu)$ for proton and neutron are to be empirically determined from neighboring odd-A nuclei and are used to calculate

$\Delta\mu_p$ and $\Delta\mu_n$. For Rb^{86}, the configuration mixing value of the moment is no better than the prediction by the extreme single-particle model.

The single-particle configuration of the Rb^{86} nucleus is written $(\pi f_{5/2})^{-1} (\nu g_{9/2})^{-1}$; that is, there is a proton hole in the closed shell of six protons with $j_p = \ell_p - 1/2$, where $\ell_p = 3$; there is a neutron hole in a closed shell of 10 neutrons with $j_n = \ell_n + 1/2$, with $\ell_n = 4$. By Nordheim's strong rule, Eq. (VII. 3), one has

$$I = |9/2 - 5/2| = 2,$$

as is observed experimentally. The coupling rules of Gallagher and Moszkowski also correctly predict the spin. Table VIII summarizes the predictions of these nuclear models as applied to Rb^{86}.

Table VIII

Nuclear moment of Rb^{86}

μ_{exp}	SP, g(free)	SP, g(emp)	Collective (BOH 53)	Collective (GAL 58)	Config. mixing (NOY 58)
-1.686	-2.13	-1.7	-1.56	-1.14	-1.0

B. Application of Models to Bohr-Weisskopf Theory

It will be useful to try to predict the hfs anomaly for the two isotopes Rb^{85} and Rb^{86} by using three stages of the theory:

(a) the original theory as modified by Bohr,

(b) the extension by Eisinger and Jaccarino,

(c) the extension by Stroke to include effects of the charge distribution.

Unfortunately, it is not feasible at this stage of development to apply the more sophisticated configuration mixing and collective models of odd-odd nuclei to this theory because of the additional arbitrary conditions which must now be set on the apportioning of the spin and orbital fractional contributions among the many particles which now contribute to the value of the moment. It is hoped that progress will be made soon on this problem.

Two models are considered here, both of which are of single-particle type. In Model 1, the difference between the observed g value and the Schmidt g value is eliminated by a reduction of the intrinsic spin moment of the odd nucleon (BLO 51), which may be considered to be caused by exchange currents in the nucleus. In Model 2, g_ℓ instead of g_s is to be modified by exchange currents to give g(exp). Each of these is then applied to the three stages of the anomaly theory above to give a predicted Δ for Rb^{85} - Rb^{86}. As is readily seen, the theory of Eisinger and Jaccarino corresponds to the uniform charge distribution of Stroke (STR 59), and theory (c) assumes a surface-charge distribution as presented by Stroke.

Fortunately, the use of empirical g factors of neighboring nuclei gives very close agreement to the observed moment for Rb^{86}, so that these models are equivalent to the use of the adjacent g factors.

C. Predictions of the Rb^{85} - Rb^{86} hfs Anomaly

Model 1

For a nucleon in a single-particle state, the g factor is given by Eq. (III. 6) and a_s and a_ℓ are given by Eq. (III. 7). For Rb^{85} the odd proton is in a $f_{5/2}$ state and one finds, assuming g_ℓ (proton) = 1,

g_ℓ(neutron) = 0,

$$g = -\frac{1}{7} g_p^{eff} + \frac{8}{7} .$$

Using the empirical value of g for Rb^{85}, .539, one finds $g_p^{eff} = 4.22$. Then $a_s = -1/7\ g_p^{eff} = -1.14$ and $a_\ell = (1 - a_\epsilon) = 2.114$. For Rb^{86} the nuclear g factor is given by Eq. (VII. 1). It is assumed that the addition of the odd neutron does not affect the proton state, so for g_p the value $g_{exp}(Rb^{85})$ is used. With $I_p = 5/2$ and $I_n = 9/2$, Eq. (VII. 1) gives $g_n = -0.215$, using the experimental g factor of Rb^{86}. From Eq. (VII. 2), with g_ℓ(neutron) = 0, one finds $g_{sn}^{eff} = -1.94$. Using these values in Eq. (VII. 1), one obtains

$$g = -\frac{5}{6} g_p + \frac{11}{6} \left(\frac{g_{sn}^{eff}}{9}\right)$$

and $a_{sp} = -5/6\ a_s(Rb^{85})$, $a_{\ell p} = -5/6\ a_\ell(Rb^{85})$, and $a_{sn} = \frac{11}{6} \frac{1}{g} \left(\frac{g_{sn}^{eff}}{9}\right)$, giving the values 0.928, -1.762, and 0.466, respectively.

Model 1(a)

With the fractional contributions obtained above, ϵ is calculated with Eq. (III. 4) as derived by Bohr. For Rb, b = 0.58, and for the odd $f_{5/2}$ proton, $(R/R_0)^2 \simeq 0.8$ (BOH 50), and from Eq. (III. 2), $\zeta = 4/5$. For the $g_{9/2}$ neutron, $\zeta = 4/11$, $(R/R_0)^2 \simeq 0.9$ and the ϵ's are summed for the two odd particles in Rb^{86}.

Model 1(b)

The extension of the Bohr-Weisskopf theory by Eisinger and Jaccarino (EIS 58) is used, which assumes a uniform nuclear charge distribution. The ϵ is calculated from Eq. (III. 1), using the $\bar{K}_\ell$ and $\bar{K}_s$ calculated from Eq. (III. 5). From these authors' tables, for the $f_{5/2}$ neutron, $\mathcal{R} e_2 = 0.89$ and $\mathcal{R} e_4 = 0.88$, and the b coefficients for Z = 37 are used.

Model 1(c)

A surface charge distribution is assumed in determining the b coefficients used in Eq. (III. 5). For comparison the b coefficients for the surface and uniform distribution are compared for Z = 37.

Charge Distribution	b_{s2}	b'_{s2}	$b_{\ell 2}$	b_{s4}	b'_{s4}	$b_{\ell 4}$
uniform	0.53	0.21	0.32	0.065	0.037	0.028
surface	0.34	0.14	0.21	0.004	0.002	0.001

The $\mathcal{R}_{ei}$ are the same as for Model 1(b). The results are given in Table IX.

Model 2

Instead of obtaining g_s^{eff}, one modifies g_ℓ to obtain g(exp) by using the "free" nucleon values for g_s. For Rb^{85}, as before,

$$g = -\frac{1}{7} g_s + \frac{8}{7} g_\ell^{eff},$$

where $g_\ell^{eff} = 1.117$. One finds $a_s = -1.46$ and $a_\ell = 2.46$. For Rb^{86},

$$g = -\frac{5}{6} g_p + \frac{11}{6} g_n,$$

which yields $g_n = -0.216$. Using Eq. (VII. 2) (where now the neutron has an " effective" g_ℓ), one finds $g_{\ell n}^{eff} = 0.119$, g_{sp} and g_{sn} have their "free" values, and $g_{\ell p} = g_\ell^{eff}(Rb^{85})$.

Then

$$a_{sp} = -\frac{5}{6} a_s(Rb^{85}),\ a_{\ell p} = -\frac{5}{6} a_\ell(Rb^{85}),\ a_{\ell n} = \frac{11}{6}\left[\frac{8}{9}\ \frac{g_{\ell n}^{eff}}{g_n}\right],$$

$$a_{sn} = \frac{11}{6}\left[1 - \left(\frac{8}{9}\ g_{\ell n}^{eff}/g_n\right)\right],$$

which give the values 1.22, - 2.05, -0.905, and 2.72 respectively.

Model 2(a)

With the fractional contributions calculated with this model, ϵ is calculated by using Eq. (III. 4) with the parameter values as given under Model 1(a).

Model 2(b)

Eqs. (III. 1) and (III. 5) are used, as was done with Model 1(b). The parameters for the uniform charge distribution are unchanged.

Model 2(c)

A surface charge distribution is assumed and the b coefficients appropriate to it are used as listed under Model 1(c). Results are shown in Table IX.

Table IX

hfs Anomalies - Comparison with Theory (percent)

	$\epsilon(Rb^{85})$	$\epsilon(Rb^{86})$	Δ
Experiment	...	...	0.17(9)
Model 1a	0.066	-0.331	0.40
Model 1b	0.030	-0.293	0.32
Model 1c	0.037	-0.219	0.26
Model 2a	0.177	-1.46	1.64
Model 2b	0.024	-1.11	1.13
Model 2c	0.102	-1.00	1.10

VIII. CONCLUSIONS

An apparatus constructed to measure the hyperfine-structure anomalies of radioactive alkali isotopes was used to measure the hfs separations and nuclear moments of Rb^{85} and Rb^{86} and the hfs anomaly was calculated from these results.

Comparison of the Δ(exp) with predictions of the several stages of the Bohr-Weisskopf theory show that a modification of g_ℓ to get g(exp) gives very poor agreement because of the large intrinsic "free" neutron-spin g factor that is assumed. However, Model 1(c) (Table IX) for a surface charge distribution with g_s modified gives the best agreement with the experimental result. It is interesting to note the effect of the extensions of the theory to include terms in $(R/R_0)^4$ and the use of the later value of the nuclear radius; both for the uniform and surface charge distributions the agreement with experiment is better than the original formulation predicts. With three sets of anomalies involving three adjacent isotopes (potassium-39, -40, and -41; rubidium-85, -86, and -87; and cesium-133, -134, and -135) now measured, it is worth while to try to extend the theory to include the configuration mixing and collective models of odd-odd nuclei.

The apparatus and technique described for measuring the nuclear g factor are not capable of giving the ultimate accuracy desired for a measurement of the anomaly. A new atomic-beam apparatus now under construction in this Laboratory will permit g factors to be measured with about ten times the accuracy that can be obtained with this machine. The measurements made here do indicate, however, that, to at least one part per million, the Breit-Rabi equation accurately represents the energy levels of the hyperfine interaction for atoms in the $^2S_{1/2}$ electronic state.

ACKNOWLEDGMENTS

It is a pleasure to acknowledge the support, both moral and material, by Professor William A. Nierenberg during the course of this research.

I am indebted to Dr. Gil Brink who conceived the machine design, directed its construction, and contributed much to its successful operation.

Professor Howard Shugart has been a fountain of wisdom, support during dark hours, and moderator of rash and hasty decisions. I appreciate his interest and help.

To the Atomic Beam Group, especially Dr. Bruce Ewbank, Vernon Ehlers, and Russ Petersen, I am grateful for discussions, assistance, and sympathetic attention to my occasional wailing and gnashing of teeth. To Jhan M. Khan and John Faust, who inherit this machine, I express my thanks for their assistance during the long hours of operation and counting. I wish to thank the Health Chemistry Division of the Lawrence Radiation Laboratory for their competent assistance during the handling of the radioisotopes. I also wish to thank Mr. Douglas McDonald of the Lawrence Radiation Laboratory for his advice on mechanical design and his efforts to get work in and out of the shops with utmost dispatch.

I am grateful to my mother and father, who instilled in me an appreciation of scholarship and enabled me by their support to reach this point.

Words cannot adequately express my thanks to my wife Adele, who so graciously accepted the life of a graduate student's wife and has so competently kept husband, son, and home in running order.

This work was done under the auspices of the U. S. Atomic Energy Commission and supported in part by the Office of Naval Research.

APPENDIX A: CONSTANTS USED IN THIS WORK

The values of the physical constants used in this work have been taken from E. R. Cohen, K. M. Crowe, and J. W. M. duMond, The Fundamentals Constants of Physics (Interscience Publishers, New York, 1957):

$$h = 6.62517(23) \times 10^{-27} \text{ erg sec},$$

$$\mu_0 = 0.92731(2) \times 10^{-20} \text{ erg/gauss},$$

$$k = 1.38042(10) \times 10^{-16} \text{ erg deg}^{-1},$$

$$M_p/m_e = 1836.12(2),$$

$$\mu_N = \mu_0(m_e/M_p) = 0.505038(18) \times 10^{-23} \text{ erg/gauss}.$$

The following measured constants are used in this work and are summarized here for convenience:

$g_J(\text{Rb}) = -2.00238(2)$	(KUS 49)
$\Delta\nu(\text{Rb}^{85}) = 3035.735(2)$ Mc	(BED 52)
$\Delta\nu(\text{Rb}^{87}) = 6834.7005(11)$ Mc	(BED 52)
$g_I(\text{Rb}^{85}) = 2.93704 \times 10^{-4}$	(YAS 51)
$g_I(\text{Rb}^{87}) = 9.95359 \times 10^{-4}$	(YAS 51)
$I(\text{Rb}^{85}) = 5/2$	(KOP 33)
$I(\text{Rb}^{87}) = 3/2$	(KOP 33)

APPENDIX B: DETAILS OF TRANSITION CALCULATIONS

All transitions of interest are of the type $\Delta F = \pm 1$. From Eq. (II. 20), the general equation of a transition is

$$\nu = g_I \mu_0 H_0 (m_+ - m_-) + \frac{\Delta\nu}{2} \left[\left(1 + \frac{4m_+}{2I+1} x + x^2\right)^{1/2} + \left(1 + \frac{4m_-}{2I+1} x + x^2\right)^{1/2} \right] \quad \text{(B. 1)}$$

A. Transitions in Rb^{85} ($I = 5/2$)

The doublet of interest for measuring g_I has the m values $m_+ = -1$, $m_- = -2$, and $m_+ = -2$, $m_- = -1$. From Eq. (B. 1) the mean frequency of this doublet is

$$\bar{\nu} = \frac{\Delta\nu}{2} \left[\left(1 - \frac{2}{3} x + x^2\right)^{1/2} + \left(1 - \frac{4}{3} x + x^2\right)^{1/2} \right], \quad \text{(B. 2)}$$

and the separation of the two lines is

$$\nu^+ - \nu^- = 2g_I \frac{\mu_0 H_0}{h} . \quad \text{(B. 3)}$$

The value of x for which $\bar{\nu}$ is a minimum is found by differentiating $\bar{\nu}$ with respect to x and setting the derivative equal to zero,

$$\frac{\partial \bar{\nu}}{\partial x} = 0 = \frac{2x - 2/3}{\left(1 - \frac{2}{3} x + x^2\right)^{1/2}} + \frac{2x - 4/3}{\left(1 - \frac{4}{3} x + x^2\right)^{1/2}} .$$

Solving for x,

$$x = \frac{11 - 2\sqrt{10}}{9} = 0.519\ 493\ 84.$$

On the basis of Eq. (II. 19b) and the constants for Rb^{85} given in Appendix A, this value of x corresponds to a field of 562.61(3) gauss. Substituting this value of x in Eq. (B. 2) gives

$$\bar{\nu} = \frac{\Delta\nu}{2} \left[(.923\ 544\ 623)^{1/2} + (.577\ 215\ 397)^{1/2} \right]$$

$$= \frac{\Delta\nu}{2} \left[.961\ 012\ 291 + .759\ 746\ 930 \right]$$

$$= .860\ 379\ 61\ \Delta\nu$$

$$= 2611.8845(20)\ \text{Mc} \qquad \text{(B. 4)}$$

Since the term $(m_+ - m_-)$ in Eq. (B. 1) has the value ± 1 for these transitions, the two lines are symmetrically above and below $\bar{\nu}$ by $g_I \frac{\mu_0 H_0}{h}$, and have the values

2611.6532(20) Mc,
2612.1158(20) Mc.

When the resonance frequencies have been observed, as summarized in Table III, g_I can be calculated from Eq. (B. 3) and $\Delta\nu$ from Eq. (B. 4) by using the minimum observed value of $\bar{\nu}$.

B. Transitions in Rb^{86} (I = 2)

For the doublet used to measure g_I, the values of m are $m_+ = 1/2$, $m_- = 3/2$ and $m_+ = 3/2$, $m_- = 1/2$. From Eq. (B. 1),

$$\bar{\nu} = \frac{\Delta\nu}{2} \left[(1 - \tfrac{6}{5}x + x^2)^{1/2} + (1 - \tfrac{2}{5}x + x^2)^{1/2} \right],$$

so that

$$\frac{\partial\bar{\nu}}{\partial x} = 0 = \frac{2x - 6/5}{(1 - \frac{6}{5}x + x^2)^{1/2}} + \frac{2x - 2/5}{(1 - \frac{2}{5}x + x^2)^{1/2}},$$

$$x = \frac{14 - 4\sqrt{6}}{10} = .420\ 204\ 103;$$

then

$$\bar{\nu} = \frac{\Delta\nu}{2}\left[(.672\ 326\ 564)^{1/2} + (1.008\ 489\ 847)^{1/2}\right]$$

$$= \frac{\Delta\nu}{2}\left[.819\ 955\ 221 + 1.004\ 235\ 951\right]$$

$$= .912\ 095\ 585\ \Delta\nu. \qquad \text{(B. 5)}$$

Using the value of $\Delta\nu$ calculated in low field (Table V) the value of x above corresponds to a field of 591.89(3) gauss, from Eq. (II. 20b), and $\bar{\nu}$ = 3599.935(3) Mc. Again, the separation of the doublet is $2g_I\ \mu_0 H_0/h$, with the lines symmetrically above and below the mean value so that the transitions were expected at

3599.553(5) Mc,

3600.317(5) Mc.

When the transitions have been found, $\Delta\nu$ can be calculated from Eq. (B. 5) by using the observed minimum value of $\bar{\nu}$.

For $x \ll 1$ (Zeeman region), where $\Delta\nu$ is first determined before the search for the doublet above is undertaken, the g_I term in Eq. (B. 1) can be neglected, and an expansion of the equation to second order in x yields

$$\nu = \frac{\Delta\nu}{2}\left\{2 + \frac{2x}{2I+1}(m_+ - m_-) + x^2\left[1 - \frac{2}{(2I+1)2}(m_+^2 + m_-^2)\right]\right\}. \qquad \text{(B. 6)}$$

The $\Delta F = \pm 1$ line of interest is the one which is field-independent to second order, and for I = 2 this is an unresolved doublet with the m values $m_+ = \pm 1/2$, $m_- = \mp 1/2$. Substituting these values in Eq. (B. 6),

$$\nu = \Delta\nu\ (1 + \frac{12}{25}\ x^2). \qquad \text{(B. 7)}$$

Now, to sufficient accuracy, from Eq. (II. 19b), one has

$$x \cong \frac{2.8\ \hat{H}_0}{\Delta\nu},$$

and the low-field calibrating resonance is given by Eq. (II. 23) as

$$\nu_{cal} = \frac{2.8\ H_0}{2I_{cal} + 1} .$$

Substituting these relations in B. 7) and solving for $\Delta\nu$ gives

$$\Delta\nu = \nu - \frac{12}{25} \frac{\nu_{cal}^{\ 2}(2I_{cal}+1)^2}{\Delta\nu} .$$

Using Rb^{87} ($I = 3/2$) as the calibrating isotope, one obtains

$$\Delta\nu = \nu - .00194(\nu_{Rb^{87}})^2 \text{ Mc.}$$

APPENDIX C

Reprinted from THE REVIEW OF SCIENTIFIC INSTRUMENTS, Vol. 30, No. 8, 670–674, August, 1959
Printed in U. S. A.

Atomic-Beam Magnet-Stabilization System

GILBERT O. BRINK AND N. BRASLAU
Lawrence Radiation Laboratory and Department of Physics, University of California, Berkeley, California
(Received March 5, 1959; and in final form, April 15, 1959)

A system is described which allows the magnetic field of the "C" magnet of an atomic-beam magnetic-resonance apparatus to be locked to a resonance in the beam. The construction of the system is discussed and representative performance data are presented.

INTRODUCTION

ONE of the greatest difficulties associated with the use of an atomic-beam apparatus for the measurement of atomic properties of radioactive nuclides is the drift of the magnetic fields with time. This is especially true if the beam detection is done by radioactive counting of collected samples. In the work referred to here the machine is to be used to measure a series of hyperfine-structure anomalies of cesium and rubidium isotopes. Since the measurements must be made to a high accuracy, it is necessary for the machine to be stable for long intervals of time. In order to achieve this, it was decided to develop a system by which the magnets could be locked to a resonance in the carrier beam. This has the added advantage that the locking and experimental beams see the same magnetic field, and thus the region of the field that is being locked is that in which the experiment is being performed. The magnetic field calibration is also done in this region. The system has proved very satisfactory and has been a great aid in working with narrow lines.

THEORY OF SYSTEM

The general shape of the peak of an atomic-beam resonance[1] is shown in Fig. 1.[2] In order to lock the magnet system to this resonance, it is necessary to develop an error signal that is capable of deciding which side of the resonance the machine is observing at a given time. To do this the radio frequency that is being used to examine the resonance is frequency-modulated by an amount that is small compared with the resonance width. As can be seen from Fig. 1, the output signal then contains an ac component at the modulation frequency, the phase of which, when compared with the modulating signal, depends upon which side of the resonance is being examined. At the exact resonance frequency, this component has a null. This ac signal is detected with a phase detector whose reference is supplied by the modulation signal. The dc output of the phase detector then depends upon which portion of the resonance is being examined. This dc signal is used to regulate the current through the "C" magnet.

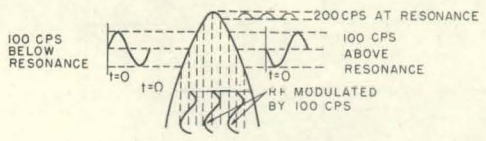

FIG. 1. Production of error signal.

It can also be seen from Fig. 1 that, at exact resonance, there is an ac component produced at twice the modulation frequency. It is convenient to monitor this component so that one can tell at a glance if the machine is properly locked.

GENERAL DISCUSSION

A block diagram of the system is shown in Fig. 2. The primary frequency source is a Gertsch model AM-1 frequency generator,[3] which was modified to allow frequency modulation of the low-frequency oscillator. The output of the low-frequency oscillator is either fed to a frequency multiplier, which supplies signals from 1 to 20 Mc and 100 Mc, or is used to lock the high-frequency oscillator, which supplies signals from 20 to 40 Mc, plus harmonics. For frequency below 200 Mc, the signals are fed to a pair of distributed amplifiers and then to the transition hairpins.

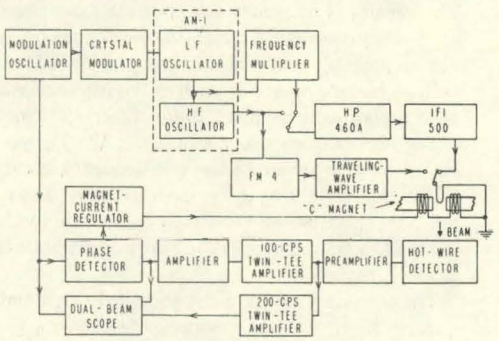

FIG. 2. Block diagram of system.

[1] For a discussion of general atomic-beam technique see N. F. Ramsey, *Molecular Beams* (Oxford University Press, New York, 1955).

[2] Permission to use this figure through the courtesy of the National Company.

[3] Gertsch Products, Inc., 11846 Mississippi Avenue, Los Angeles 25, California.

Reproduced with permission of
The Review of Scientific
Instruments - April 1960

In this system no provision is made to generate signals in the range between 40 and 500 Mc, except at 100 Mc. Frequencies from 500 to 1000 Mc are generated with the Gertsch model FM-4, which is locked to the output of the AM-1. The output of the FM-4 goes to a 1-w traveling-wave amplifier that drives the hairpin. In this manner an FM signal is provided in the range 1 to 40, at 100, and in the range 500 to 1000 Mc.

The beam is detected by means of a hot-wire surface-ionization detector.[4] The output of the detector goes directly to a preamplifier which, in turn, feeds the "lock-in amplifier," consisting of two twin-tee amplifiers, one of which feeds a monitoring oscilloscope while the other feeds a phase detector. The output of the phase detector goes directly to the magnet current regulator that supplies current to the "C" magnet. The loop is completed through the beam to the rf system.

RADIO-FREQUENCY SYSTEM

The Gertsch model AM-1 is a VHF interpolater that is capable of generating fundamental frequencies between 1 and 2 Mc and 20 to 40 Mc, plus harmonics up to 1000 Mc. It consists of two oscillators that can be phase-locked together. The low-frequency oscillator is used as a free-running oscillator and tunes from 1 to 2 Mc. For use in this application, it was modified as shown in Fig. 3. The low-frequency oscillator is frequency-modulated by means of a crystal diode which is capacitance-coupled to the oscillator tank circuit. The diode is driven from the modulation oscillator (which is described later). The frequency deviation can be adjusted either by the amplitude of the modulation signal or by the variable coupling capacitor. The amount of frequency deviation available also depends upon the frequency to which the oscillator is tuned. The circuit probably could be improved by substitution of a voltage-tunable capacitor, such as the International Rectifier Corporation type 6.8SC20 for the crystal diode.

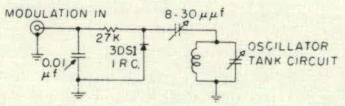

FIG. 3. Modification of AM-1

The high-frequency oscillator in the AM-1 can be phase-locked to a harmonic of the low-frequency oscillator. In this manner, the frequency modulation is transferred to the HF oscillator, which is used to provide fundamental frequencies from 20 to 40 Mc and to generate harmonics of these frequencies.

The output of the LF oscillator is fed to a standard frequency multiplier which supplies frequencies from 2 to 20 Mc and 100 Mc. The output of the multiplier goes to a Hewlett-Packard model 460A distributed amplifier and then to an Instruments for Industry model 500 distributed power amplifier which drives the hairpin. The output of the HF oscillator can also be fed to the distributed amplifiers and thence to the hairpin. This system is capable of supplying up to 3 w of power from 1 to 40 and at 100 Mc.

The Gertsch model FM-4 is used to generate frequencies from 500 to 1000 Mc. It consists of an oscillator which tunes from 500 to 1000 Mc and which can be phase-locked to a harmonic of the AM-1. A frequency-modulated signal is thus produced which is fed to a 1-w 500- to 1000-Mc traveling-wave amplifier,[5] which feeds the hairpin.

This rf system has proved very satisfactory for this purpose. The center frequency of the Gertsch oscillator has a short-term stability of about 1 part in 10^7, and the generated frequencies are quite adequate for most atomic-beam experiments. The frequency deviation in the region of 1 Mc is somewhat low, but this probably could be improved with the above-mentioned substitution for the crystal diode.

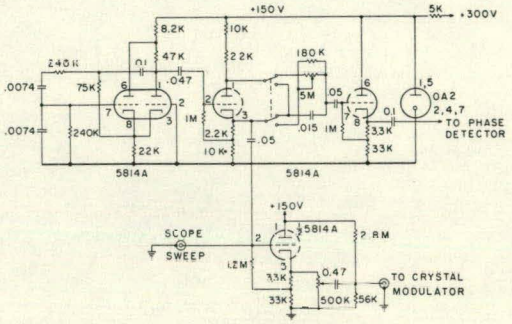

FIG. 4. Modulation oscillator.

MODULATION OSCILLATOR

The modulation oscillator is shown in Fig. 4. It is an RC oscillator using a 5814A tube, and it runs at a frequency of 100 cps. The output of the oscillator is coupled to a second 5814A which serves as a phase shifter and cathode follower. The output of the phase shifter is used

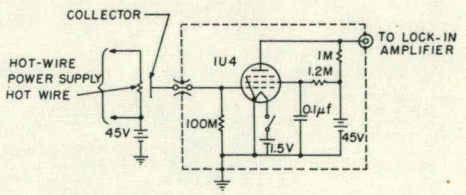

FIG. 5. Preamplifier.

[4] See reference 1, p. 379.

[5] The traveling-wave amplifier used here is no longer available commerically. There are, however, several other traveling-wave amplifiers available that are suitable for this purpose.

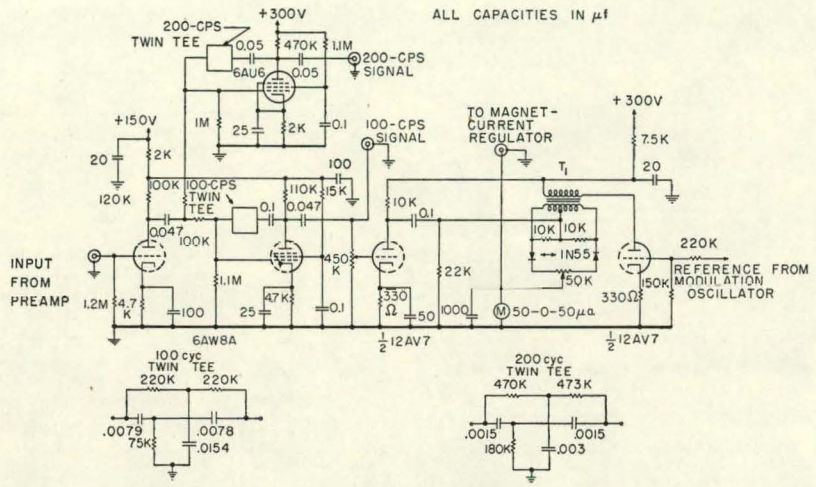

FIG. 6. Lock-in amplifier. T_1 is a United Transformer Company A-19 Interstage.

to provide the reference signal for the phase detector. The output of the cathode follower drives one section of another 5814A cathode follower, which is used to drive the crystal modulator. It also supplies the dc bias for the crystal and allows the amplitude of the modulation signal to be controlled. Horizontal sweep for the monitoring oscilloscope is taken from the grid of this tube.

BEAM DETECTOR AND PREAMPLIFIER

The beam is detected on a surface ionization detector which consists of a 0.002×0.010-in. potassium-free tungsten ribbon.[6] The collector of the detector goes directly to the grid of the preamplifier. The preamp, which is shown in Fig. 5, is mounted very near the detector and is completely enclosed in an aluminum box to provide shielding against 60-cps pickup. The amplifier is battery-powered; the batteries are also contained inside the shield. For the beam intensities that are usually used in radioactive work, it was not necessary to use an electron multiplier, and this detector proved very satisfactory. The exit beam in the machine is about 0.060 in. wide and the detector, which is mounted vertically in the center of the beam, does not block very much of it.

LOCK-IN AMPLIFIER

The lock-in amplifier is shown in Fig. 6. The first half of the 6AW8A is used as an input amplifier which drives two twin-tee amplifiers. One of these, which uses the second half of the 6AW8A, is tuned to 100 cps and provides the signal for the phase detector. The second twin-tee amplifier is a 6AU6 tube, and is tuned to 200 cps. When the system is properly locked on the peak of the carrier resonance, there is a 200-cps component present in the signal and it is monitored through this amplifier.

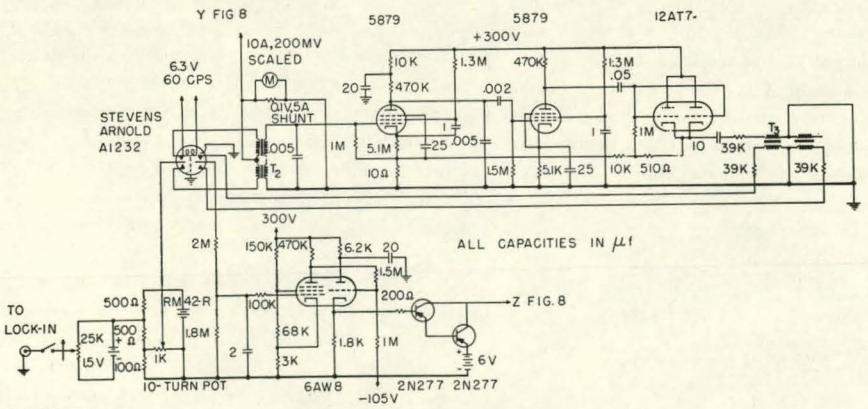

FIG. 7. Magnet-current regulator. T_2 is Triad G-10 Geoformer; T_3 is Chicago Standard Transformer Company A-4774 Universal Interstage.

[6] This ribbon was obtained from A. D. Mackay, Inc., 198 Broadway, New York 38, New York.

TABLE I. Representative performance of the lock-in system: Frequencies as a function of time, Rb^{87} resonance (in Mc).

	Run Number 6: System locked on $\Delta F = 0$ resonance of Rb^{85} at 100.0 Mc. Time					
	1315	1410	1505	1600	1700	1825
First reading	136.960	136.986	136.972	136.986	136.984	136.948
Second reading	136.981	136.986	136.982	136.981	136.985	136.953
Third reading	136.968	136.964	137.011	136.998	...	136.974
Average	136.970	136.979	136.988	136.988	136.985	136.958
	Run Number 10: System locked on $\Delta F = 0$ resonance of Rb^{85} at 503.5 Mc. Time					
	1505	1555	1643	1730	1815	1915
First reading	537.408	537.417	537.360	537.348	537.351	537.324
Second reading	537.336	537.408	537.411	537.357	537.354	537.324
Third reading	537.414	537.444	537.420	537.321	537.357	537.342
Average	537.386	537.423	537.397	537.342	537.354	537.330
	Run Number 15: System locked on $\Delta F = 0$ resonance of Rb^{85} at 1.9 Mc. Time						
	1510	1610	1705	1745	1805	1830	1907
First reading	2.848	2.846	2.845	2.844	2.846	2.847	2.844
Second reading	2.849	2.836	2.845	2.845	2.842	2.844	2.845
Third reading	2.849	2.834	2.846	2.848	2.845	2.847	2.843
Average	2.849	2.839	2.845	2.846	2.844	2.846	2.844

The output of the first twin-tee amplifier drives the phase detector, which is similar to that used in the National Company Atomichron. It has the advantage that both the input and output signals are single-ended, while the reference signal is introduced in push-pull. The output of the phase detector, after being filtered, is fed to the magnet-current regulator, which is shown in Fig. 7.

MAGNET-CURRENT REGULATOR

The magnet-current regulator is a current-regulated power supply which uses power transistors as the series element. The regulator consists of a chopper amplifier followed by a synchronous detector, the output of which drives the transistors. Since the output of the phase detector is at zero volts, it is necessary to use a bucking battery in order to match it to the input of the regulator. The regulator supplies 0 to 5 amp to the "C" magnet.

When it is necessary to run the "C" magnet at more than 5 amp, the current is obtained from submarine storage batteries, as shown in Fig. 8. The variable resistor allows the current to be varied in 5-amp steps, and the regulator provides the fine control. In this manner, the magnet can be locked at any field desired.

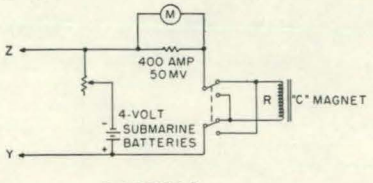

FIG. 8. Magnet storage-battery circuit.

PERFORMANCE

The locking system has been used in many runs on stable potassium and rubidium and in several runs on radioactive Rb^{86}. The actual degree of field stabilization is dependent upon the line width of the carrier resonance and on its field dependence. Representative performance of the system is indicated by observing the peak frequency of the calibrating resonance at various times during a run. Table I gives data from Rb^{86} investigations at three different values of the magnetic field. The system is operated with maximum loop gain, with the frequency deviation adjusted to give best operation. Both Rb^{85} and Rb^{87} are present as carrier isotopes and either may be used to lock the field. For isolation of the oscillators, separate closely spaced hairpins were used, one for locking the field and the other for calibration and search.

In run Number 6, the field was locked to the $(3, -3 \leftrightarrow 3, -2)$ line of Rb^{85} at a frequency of 100 Mc. The frequency-modulated signal was obtained from the LF oscillator of the AM-1, having been multiplied by a factor of 60. The calibrating frequency was obtained from a Hewlett-Packard 608A signal generator, its frequency being monitored by a Hewlett-Packard 525 frequency counter. The calibrating line was the $(2, -2 \leftrightarrow 2, -1)$ line of Rb^{87}, having a line width in this instance of about 150 kc.

In run Number 10, the system was locked to the same Rb^{85} line at a frequency of 503.5 Mc, with the AM-1, FM-4 combination. The line in this instance was 400-kc wide (due to field inhomogeneities), and since the frequency deviation of the signal was limited so as not to pull the FM-4 off its phase-locked condition, the oscillator

could not be swept very far down the sides of the resonance lines. Some decrease in performance was expected owing to the reduced strength of the error signal; however, the Rb^{86} resonance obtained in this run was quite satisfactory. The calibrating frequency was obtained from another AM-1, FM-4 combination with its frequency monitored by a Hewlett-Packard 540A transfer oscillator.

In run Number 15, the system was locked to the same Rb^{85} line at 1.9 Mc with the LF oscillator of the AM-1, the line width being about 150 kc. The Rb^{87} calibrating frequency was obtained from a Tektronix Type 190A signal generator.

ACKNOWLEDGMENTS

The authors wish to thank Mr. George Schrader of the Lawrence Radiation Laboratory for designing and constructing the magnet-current regulator. This work was supported in part by the National Science Foundation, the U. S. Office of Naval Research, and the U. S. Atomic Energy Commission.

REFERENCES

ARD 58 M. Arditi and T. R. Carver, Phys. Rev. 109, 1012 (1958).

ARI 54 A. Arima and H. Horie, Progr. Theoret. Physics (Kyoto) 12, 623 (1954).

BED 52 B. Bederson and V. Jaccarino, Phys. Rev. 87, 228 (1952).

BEL 51 E. H. Bellamy, Nature 168, 556 (1951).

BEL 53 E. H. Bellamy and K. F. Smith, Phil. Mag. 44, 33 (1953).

BEM 53 G. Bemski, The Fluorine Resonance in Molecular Beams (Thesis), University of California, 1953.

BEN 58 P. L. Bender, E. C. Beatty, and A. R. Chi, Phys. Rev. Letters 1, 311 (1958).

BIT 49 F. Bitter, Phys. Rev. 76, 150 (1949).

BLI 53 R. J. Blin-Stoyle, Proc. Phys. Soc. (London) A66, 1158 (1953).

BLI 57 R. J. Blin-Stoyle, The Theories of Nuclear Moments (Oxford University Press, London, 1957).

BLO 51 F. Bloch, Phys. Rev. 83, 839 (1951).

BOH 50 A. Bohr and V. Weisskopf, Phys. Rev. 77, 94 (1950).

BOH 51a A. Bohr, Phys. Rev. 81, 134 (1951).

BOH 51b A. Bohr, Phys. Rev. 81, 331 (1951).

BOH 53 A. Bohr and B. R. Mottelson, Kgl. Danske Videnskab. Selskab Mat. -fys. Medd. 27, 16 (1953).

BRE 31 G. Breit and I. I. Rabi, Phys. Rev. 38, 2082 (1931).

BRI 58 G. O. Brink, N. Braslau, and J. M. Khan, Bull. Am. Phys. Soc. Ser II, 3, 185 (1958).

CAI 56 C. A. Caine, Proc. Phys. Soc. (London) A69, 635 (1956).

CLE 54 W. W. Clendennen, Phys. Rev. 94, 1590 (1954).

CON 35 E. U. Condon and G. H. Shortley, Theory of Atomic Spectra (Cambridge University Press, London, 1935).

CRA 49 M. F. Crawford and A. L. Shawlow, Phys. Rev. 76, 1310 (1949).

EIS 52 J. Eisinger, B. Bederson, and B. T. Feld, Phys. Rev. 86, 73 (1952).

EIS 58 J. Eisinger and V. Jaccarino, Revs. Modern Phys. 30, Part 1, 528 (1958).

ESS 58 W. Markowitz, R. Glenn Hall, L. Essen, and J. V. L. Parry, Phys. Rev. Letters 1, 105 (1958).

EVA 55 R. D. Evans, The Atomic Nucleus (McGraw-Hill Book Co., New York, 1955).

FEH 56 G. Feher, Phys. Rev. 103, 500 (1956).

FEH 58 J. Eisinger and G. Feher, Phys. Rev. 109, 1172 (1958).

FER 30 E. Fermi, Z. Physik 60, 320 (1930).

FOR 55 K. W. Ford and D. L. Hill, Ann. Rev. Nuclear Sci. 5, 25 (1955).

FRI 59 G. Fricke, S. Penselin, and E. Recknagel (Heidelberg Univ.), to be published.

GAL 58 C. G. Gallagher and S. A. Moszkowski, Phys. Rev. 111, 1282 (1958).

GIN 57 E. L. Ginzton, Microwave Measurements (McGraw-Hill Book Co., New York, 1957).

HOL 59 J. Holloway, W. Mainberger, F. H. Reder, G. M. R. Winkler, L. Essen, and J. V. L. Parry, Proc. I. R. E. 47, 1730 (1959).

HOL 60 Joseph H. Holloway (National Company, Malden, Mass.), private communication.

HUB 59 J. C. Hubbs and W. A. Nierenberg, The Investigation of Short-Lived Radionuclei by Atomic Beam Methods, UCRL-8724, Jan. 1959.

KAS 50 A. Kastler, J. Phys. Radium 11, 225 (1950).

KIN 52 D. D. King, Measurements at Centimeter Wavelength (D. Van Nostrand Co., New York, 1952).

KOP 33 H. Kopfermann, Naturwiss. 21, 24 (1933).

KOP 58 H. Kopfermann, Nuclear Moments, Schneider, Translator (Academic Press, New York, 1958).

KUS 40 P. Kusch, S. Millman, and I. I. Rabi, Phys. Rev. 57, 765 (1940).

KUS 49 P. Kusch and H. Taub, Phys. Rev. 75, 1477 (1949).

KUS 59 P. Kusch and V. W. Hughes, Atomic and Molecular Beam Spectroscopy, in Handbuch der Physik, Flugge, Ed., Vol 37/1 (Springer Verlag, Berlin, 1959), p. 1.

LAM 41 W. E. Lamb, Phys. Rev. 60, 817 (1941).

LAU 58 G. Laukin, Kernmagnetiche Hochfrequenz-Spectroskopie, in Handbuch der Physik, Flugge, Ed., Vol. 38/1 (Springer Verlag, Berlin, 1958), p. 120.

LUR 56 A. Lurio and A. G. Prodell, Phys. Rev. 101, 79 (1956).

MAJ 32 E. Majorana, Nuovo cimento 9, 43 (1932).

MAY 55 M. Mayer and J. H. D. Jensen, Elementary Theory of Nuclear Shell Structure (John Wiley and Sons, New York, 1955).

MOT 55 B. R. Mottelson and S. G. Nilsson, Phys. Rev. 99, 1615 (1955).

NIE 57 W. A. Nierenberg, Ann. Rev. Nuclear Sci. 7, 349 (1957).

NIL 55 S. G. Nilsson, Kgl. Danske Videnskab. Selskab Matt. - fys. Medd. 29, 16 (1955).

NOR 50 L. W. Nordheim, Phys. Rev. 78, 294, (1950).

NOY 58 H. Noya, A. Arima, and H. Horie, Progr. Theoret. Phys. (Kyoto) Suppl. 8, 33 (1958).

PAC 57 K. S. Packard, I. R. E. PGMTT-5, 244 (1957).

PAU 24 W. Pauli, Naturwiss. 12, 741 (1924).

RAB 38 I. I. Rabi, S. Millman, P. Kusch, and J. R. Zacharias, Phys. Rev. 53, 318 (1938).

RAM 44 S. Ramo and J. R. Whinnery, Fields and Waves in Modern Radio (John Wiley and Sons, New York, 1944).

RAM 50 N. F. Ramsey, Phys. Rev. 78, 695 (1950).

RAM 53 N. F. Ramsey, Nuclear Moments (John Wiley and Sons, New York, 1953).

RAM 56 N. F. Ramsey, Molecular Beams (Clarendon Press, Oxford, 1956).

ROS 32 J. E. Rosenthal and G. Breit, Phys. Rev. 41, 459 (1932).

SAN 59 P. G. H. Sandars, Investigations of Hyperfine Structure by the Method of Magnetic Resonance in Atomic Beams (Thesis), Oxford University, 1959.

SCH 53 H. M. Schwartz, Phys. Rev. 89, 1293 (1953).

SCH 57 C. Schwartz, Phys. Rev. 105, 173 (1957).

SEA 58 D. Strominger, J. M. Hollander, and G. T. Seaborg, Revs. Modern Phys. 30, 585 (1958).

SHU 57 H. A. Shugart, The Nuclear Spins, Hyperfine-Structure Separations, and Magnetic Moments of Cs^{127}, Cs^{129}, Cs^{130}, and Cs^{132}. (Thesis), University of California, 1957.

SMI 55 K. F. Smith, Molecular Beams (Methuen and Co., Ltd., London, 1955).

STR 57 H. H. Stroke, V. Jaccarino, D. S. Edmonds, and R. Weiss, Phys. Rev. 105, 590 (1957).

STR 59 H. H. Stroke, Quarterly Progress Report No. 54, Research Lab of Electronics, M. I. T., July 15, 1959.

SUN 56 R. J. Sunderland, The Nuclear Spins of Rb^{82}, Rb^{83}, and Rb^{84} (Thesis), University of California, 1956.

TIN 57 Y. Ting and H. Lew, Phys. Rev. 105, 581 (1957).

TOR 41 H. C. Torry, Phys. Rev. 59, 293 (1941).

WOO 56 G. K. Woodgate and R. W. Hellworth, Proc. Phys. Soc. (London) A69, 588 (1956).

WOO 58 G. K. Woodgate and P. G. H. Sandars, Nature 181, 1395 (1958).

YAS 51 E. Yasaitis and B. Smaller, Phys. Rev. 82, 750 (1951).

ZAC 42 J. R. Zacharias, Phys. Rev. 61, 270 (1942).

This report was prepared as an account of Government sponsored work. Neither the United States, nor the Commission, nor any person acting on behalf of the Commission:

A. Makes any warranty or representation, expressed or implied, with respect to the accuracy, completeness, or usefulness of the information contained in this report, or that the use of any information, apparatus, method, or process disclosed in this report may not infringe privately owned rights; or

B. Assumes any liabilities with respect to the use of, or for damages resulting from the use of any information, apparatus, method, or process disclosed in this report.

As used in the above, "person acting on behalf of the Commission" includes any employee or contractor of the Commission, or employee of such contractor, to the extent that such employee or contractor of the Commission, or employee of such contractor prepares, disseminates, or provides access to, any information pursuant to his employment or contract with the Commission, or his employment with such contractor.